MECHANISM OF HEAT GENERATION FROM LOADING GASEOUS HYDROGEN ISOTOPES INTO PALLADIUM NANOPARTICLES

by

OLGA DMITRIYEVA

M.S., Physics, Voronezh State University, Voronezh, 1996

M.S., Electrical Engineering, University of Colorado, Boulder, 2010

A thesis submitted to the

Faculty of the Graduate School of the

University of Colorado in partial fulfillment

of the requirement for the degree of

Doctor of Philosophy

Department of Electrical Engineering

2012

This thesis entitled:

Mechanism of heat generation from loading gaseous hydrogen isotopes into palladium nanoparticles

written by Olga Dmitriyeva

has been approved for the Department of Electrical Engineering

_____

Prof. Garret Moddel

_____

Prof. Alan Gallagher

Date_____

The final copy of this thesis has been examined by the signatories, and we
Find that both the content and the form meet acceptable presentation standards
Of scholarly work in the above mentioned discipline.

Dmitriyeva, Olga (Ph.D., Electrical Engineering)

Mechanism of heat generation from loading gaseous hydrogen isotopes into palladium nanoparticles

Thesis directed by Prof. Garret Moddel

I have carried out the study of hydrogen isotope reactions in the presence of palladium nanoparticles impregnated into oxide powder. My goal was to explain the mechanisms of heat generation in those systems as a result of exposure to deuterium gas. Some researchers have associated this heating with a nuclear reaction in the Pd lattice. While some earlier experiments showed a correlation between the generation of excess heat and helium production as possible evidence of a nuclear reaction, the results of that research have not been replicated by the other groups and the search for radiation was unsuccessful. Therefore, the unknown origin of the excess heat produced by these systems is of great interest.

I synthesized different types of Pd and Pt-impregnated oxide samples similar to those used by other research groups. I used different characterization techniques to confirm that the fabrication method I used is capable of producing Pd nanoparticles on the surface of alumina support. I used a custom built gas-loading system to pressurize the material with hydrogen and deuterium gas while measuring heat output as a result of these pressurizations. My initial study confirmed the excess heat generation in the presence of deuterium. However, the in-situ radiometry and alpha-particle measurements did not show any abnormal increase in counts above the background level. In the absence of nuclear reaction products, I decided to look for a conventional chemical process that could account for the excess heat generation.

It was earlier suggested that Pd in its nanoparticle form catalyzes hydrogen/deuterium (H/D) exchange reactions in the material. To prove the chemical nature of the observed phenomena I demonstrated that the reaction can be either exo- or endothermic based on the water isotope trapped in the material and the type of gas provided to the system. The H/D exchange was confirmed by RGA, NMR and FTIR analysis. I quantified the amount of energy that can be released due to the H/D exchange and proved that the heat generated during the experiments can be fully accounted for by this chemical reaction. Based on these results I concluded that the origin of the excess heat generated during deuterium loading of Pd-nanoparticle materials is chemical rather than nuclear.

I also looked at which measurement artifacts can result in apparent heat generation. I suggested that the presence of a thermal gradient within the system can alter the temperature measurement baseline, which would then look like anomalous heating under gas pressure. To test the hypothesis I experimentally enhanced thermal gradients in the gas-loading system and successfully demonstrated the effect. By using a commercially available finite element solver I matched experimental and simulated data to quantify the magnitude of the thermal gradient required to produce a measurable effect. Based on my observations I proposed a technique that would ensure the proper gas-loading system calibration and help to avoid any misinterpretation of the results.

ACKNOWLEDGMENTS

My deepest gratitude goes to Prof. Garret Moddel, my advisor and great mentor, who for the last 8 years influenced my life in many ways including my decision to go back to school to pursue my degree in Electrical Engineering.

I thank the faculty members in my committee, Profs. Alan Gallagher, Alan Mickelson Charles Musgrave, and Won Park for sharing their expertise on various aspects of my thesis.

This work would never be completed without the support of Coolescence's team. My very special thanks go to Matt McConnell and Rick Cantwell for the opportunity to work on the project and to learn from their engineering talents. I sincerely thank Garry Stanish for shaping up my sometimes vague ideas into a solid form of experimental apparatus and measurement setup. I also thank Judy Bebber for her enthusiasm towards my research and her ability to keep my spirit up during the uneasy times.

I thank Dr. David Kidwell for his generous invitation to visit the Naval Research Laboratory where a big part of my process characterization work was done. I also would like to thank Drs. Dennis Eberl, Alex Blum, Hans Funke and Natalia Varaksa along with Troy Gould for their assistance in the characterization of my samples. I also thank Joshua Solomon for our collaboration.

I wish to thank current and former members of the Quantum Engineering Lab including Sachit Grover, David Doroski, James Zhu, Saumil Joshi, Weiming Peng, Bradley Pelz, and Michael Cromar for their helpful comments, ideas, and criticism, and most importantly for making my grad school years an enjoyable experience.

I also thank my friends Ginni Sharma, Yulyia Kokoshinskiy, Anna Belous, and Maria Pereskokova for being supportive and caring.

I am eternally grateful to my mother, Veronika for her love and everlasting support. Even though my father, Yuri, did not live long enough to witness my work, his memory was giving me strength throughout these years. I thank my husband, Michael, for believing in me and being there for me. Finally, with all my heart, I thank my son Zakhar for his love, patience and understanding, and for looking up to me while always encouraging me to move forward.

TABLE OF CONTENTS

LIST OF TABLES

LIST OF FIGURES

CHAPTER I

INTRODUCTION AND THESIS OUTLINE

A. Introduction

According to the International Energy Outlook 2011 (IEO2011) reference case (U.S. Department of Energy, 2011) the world energy consumption is expected to grow by 53% from 2008 to 2035. As a result of growing demand and limited supply conventional energy sources' prices are on the rise. Once again we are in a search for alternative energy sources. Shifts from primary to alternative energy sources have happened before; the reason for the transition from wood to soft coal in the early 19^{th} century was economic: coal was cheap and abundant. These days society is looking for not only cost-effective, but also environmentally friendly and safe alternative energy sources that have an inexhaustible supply.

Alternative energy is a broad term usually applied to nuclear power and renewable sources such as solar, wind, hydro, and geothermal. My research interests lie within a couple of less common options. The two cases which I will discuss are (1) the investigation of the results from deuterium loading in palladium-based powdered materials associated with low energy nuclear reaction (LENR), and (2) the observation of a zero-point energy (ZPE) radiation from Casimir cavities as a potential vehicle for vacuum energy harvesting.

1) Hydrogen isotopes loading into Pd

In 1989 two electrochemists, Profs. Martin Fleischmann and Stanley Pons, ran an experiment that resulted in thermal energy production that could not be explained by conventional chemistry. The two scientists used an electrochemical cell with a Pd cathode submerged in a D_2O + LiOD electrolyte (Fleischmann, et al., 1989). The process proposed to involve a nuclear fusion reaction between deuterons, resulting in helium production at low

radiation levels. The phenomenon was called cold fusion, or a low energy nuclear reaction (LENR). The idea of harvesting clean energy in the absence of harmful nuclear products or waste was an attractive alternative to the known energy generation approaches. The announcement made by Fleischmann and Pons in 1989 resulted in a massive experimental effort undertaken by scientists around the world. After multiple unsuccessful replications and withdrawal of some positive results, a US Department of Energy (DOE) review panel statement was issued in 1989: "the evidence for the discovery of a new nuclear process was not persuasive enough to start a special program". The following DOE review, organized in 2004 to look at new research, reached similar conclusions, adding that, "internal inconsistencies and lack of predictability and reproducibility remain serious concerns" (U.S. Department of Energy, 2004). The statement issued by DOE reflected the skepticism of mainstream science towards the cold fusion phenomenon. From that point on the research was limited and only took place after the occasional financial infusion. In addition to the original Fleischmann-Pons electrochemical experiments, LENR research included: co-deposition, plasma glow-discharge, D_2 and H_2 gas-loading in Pd and other transition metals, metal bombardment with energetic particles, bubble collapse of various metals in D_2O using ultrasound, and more (Storms, 2007) (Storms, 2010). Despite the scientific community's best efforts, poor reproducibility remained a problem. Scientists were in a search of an experiment that would produce consistent results in a repeatable manner. In recent years attention has been focused on gas-loading in a variety of Pd-nanoparticle materials, because they have consistently exhibited anomalous heat production.

During gas-loading the material remains in a bulk or powdered form while deuterium is supplied in a gas form (Biberian, 2008). The advantages of gas-loading over electrochemical experiments are:

- pressures are easily controlled,
- operational temperatures can be high,
- clean environment: the experiment is sealed in the vacuum chamber,
- somewhat easier analysis: the gaseous reaction products can be analyzed with a residual gas analyzing (RGA) unit.

The disadvantages are:

- it is difficult to achieve very high pressures,
- an advanced vacuum system is required,
- hydrogen isotopes, pressurized at high temperatures, possess potential danger if handled without care.

The most encouraging gas-loading results were presented by Arata et al. (Arata & Zhang, 2008), where anomalous heat along with nuclear fusion products (^{4}He) were observed. Arata used nano-Pd material in the form of a ZrO_2+Pd mixture, and an alloy composed of Zr+Ni+Pd in powdered form. Figure I - 1 shows the heat measurement results done on the samples during the exposure of both materials to deuterium and hydrogen gases. The temperature change as a function of time is shown after the material made contact with the gas. The temperature change was monitored by two thermocouples: T_{in} is the reading from the probe installed inside the cell at the location of the sample, while T_s is the temperature of the outside surface of the cell. When gas was introduced into the system the amount of heat produced was apparently greater for the ZrO_2+Pd sample than for the Zr+Ni+Pd sample. The reaction in the presence of deuterium gas generated more heat than the reaction with hydrogen – the phenomenon known as an isotope effect.

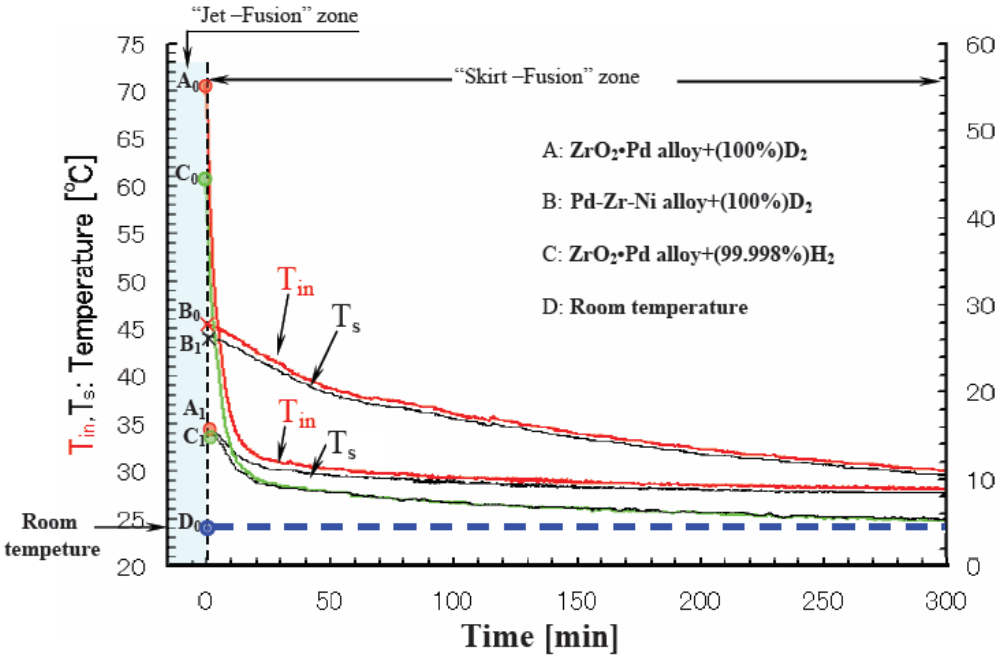

Figure I - 1 Heat evolution after exposing ZrO2+Pd and Zr+Ni+Pd to hydrogen and deuterium (Arata & Zhang, 2008).

Figure I - 2 represents a quadrupole mass spectroscopy (QMS) analysis of the gas and the powdered sample. QMS is capable to distinguish between deuterium molecule and helium atom, where the conventional RGA would fail. However, no clear explanation on experimental protocol was supplied by the authors, besides the statement that deuterium exposures resulted in the clearly visible helium traces.

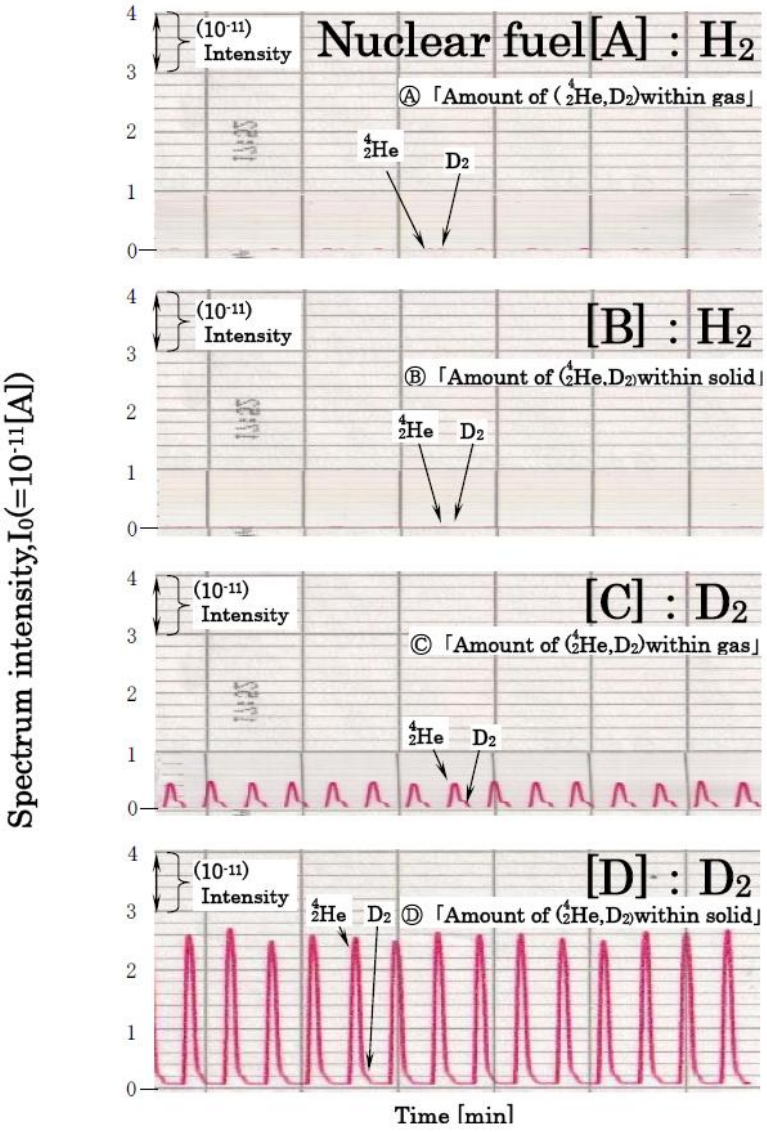

Figure I - 2 QMS mass spectroscope data: cases [A] and [B] show relative concentration of 4He found in the gas and the powder as a result of hydrogen exposure, while [C] and [D] show 4He concentration in the gas and the powder due to deuterium exposures (Arata & Zhang, 2008).

Important details were missing from the report, which diminish the value of this work. No data were given on the QMS detector calibration, and there was no information on the time scale of the helium generation events or their correlation with the gas cycling. Still, the reported

results (even with the patches of missing information), generated a great deal of interest in nano-materials.

In the years that followed, several groups reported very similar results on Pd nanoparticle materials. A. Kitamura and his colleagues from Kobe University, Japan, in collaboration with A. Takahashi from Osaka University, Japan, constructed a system to replicate Arata's results on heat and helium generation in nano-sized Pd powders, and to investigate the underlying physics. Pd-Zr oxide nano-powder demonstrated an anomalous heating in the presence of deuterium, but "nothing other than steady background both in neutron counter and scintillation probe [used for the ionizing radiation measurements] was observed" (Kitamura, et al., 2008). Scientists from the Naval Research Laboratory, USA, reported exothermic heat generation during gas-loading experiments on Pd enriched zeolite and alumina powders using a high precision calorimeter (Kidwell, et al., 2009). Toyota's Central Research and Development Laboratories Inc., Japan, used Pd-ZrO_2 nanocomposites and reported anomalous heating in the presence of deuterium (Hioki, et al., 2009).

All of the previously reported works has provided enough evidence that gas-loading systems are capable of producing excess heat in a repeatable manner, which can be studied and evaluated in a laboratory setup.

2) Zero-point energy radiation detection

In quantum mechanics the energy of the system at temperature T=0 K (or at its lowest quantized energy level) is called zero-point (ZP) energy. ZP energy is the energy that remains when all other energy is removed from a system. The most frequently used examples are (i) the current noise in a resistively shunted Josephson junction, (ii) the fact that helium remains liquid

at absolute zero and atmospheric pressure, and (iii) the Casimir force, which is now experimentally measured to the very high precision.

ZP radiation has a frequency-cubed dependence, and assuming that ZP fluctuations continue to the Planck frequency (10^{43} Hz), the density of ZP field is enormous. Different approaches were suggested for harvesting ZP energy to use it as a power source (Davis, et al., 2006), (Moddel, 2009).

A recently issued patent (Haisch & Moddel, May 27, 2008) describes a method by which vacuum energy is extracted from gas flowing through a Casimir cavity. According to stochastic electrodynamics (SED) the ground state of an electron orbital is assumed to emit Larmor radiation, which would cause the electron to spiral inward if it were not balanced by absorption of ZP energy from the vacuum. Mode suppression of quantum vacuum radiation is known to take place in Casimir cavities, which gives a rise to already mentioned Casimir force.

Figure I - 3 shows a schematic representation of the vacuum energy extraction process. In the upper part of the loop gas is pumped first through a region surrounded by a radiation absorber, and then through a Casimir cavity. As the atoms enter the Casimir cavity their orbitals spin down in accordance with SED and release electromagnetic radiation (the process is depicted by the outward pointing arrows), that get absorbed by the absorbing media. On exiting the cavity at the top left, the ambient ZP field re-energizes the orbitals (depicted by the inward pointing arrows). The gas then flows through a pump and is re-circulated through the system. The system functions like a heat pump, pumping energy from an external source to a local absorber.

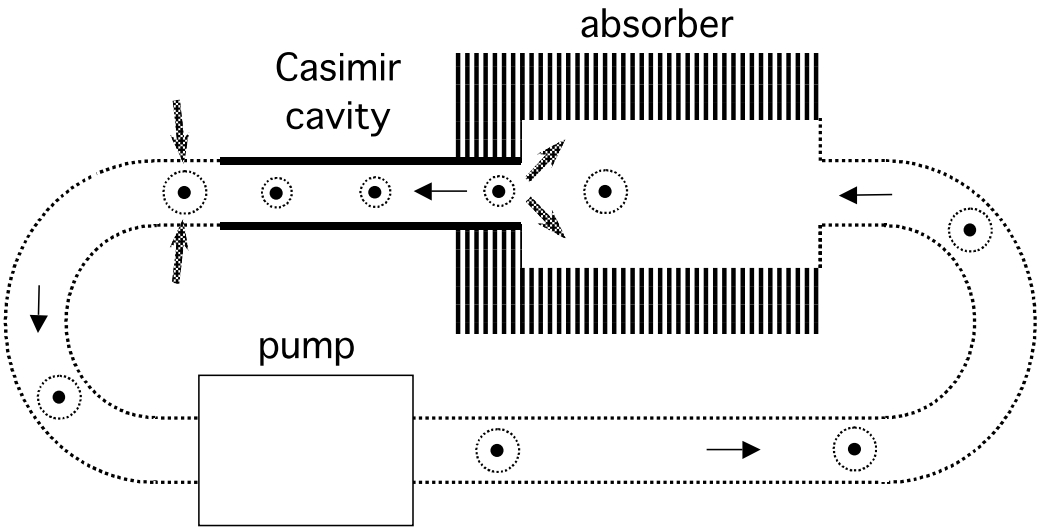

Figure I - 3 Schematic representation of the vacuum-energy extraction process. Gas circulates through the system. The electronic orbitals of the gas atoms spin down to a lower level as the gas enters the Casimir cavity, radiating the excess energy to the absorber. Upon exiting the cavity the orbitals are re-energized by the ambient zero-point field. In this way, energy is collected from the ambient zero-point field and deposited on the absorber.

To establish the feasibility of this energy-harvesting approach I carried out a series of experiments to test whether energy is, in fact, radiated from Casimir cavities when the appropriate gas flows through them.

B. Thesis outline

In Chapter II I discuss the properties of nanomaterials. I hypothesize that the positive results reported by LENR research with Pd nanomaterials is a manifestation of the strong catalytic properties of Pd heterogeneous catalysts.

In Chapter III I describe the techniques I used to fabricate Pd and Pt nanomaterials that are used later in my experimental work. I discuss the characterization techniques I used to gather information on the structure and composition of the fabricated samples.

In Chapter IV I describe the measurement methods I used throughout the experimental phase.

Chapter V is dedicated to the discussion of the heat measurements I did while pressurizing Pd-infused oxide powders with deuterium and hydrogen. In the absence of nuclear byproducts an H/D exchange chemical reaction was proposed to explain the heat production in Pd material in the presence of deuterium, but not hydrogen.

I proceed with a discussion of the H/D exchange in Chapter VI. I support the heat measurements with an extensive process characterization study.

The suggested concept of fuel, consisting of water isotopes trapped in the material that react with gas, is discussed in Chapter VII. By measuring the material weight loss as a result of a bakeout I assessed the amount of water and the reaction's energy content. I confirm that generated heat can be fully accounted for by the H/D exchange reaction.

In Chapter VIII I describe the study of measurement artifacts that can be misinterpreted as excess energy production during gas-loading experiments at elevated temperature.

In Chapter IX I apply the H/D exchange theory to electrolytic experiments to quantify the H/D exchange contribution in excess heat generation.

Conclusions and directions for future work are discussed in Chapter X.

In Appendix - A, I describe the experimental work on detection of the zero-point energy radiation as a result of the gas flowing through the Casimir cavities. The Appendix - A contains a reprint of a paper published earlier.

CHAPTER II

REVIEW OF NANO-CATALYSTS

The anomalous effects described in the previous chapter were demonstrated in nano-Pd-on-oxide materials, which are well known catalytic systems. Catalysis is a surface phenomenon, and hence an efficient catalyst must have a large surface area, implying that the active particles must be small. Small metal particles can be unstable and prone to sintering in order to reduce their surface area. Therefore, most heterogeneous catalysts consist of particles inside the pores of inert substrates such as alumina, silica, titania, magnesia, zinc oxide, zirconia, zeolite and others. Thus, Pd-impregnated alumina appears to be a suitable system to promote chemical reactions in the presence of hydrogen isotopes.

Let us look closer at the important parameters to consider for a successful catalyst:

- high activity per unit of volume,
- sufficiently long lifetime before a catalyst is considered to be "dead" or needed to be reactivated,
- cheap and reproducible synthesis.

Obviously, a high volume manufacturer will impose more strict and detailed requirements on catalyst's properties, but these three still will be valid.

Metal catalysts (the system I was dealing with) are used in the fine-chemical industry to perform hydrogenations and oxidations. The ability of a metal catalyst to dissociate hydrogen and oxygen molecules is directly related to this study and will be discussed in great detail in Chapter V.

Elements forming groups VIII and I-B of the periodic system are considered to be the most important metals for catalytic applications. I was especially interested in Pd, Pt and Ni in

conjunction with LENR research. All three of these metals have face-centered cubic crystal structure (fcc). The reactivity properties of catalytic surface depend on the number of unsaturated bonds, available for reaction. An atom of fcc (100) surface would have four neighbors missing, which makes it more active than the atom in (111) orientation. However, there are other factors that come into play during the synthesis. The morphology of the particle determined by the surface energy of the particle itself and the oxide support, on which the particle is deposited. These two factors determine the thermodynamically most stable configuration and the surface planes that the particle will expose.

Energy is needed to create a surface, because bonds need to be broken. Thus, in an ideal situation in free space, small metal particles will always want to agglomerate to minimize the surface energy. The oxide surface support is what prevents particles from clumping together.

Minimization of the surface free energy is a driving mechanism of the surface processes. For Pd and other group VIII fcc metals the smallest free surface energy is associated with (111) crystal plane. For example, the surface free energy values for Pd at different crystal face orientation are (Vitos, et al., 1998):

$$\gamma_{111} = 1.920 \text{ J m}^{-2}, \gamma_{100} = 2.326 \text{ J m}^{-2}, \gamma_{110} = 2.225 \text{ J m}^{-2}$$

However, in the presence of support, the interface energy also plays a role in metal particle formation. For example, for Pd particles on the surface of alumina the interface energy was found to be 2.8 J m^{-2} (Hansen, et al., 1999), which is higher than γ_{111}, γ_{100} , or γ_{110}. That means that Pd on alumina surface forms particles exhibiting (111) facets rather than spreading over the support, which was experimentally confirmed by the STM imaging (Hansen, et al., 1999). I observed similar results on crystal plane orientation using XRD technique (discussed in Chapter III).

CHAPTER III

PALLADIUM AND PLATINUM CATALYST FABRICATION AND CHARACTERIZATION

A. Fabrication.

Table 1 lists different catalysts that I used throughout my study. More than 20 batches were fabricated. Incipient wetness and ionic exchange methods were used to prepare samples of different concentration of Pd or Pt. I used different precursors and three different types of supports. In addition to the fabricated materials, I experimented with commercially available catalyst from Acros Organic. Samples showed some limited variation during gas loading experiments, however in regard to the phenomena investigated here, they all responded similarly.

TABLE 1. List of the catalysts.

Sample type	Precursor	Support
type 1: 5% Pd-on-alumina (commercially available)	Acros Organic CAS:7440-05-3	
type 2: 2% Pd-on-zeolite	$Pd(NH_3)_4Cl_2$	molecular sieve 13X: Sigma-Aldrich 283592
type 3: 2%, 1%, 0.5% Pd-on-alumina	$Pd(NH_3)_4Cl_2$ $Pd(ND_3)_4Cl_2$ H_2PdCl_4	80-200 mesh Al_2O_3 Fisher Scientific P/N: CAS 1344-28-1; high crystalline α-alumina: American Elements P/N AL-OX-O2-P.30UM 30-50 μ particle size
type 4: 2% Pt-on-alumina	H_2PtCl_6	80-200 mesh Al_2O_3 Fisher Scientific P/N: CAS 1344-28-1

Wet impregnation and ionic exchange methods are based on the loading of the high surface area oxide support with a catalytically active phase (precursor). The way the catalytic material is loaded into the support is a several step process that includes filling the pores of the support with liquid precursor followed by baking out the sample at elevated temperature. The chemical interactions between the solid support and the precursor may play a significant role in the quality of the resulting material (Chorkendoff & Niemantsverdriet, 2007). The precursor may be chosen based on the charge state of the hydroxyl groups on the surface of the support. For example, negatively charged $PdCl_4^{2-}$ or $PtCl_6^{2-}$ will exchange readily with basic OH groups in alumina. In the case of the zeolite the ionic-exchange takes place between the positive Pd^+ ions and the sodium ions in the zeolite cage.

For the catalyst's synthesis I mostly used 80-200 mesh Al_2O_3. The blank alumina was baked in vacuum at 350° C for 12 hours to remove residual water. Samples containing different percentages of Pd by weight were fabricated by impregnating alumina powder with hot $Pd(NH_3)_4Cl_2$ or H_2PdCl_4 in water, forming a slurry. This slurry was later dried either in air or in an argon atmosphere at room temperature without calcination. Prior to loading into the measurement apparatus, all the samples were baked in a vacuum oven at 120° C for 24 hours. This prebaking step results in 2% weight loss due to water evaporation, based on thermogravimetric analysis (TGA). Some water was still trapped in the material even after prebake. During the loading there was a 2-5 minutes period during which the samples were exposed to air, which resulted in an additional absorption of the moisture from air. I will discuss this in more details in Chapter VI and VII.

B. Nanocatalysts characterization

I carried out the material characterization to establish the basic understanding of the structure and composition of the fabricated samples. There are several standard methods for characterizing metals in the catalysts. The three most widely used are: X-ray diffraction, chemisorptions, and electron microscopy. The combination of these three techniques provides the information on the metal particles' size distribution, dispersion, phase and predominant crystal structure. Another purpose for characterizing the material was to establish a correlation between the sample's performance and structural features modification as a result of an experiment.

a) X-ray diffraction

The primary purpose of the X-ray measurement was to identify the size of the Pd metal particles in alumina powder. All measurements were carried out at the US Geological Survey (courtesy of Dr. Alex Blum). The powdered sample was wetted with alcohol and dried on the surface of a polished Si wafer, forming a film. The wafer was loaded into the X-ray apparatus and scanned at angles $15^o < 2\theta < 90^o$. Figure III - 1 shows the scan of 2% Pd by weight impregnated into highly crystalline alumina powder – type 2 sample from Table 1. The major peaks on the scan were identified as alumina and Pd of different facet formation which agrees with the study by Datye et al. (Datye, et al., 2000).

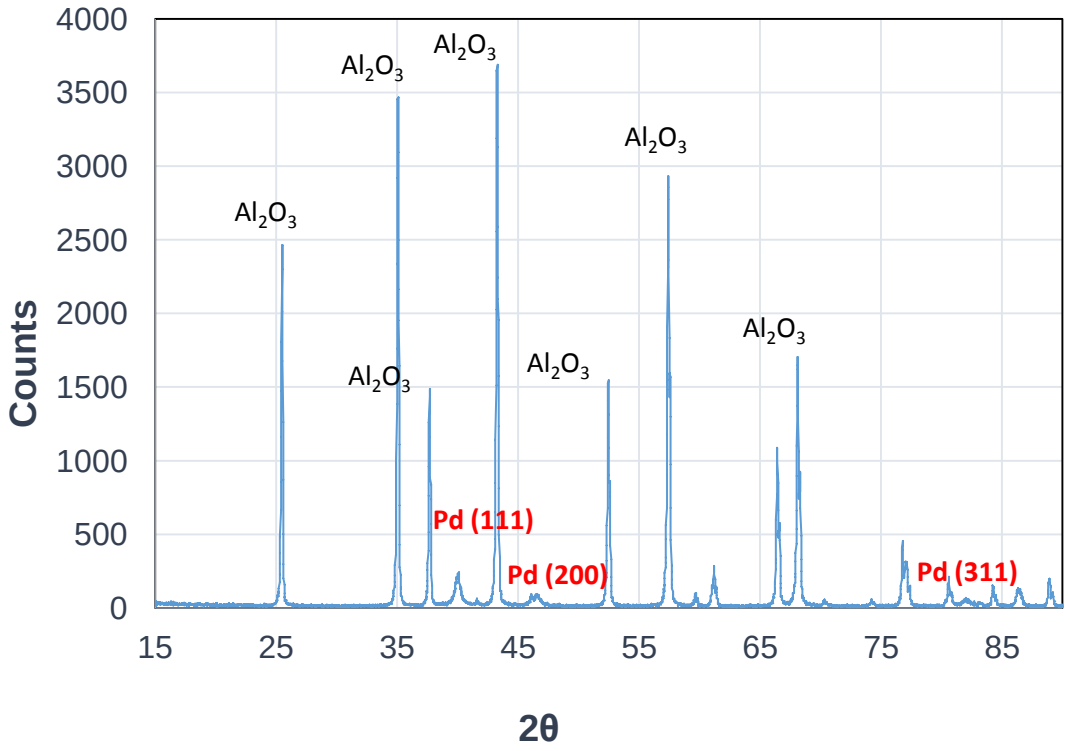

Figure III - 1 X-ray diffraction scan of 2%Pd impregnated alumina sample.

The Pd (111) particles size information can be obtained from the full width at the half maximum peak intensity using the Scherrer equation (Scherrer, 1918) (Langford & Wilson, 1978):

$$L = \frac{K\lambda}{(\Delta 2\theta)\cos\theta}$$

where L is the particle size; K is the dimensionless shape factor, which has a typical value of about 0.9, but varies with the actual shape of the crystallite; $\lambda = 1.54\text{Å}$ is the X-ray wavelength; $\Delta 2\theta$ is the line broadening at half the maximum intensity (FWHM) in radians; and θ is the Bragg angle. For Pd (111) peak the particle size was found to be 11.7 nm.

The value calculated using the Scherrer equation is usually an underestimate of the real

particle size, since it assumes negligible peak broadening from the other sources. Another ambiguity comes with the shape factor K, which is valid only if all crystallites are of the same size. A Bertaut-Warren-Averbach (BWA) analysis, which is based on Fourier analysis of X-ray diffraction peak shape, yields the crystallites thickness distribution and strain. The modified version of this method was developed by Drits et al. (Drits, et al., 1998) to measure the coherent scattering domain sizes and strains in minerals. Using this method my data was analyzed with MudMaster custom written software (Eberl, et al., 1996). The result of the particle size distribution is shown in Figure III - 2. The distribution shape seems to be trimodal (or may be even 4 modes) with peaks around 6, 13, and 26 nm. The multimodal distribution could be a result of multiple nucleation events during palladium crystallization. Indeed, the synthesis of Pd nanoparticles in alumina was a multistep process, as described earlier in the catalyst fabrication section.

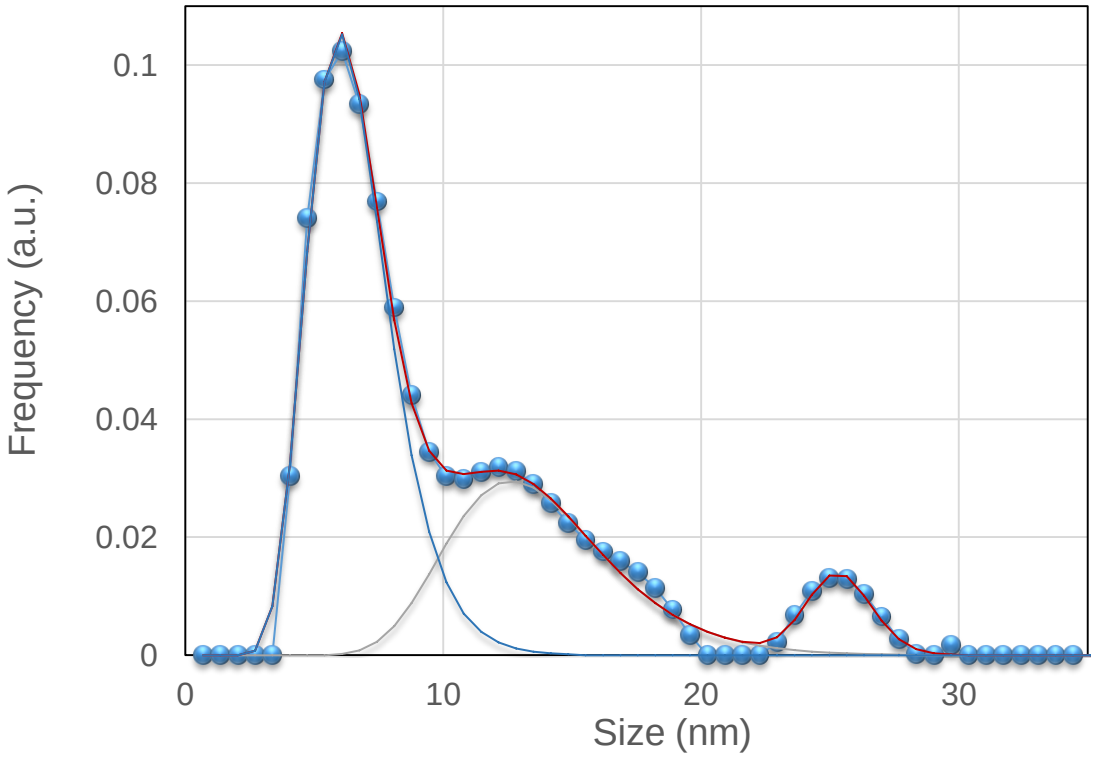

Figure III - 2 MudMaster analysis result on Pd(111) crystallite size distribution (courtesy of D. Eberl – US Geological Survey, Boulder, CO).

b) Chemisorption

I also used chemisorption (Wachs, 1992) to measure the Pd nanoparticle size and to see if it is changing as a result of my experiment. Chemisorption measures the amount of gas required to form an adsorbed monolayer on a metal surface. By knowing a total number of absorbed molecules and the amount and type of the metal, the surface area and the size of the nanoparticles can be calculated. The most common gases used for chemisorption experiments are hydrogen, oxygen, and carbon monoxide. The success of the chemisorption method depends on

knowledge of the conditions under which gases adsorb on the metal. Hydrogen dissociates on the surface of metal, and thus adsorbs atomically, forming palladium hydride with stoichiometry ratio of one (adsorption stoichiometry is the number of the gas atoms bonded to one Pd atom). The accuracy of the CO chemisorption measurements is often disputed due to the unknown adsorption stoichiometry. CO on the surface of Pd can be linearly or bridge-bonded.

The chemisorption measurement requires a metal surface to be free of contamination. Prior to the measurements my material was baked in-situ at 250°C and 390°C for 2 hours in the presence of hydrogen. After that the gas was evacuated and the temperature reduced to 40°C.

The static volumetric chemisorption method was used to measure the particle size and dispersion. The measurements were done at Prof. J. Falconer's Research facility at the Chemistry and Biological Engineering department at University of Colorado, Boulder (courtesy of Dr. Hans Funke). In the static volumetric method the pressure of a known gas is measured; then the gas is expanded into an evacuated known volume that contains a catalyst, and the pressure is measured again. The step is repeated several times for different pressures (in my case up to atmospheric pressure). The measured uptakes describe a dependency of the adsorbed volume vs. equilibrium pressure, known as an isotherm curve. Two different mechanisms contribute to the adsorption in the material. One is a chemisorptions, which is a strong bonding between gas molecules and active sites on the surface of the metallic particle (pressure increase should not affect the amount of the chemisorbed gas molecules); the second mechanism is a weak physiosorption, when gas is adsorbed on the surface of the substrate (generally this additional physisorption increases linearly as a function of gas pressure). I was interested in the amount of the chemisorbed gas, which can be extracted from the isotherm data by the extrapolation or bracketing methods (Quantachrome Instruments, 2007). Both methods evaluate the contribution of the chemi- and physiosorption to

the total adsorption on the surface of the Pd nanoparticles and alumina substrate. Using both methods would insure the accuracy of the characterization technique. This is if both methods were to give similar answers, but in the case of hydrogen adsorption, the bracketing method was giving consistently larger particle size values compared to extrapolation. This was due to the nature of the process of the PdH formation: at the temperatures and pressures used in the chemisorption experiment H_2 gets absorbed not only on the surface but also in the bulk of the Pd metal. That is why the surface area was greatly overestimated using the extrapolation method and the results were also skewed using the bracketing method. The solution was to switch to CO gas exposures. I used two as an adsorption stoichiometry for CO (Canton, et al., 2002). The results were again rather scattered: the particle size was between 6.8 and 11.4 nm and the dispersion between 9.8 and 16.5%.

To monitor the evolution of the particle size as a result of the multiple experimental runs, two samples were compared. One sample was fresh, and another one was exposed to more than 40 experimental cycles (see Chapter V for detailed explanation on the experimental procedure). I expected that the Pd particle size would increase due to the particles' agglomeration as a result of my experiments. The chemisorption measurements confirmed my hypothesis: the particles grew from 5.7 nm to 11.5 nm (the quantitative analysis may be off due to the issues described earlier, but the qualitative trend was confirmed).

c) Transmission electron microscopy (TEM)

TEM measurements were done to confirm the size of the Pd nanoparticles. TEM imaging was done in the Molecular, Cellular, and Development Biology center at University of Colorado, Boulder (courtesy of Troy Gould). Figure III - 3 (a) shows one of the several images of the 2%

Pd-impregnated alumina samples. ImageJ software was used to measure the diameter of the particles from the images. The particle size distribution is shown in Figure III - 3 (b).

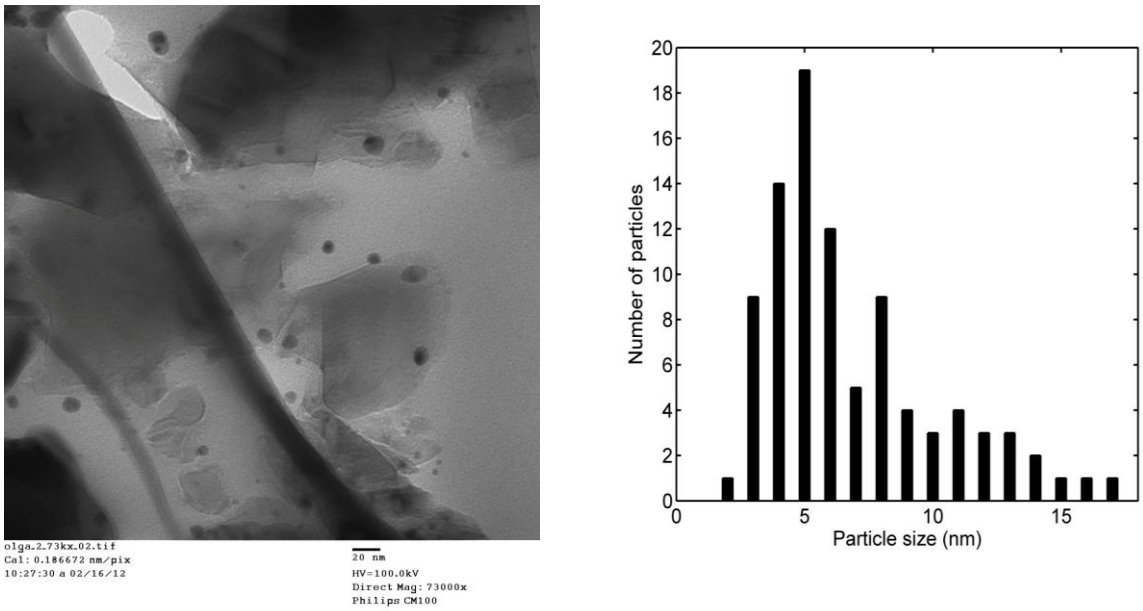

(a) (b)

Figure III - 3 2% Pd-impregnated high crystalline alumina (a) TEM image shows the Pd nanoparticles as the dark spots on the lighter alumina surface, (b) Pd particle size distribution based on the measurements done from the TEM images.

The distribution shape suggests several nucleation modes, similar to XRD. Based on the TEM, the peaks of the multimodal distribution are around 5.5, 8.5, and 11.5 nm. The main peak is around 5.5 nm. The TEM analysis has confirmed that my fabrication method results in the Pd nanoparticle formation on the surface of the oxide support with mean particle size in the order of 5-6 nm.

Chapter III conclusions

Material characterization was done using XRD, chemisorption and TEM imaging to establish a basic understanding of the catalyst's structural features. I have confirmed that the fabrication method described in Chapter II was capable of producing Pd nanoparticles incorporated into alumina powder. Based on TEM analysis, the mean size of the metal nanoparticles was 5-6 nm. Chemisorption analysis showed agglomeration of nanoparticles as a result of multiple H_2/D_2 exposures. The significance of the last statement will be discussed in Chapter VII.

CHAPTER IV

MEASUREMENT METHODS

In the absence of a unified LENR theory, the question of possible reaction products is still unanswered. A variety of measurement techniques were used to detect radiation or transmutation products (Storms, 2007), but what seems to unite all LENR experiments is the excess heat generation events. This fact explains why the majority of the experimental LENR work relies heavily on calorimetric measurements.

A. Introduction to calorimetry

Calorimetry is defined as the measurement of heat (Hemminger & Hohne, 1984) and is associated with a heat flux. By measuring heat exchange between two systems we can quantitatively assess the amount of energy (chemical, nuclear, electric) generated or absorbed inside the calorimeter. In the case of the gas-loading experiments the amount of released heat is usually small compared to the rather large applied power, which makes precise calorimetry very important.

The two systems involved in heat exchange are the measuring system, and its surroundings. The heat flux between the measuring system and its surroundings is mediated by thermal resistance.

Three operational modes of calorimeters are available:

- isothermal,
- adiabatic,
- isoperibol.

Each of these operational modes is described by three parameters:

- temperature of the surroundings,

- temperature of the measuring system,
- thermal resistance between the measuring system and the surroundings.

I worked in isoperibol operational mode, which is described by a constant temperature of the surroundings, with a possibly different temperature of the measuring system, and a finite non-zero thermal resistance between two. To satisfy the requirements of the constant surroundings' temperature I used an isothermal oven capable of maintaining the stable temperature baseline within 0.01˚C. The oven contained a measuring system made up of a stainless steel vessel filled with reactive material. This set-up is described in more detail in the next section.

B. Experimental apparatus

I used two apparatuses for my gas-loading experiments, and two different types of the sample holders (vessels). The gas-loading experiments in one apparatus were completed in a range of temperatures from 40˚C to 390˚C, while the experiments completed in the other apparatus were done at 40˚C. Figure IV - 1 shows the block diagram of the experimental set-up.

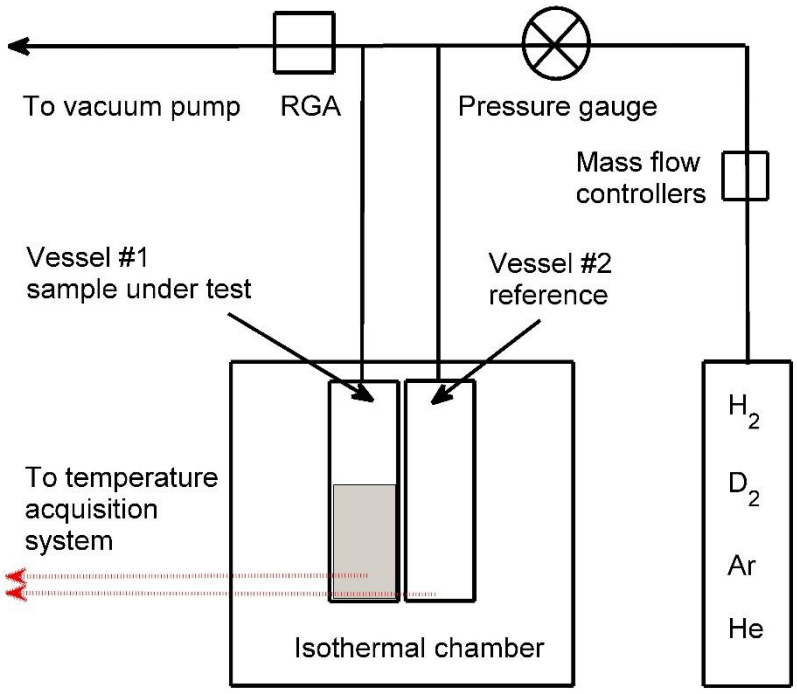

Figure IV - 1 Gas-loading system for excess heat measurements.

The main components of my gas-loading apparatus were:

- An isothermal chamber (an HP 5890A gas chromatograph oven) to provide constant temperature surroundings with a temperature baseline stable within 0.01˚C. The temperature uniformity across the oven was achieved by constant air flow produced by a heater and a fan on the back panel of the oven. The temperature of the oven could be set anywhere between 40˚C and 400˚C.
- Stainless steel vessels to hold the material in the isothermal oven (Figure IV - 2). Temperature changes due to reactions in the material were registered by either thermistors connected to the surface of the vessel (Sensor Scientific Inc. glass probe

10 kΩ thermistors p/n: SP43A10310), or with resistance temperature devices (Omega RTD-NPT-72-E-MTP-HT) screwed into the bottom of the vessels. Figure IV - 2 shows the inside of the isothermal chamber where the vessels were attached to the gas line. Temperature changes that exceeded the oven's background temperature fluctuations were associated with exothermic or endothermic heat generated in the system.

- A gas line to connect the vessels to the gas-supply cylinders. Four different gases were supplied to the vessels. H_2 and D_2 were supplied through an oxygen-removing hydrogen purifier. The D_2 gas was 99.9% pure and the H_2 gas was 99.99% pure. Ar and He were supplied directly through the gas lines bypassing the purifier. The system could be pressurized up to $2.7x10^5$ Pa (2000 torr). Evacuation of the system was done using a turbo-molecular pump down to the 10^{-5} Pa (10^{-7} torr) level. With the valve to the pump closed, the stainless steel vacuum system would outgas to the 10^{-4} Pa (10^{-6} torr) level. There was a section of the pipeline connected to the vessels that was shared by the gases. However, the pressure of the gas in the pipeline during the pressurization step was nine orders of magnitude higher than while evacuated, which made the residual gas contribution negligible.
- Mass flow controllers to control gas flow, pressure gauges, and a residual gas analyzer (SRC RGA200) to collect the data on byproducts of the reaction were also used.

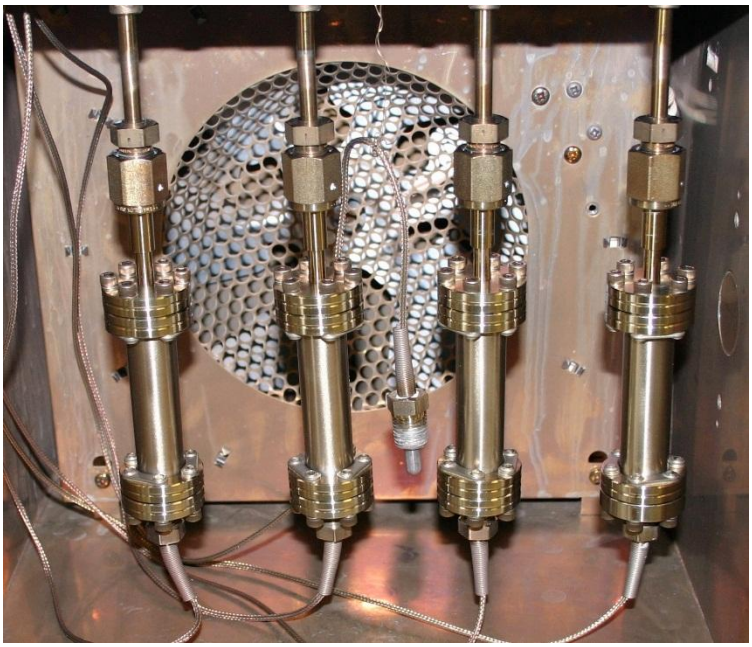

(a)

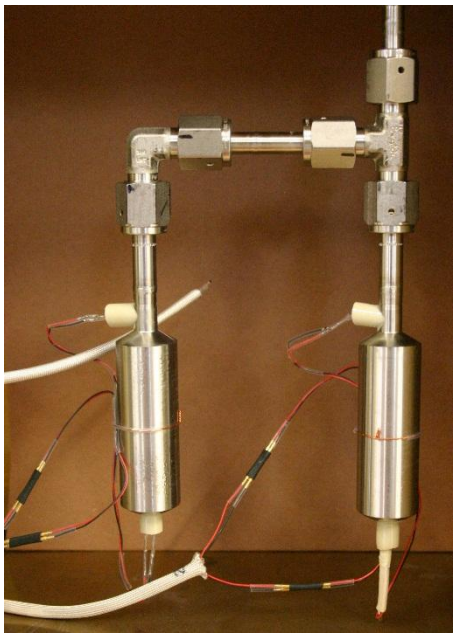

(b)

Figure IV - 2 Vessels containing material inside the isothermal chambers: (a) the high temperature set-up for experiments run up to 390˚C; (b) the low temperature set-up for experiments run at 40˚C. The temperature uniformity across the oven is achieved by constant air flow produced by a heater and a fan that can be seen at the back panel of the oven.

A typical run consisted of (1) pressurization by a gas of choice, (2) a period of time when the vacuum system remained under pressure, and (3) an evacuation step. Heat production or consumption, as a result of the reaction with the gas, was determined from temperature changes in the vessel, whose transient temperature can deviate from the constant oven temperature baseline. Net positive temperature change as measured by the temperature sensors was considered as heating, and negative change as cooling.

System control, temperature and pressure data acquisition were carried out with LabView software.

C. Calibration (isoperibol calorimetry)

Heat released or consumed by the vacuum system during the gas-load/unload cycles resulted in temperature changes for the vessel containing the sample. These temperature changes (T[t]) were measured by the temperature sensors. Since the gas-loading apparatus was not a direct calorimetric set-up, additional calibration and data manipulation was done to convert the temperature change into power. The excess power generated by the vacuum system is described by the calorimetric equation:

$$P = C_p M \frac{dT}{dt} + k_C \Delta T$$

where $C_p M$ is the equivalent heat capacity of the system, k_C is the heat transfer coefficient, and ΔT is the temperature change (Miles & Fleischmann, 2009). The $C_p M$ and k_C are parameters of the specific set-up and experimental protocol. Once determined for a given configuration, they can be used for subsequent runs on the same system.

The vessel, filled with blank alumina powder, was pressurized with hydrogen. In this case the only heat source was the heat dissipated from the gas compression. The resulting temperature change was plotted over time and shown in Figure IV - 3.

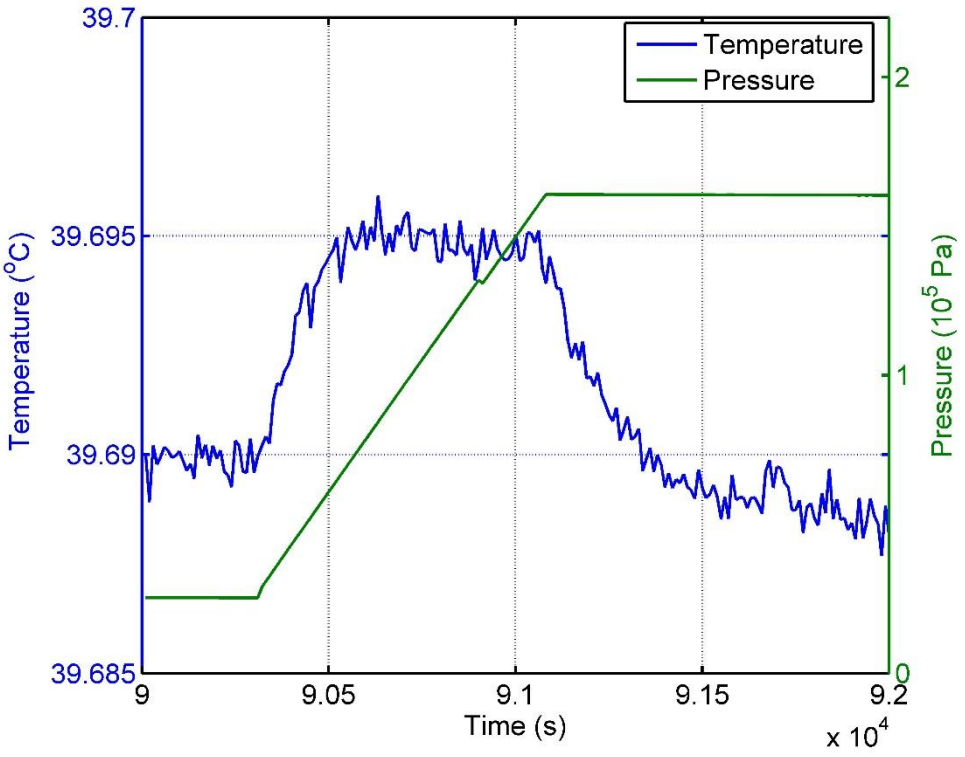

Figure IV - 3 Experimental curve for the low-temperature system set-up: (a) the temperature change due to pressurization of the system up to 1200 torr.

Using the known vessel parameters (volume and pressure) I linked the measured temperature change to the heat of the compression, which was 2.3 J. During pressurization some of the heat dissipated due to conduction. That data allowed me to calculate the heat transfer coefficient (k_c).

When pressurization was complete, it took a certain amount of time for the vessel to come back to thermal equilibrium with its surroundings (this is reflected in the cooling down portion of the temperature plot in Figure IV - 3). The cooling down process was governed by heat conduction and equivalent thermal mass (C_pM) constants, and can be written as:

$$C_p M \frac{dT}{dt} = -k_c \Delta T$$

This differential equation can be rearranged to

$$\frac{dT}{\Delta T} = -\frac{k_c}{C_p M} dt,$$

and when integrated becomes

$$\ln(T - T_{baseline}) = -\frac{k_c}{C_p M} t.$$

The equation is in the form $y = \alpha x$ and is shown in Figure IV - 4. To reduce the noise associated with the measurements I did 5th order fit of the cooling down portion of the curve from Figure IV - 3 before proceeding with C_pM calculations.

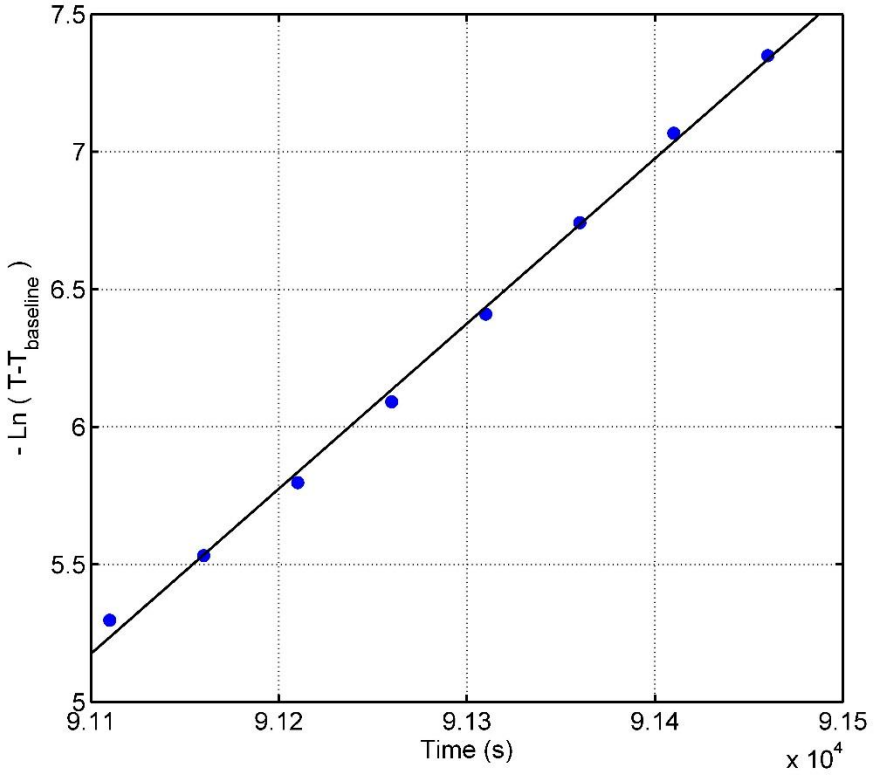

Figure IV - 4 The cooling portion of the curve from Figure IV - 3 plotted as a natural logarithm of the temperature change over time: a linear fit determines the slope of a temperature decay.

The value of C_pM was derived based on the temperature decay slope, $a = -(k_c/C_pM)t$, where k_c was calculated earlier. $T_{baseline}$ is the temperature of the vessel before the pressurization started. For the system that was equipped with vessels for the low temperature (40˚C) measurements, the calculated parameters were: $k_C = 0.63$ W K^{-1} and $C_pM = 103.2$ J K^{-1}. For the high-temperature measurement apparatus the coefficients were: $k_C = 0.79$ W K^{-1} and $C_pM = 79.1$ J K^{-1}.

D. Evaluation of the measurement error bars

Excess heat was calculated for each run by summing up heat released during pressurization step and heat consumed during evacuation which follows the chemical notion where exothermic heat is a negative value, while endothermic heat is positive. The temperature change over time T(t) was converted into power change over time P(t) using the calibration coefficients calculated in the previous section. By integrating P(t) signal over time, I evaluated the amount of heat produced/consumed by the system. Integration was done over fixed time intervals: 4000 s during pressurization and 5000 s during evacuation. Second time interval was longer since desorption of the hydrogen isotopes is slower process compare to almost instantaneous absorption.

Variation within the integration was calculated as a root mean square (RMS) of heat of desorption values from 20 different runs and was found to be 2.2 J.

The systematic error was accounted for when calibration constants $\boldsymbol{k_c}$ and $\boldsymbol{C_pM}$ were derived. Thus, the system is considered to be free of the systematic error.

E. Radiometry and alpha particles measurements

According to some LENR theories, alpha particle generation and energy release are the result of conventional deuteron fusion:

$$D + D \rightarrow {}^{4}He + \gamma$$

To test these theories, I measured radiation levels and alpha particle emission during gas pressurization cycles to trace possible nuclear products. Following the isotope effect assumptions, the nuclear products should have been released during the exposure of the material to deuterium gas, and not during exposure to hydrogen.

a) X-ray measurements

Using a Geiger counter (Ludlum Measurements model 2241, LND tube model 07-27) I tested 2%Pd-impregnated alumina in the presence of H_2 and D_2 gases to detect a radiation signal.

The stainless steel vessel had a machined opening (see Figure IV - 5 [a]) through which the Geiger tube was inserted. The tube's window was coplanar with the vessel's inner wall and the detector was permanently secured to the stainless steel vessel with two-part epoxy (see Figure IV - 5 [b]). The vessel contained 6 g of 2%Pd-impregnated material.

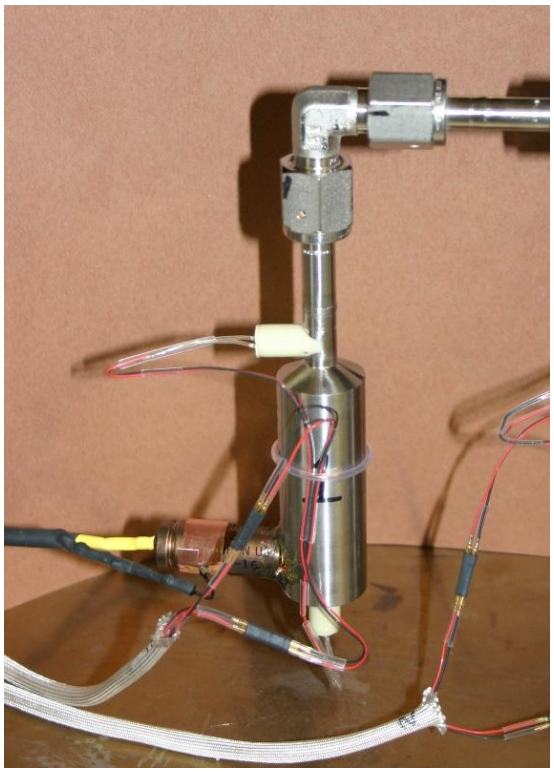

(a) (b)

Figure IV - 5 (a) The stainless steel vessel and the Geiger detector; (b) the stainless steel vessel with the Geiger detector inside the oven and ready for testing.

The Geiger detector registered an increase in counts at about $2x10^4$ Pa (150 torr) during the initial pump down. The system was then pressurized with hydrogen and deuterium four times and pressurizations were done up to atmospheric pressure. The system was evacuated down to 10^{-5} Pa between the runs. Radiation bursts were always observed during the evacuation step for all four deuterium and hydrogen runs at about $2x10^4$ Pa pressure. Similar results were observed from the runs with an empty vessel (no material): the counts increase was observed only during the evacuation step at the $2x10^4$ Pa pressure. There was no increase registered during the pressurization step, when the gas was flowing into the system. Figure IV - 6 shows the radiation counts and the pressure change inside the vessel holding 6 g of material. An explanation for this

observed effect could be a leaking Geiger tube, with gas that was ionized when pressure dropped to the certain point. The question on why the same effect was not observed when the pressure was rising during the pressurization remains unanswered.

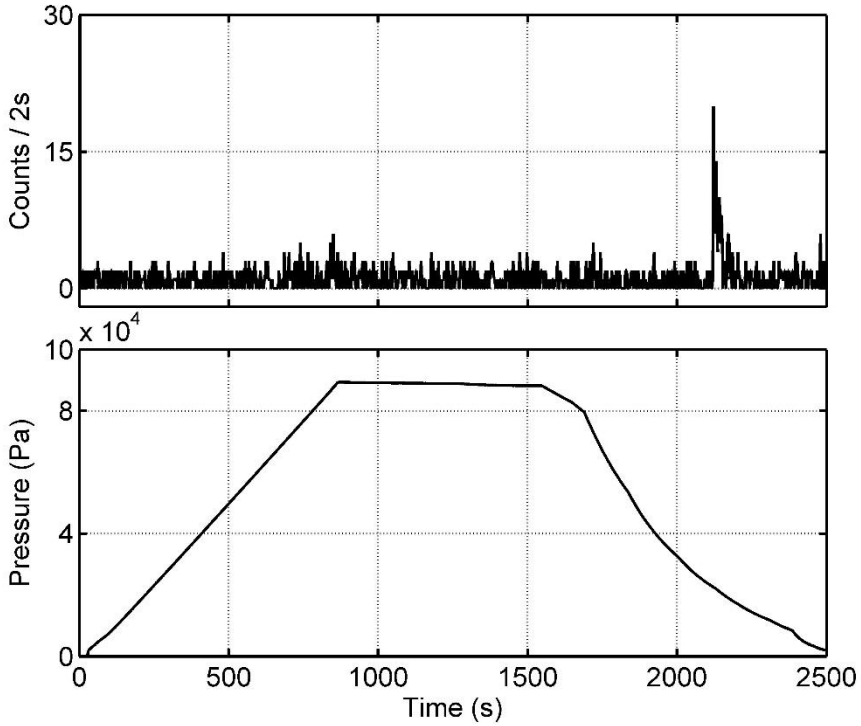

Figure IV - 6 The radiation counts and deuterium pressure changes inside the vessel. The radiation spike was observed at $2x10^4$ Pa during the evacuation step.

b) Alpha particles detection

To measure alpha particle emission I used a Quad alpha spectrometer, Model 7404, from CANBERRA. Figure IV - 7 shows a view of (a) the spectrometer and (b) a sample holder against the detector.

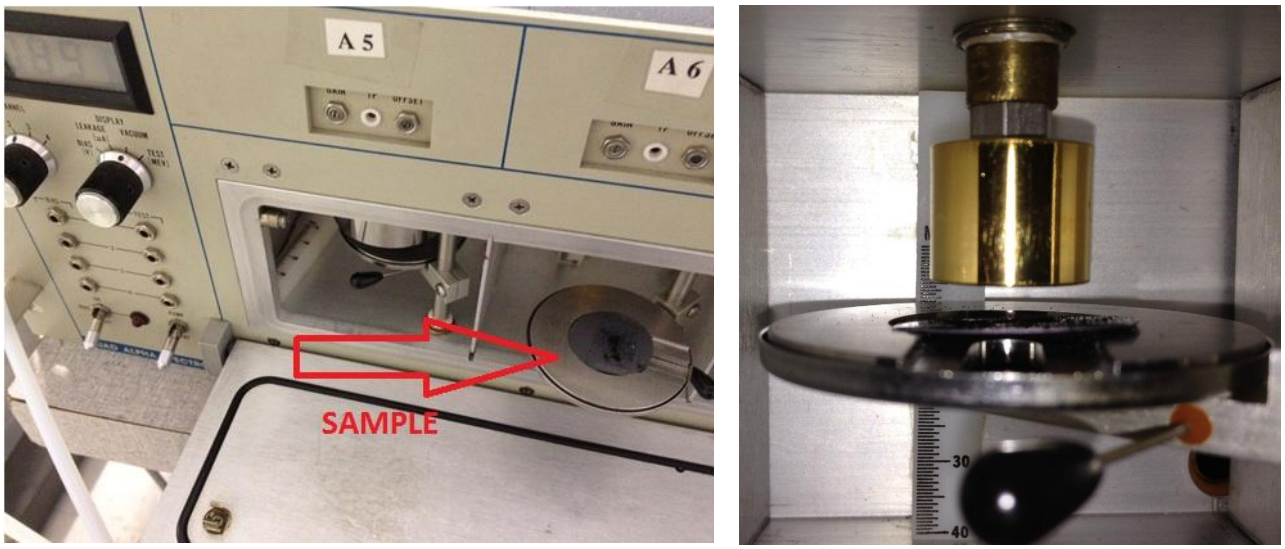

(a) (b)

Figure IV - 7 (a) The alpha spectrometer; (b) a sample holder with powdered sample against the detector.

The 2%Pd-impregnated powder sample was evenly distributed over the one-inch Si wafer and installed inside the spectrometer. Since heavy alpha-particles attenuate over a short distance the sample had to be positioned in close proximity to the detector. To calculate the attenuation of the alpha particles of different energy in the hydrogen atmosphere at a working pressure of 2.7×10^4 Pa (200 torr) I used Bethe-Bloch formula (Bloch, 1933), which gives the rate of energy of heavy charged particles in a gas. The range of the particles is approximately proportional to $E^{1.73}$ and inversely proportional to the density of the gas (Andrews, 2008). At a given pressure and room temperature the density of hydrogen is 11×10^{-3} kg/m^3. Thus, the theoretical range of particles at 25˚C and 2.7×10^4 Pa is $R = 21.1E^{1.73}$ with the energy measured in MeV and the range measured in centimeters. Graphical representation is given in Figure IV - 8. Based on the data from Figure IV - 8 the attenuation range is more than 100 cm for 3 MeV particles. In my

experiment the distance between the sample and the detector was 4 mm, which was short enough to neglect the energy attenuation in the gas.

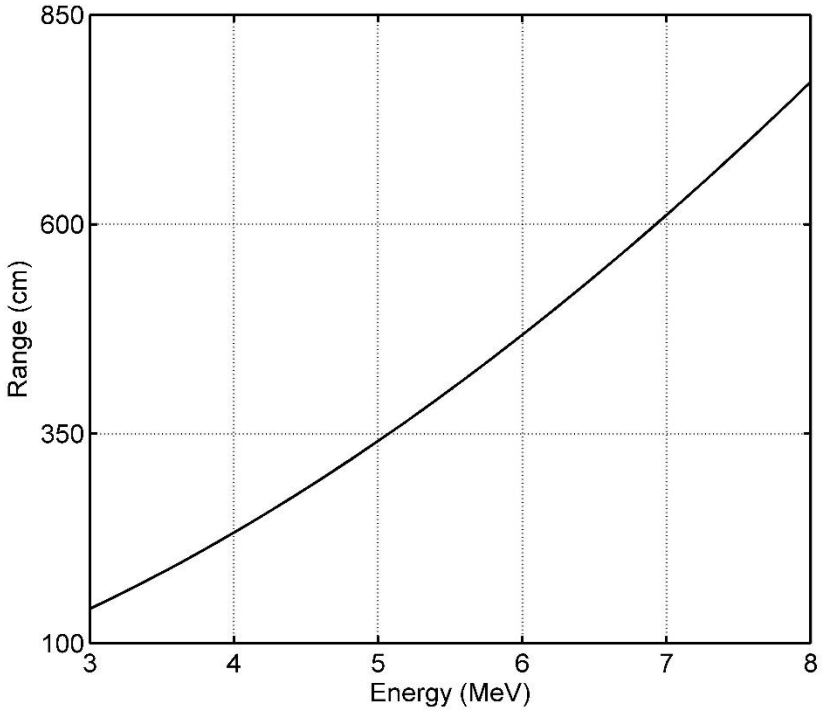

Figure IV - 8 The range of alpha particles in hydrogen at 2.7×10^4 Pa and 25˚C, represented in terms of their initial energy.

Deuterium and hydrogen gas were supplied to the system. The high-energy-resolution reverse-biased silicon detector was capable of registering alpha particles in the 3 to 8 MeV energy range with 11 keV FWHM resolution. The apparatus was calibrated in air with a Po-210 test source that emitted alpha-particles at 5.3 MeV. The 2%Pd-impregnated alumina sample was then pressurized with deuterium and hydrogen while the spectrometer was running. Figure IV - 9 shows the results from the deuterium and hydrogen runs superimposed over the calibration Po-210 curve. While Po-210 showed a distinctive peak at 5.3 MeV, no alpha particles emission traces from the gas runs were seen in the 3 to 8 MeV range.

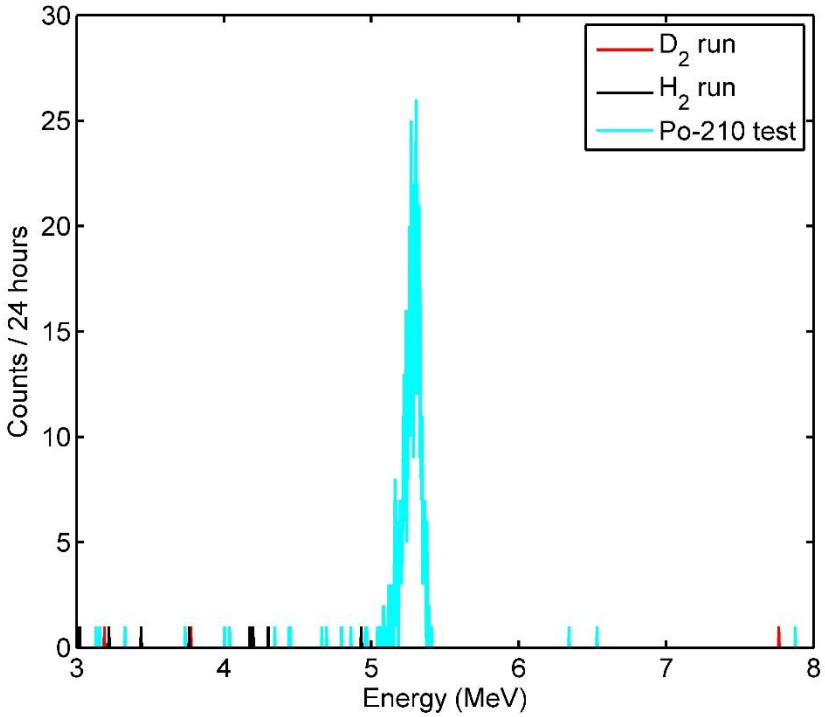

Figure IV - 9 The alpha-particles emission spectra from deuterium and hydrogen exposures of 2%Pd-impregnated alumina sample, and from the Po-210 source in air.

Chapter IV conclusions

In the absence of detectable nuclear reaction products, heat measurements were chosen as a main technique to study the phenomenon. I operated my gas-loading system as an isoperibol calorimeter. The necessary calibration was done to convert temperature changes into power.

CHAPTER V

RESULTS: HEAT MEASUREMENTS

A. Excess heat generation and isotope effect

I started my experimental work by confirming the excess heat production in Pd-impregnated materials in the presence of deuterium. Using the set-up described in Chapter IV, I pressurized the material with either deuterium or hydrogen, while measuring the temperature change (Dmitriyeva, et al., 2012, Mechanisms for heat generation during deuterium and hydrogen loading of palladium nanostructures).

The typical pressurization cycle consisted of 3 steps: (1) pressurization with hydrogen or deuterium, (2) the period of time while the system was under pressure and (3) an evacuation step. A conclusion on excess heat generation was made by comparing the amount of heat generated during the pressurization step to the amount of heat consumed during the evacuation step. The assumption was that any reversible heat released upon pressurization (heat of pressurization, heat of absorption/adsorption of hydrogen isotopes in material) would be compensated for upon evacuation. Any irreversible heat would result in a net energy excess/deficit, which I was interested in examining.

Initially, the system was checked with alumina and zeolite powders, without any Pd added. In the presence of hydrogen and deuterium I found that the exothermic heat due to the work of pressurization (*pV- work*) and the endothermic heat (recovery of *pV-work*) during evacuation equally balanced one another, and no excess heat was produced.

Figure V - 1 shows a typical run done with the 2% Pd-impregnated alumina powder in the presence of deuterium gas. A two-slope pressurization was needed to separate the process of

PdD formation (heat of loading $Q_{loading}$) from the heat of pressurization (*pV-work*). The first slope corresponds to a 0.5 sccm gas input flow, and the second slope to a 10 sccm input.

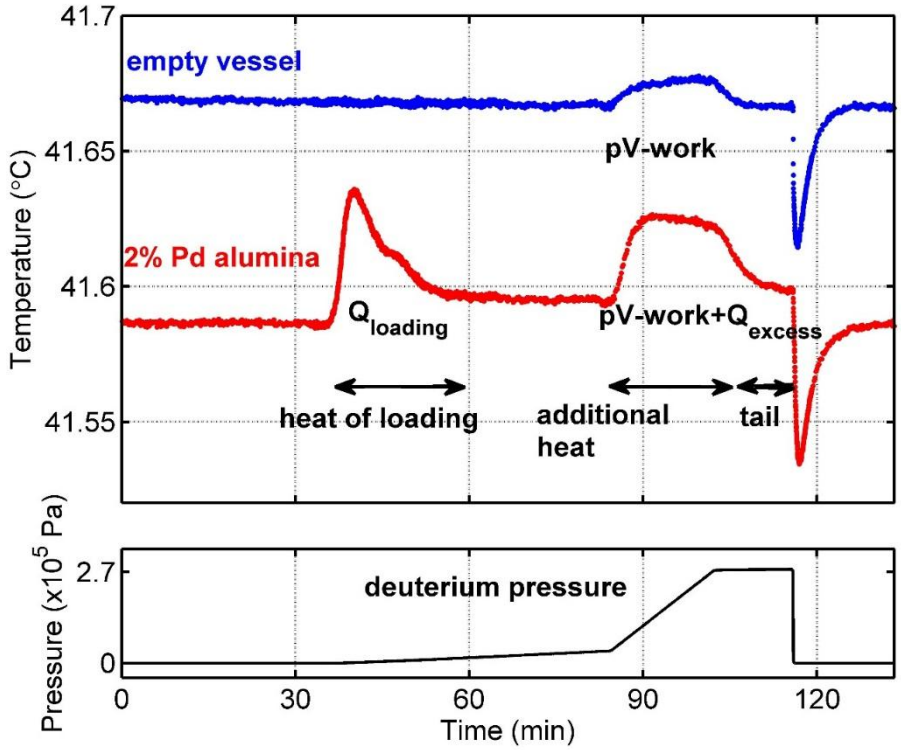

Figure V - 1 Pressure and temperature change in the system.

By looking at the area under the temperature curve that corresponds to the energy released or absorbed by the sample as a result of deuterium loading, it appears that there was excess heat generated by the material. The differences in the temperature signal between the vessel loaded with material and the reference (empty) are summarized in Table 2.

TABLE 2. Exothermic and endothermic heat generated during deuterium pressurization.

Pressurization step	**Reference (empty) vessel**	**Material loaded vessel**
Slow 0-80 min	The temperature of the empty vessel does not change because the heat of pressurization dissipates faster than it is generated.	Heat of loading we call $Q_{loading}$
Fast 80-100 min	*pV-work*	*pV-work* and extra heat we call Q_{excess}
Constant pressure 100-115 min	No temperature change	Excess heat, in the "tail". Excess heat associated with the tail typically disappears after 3-4 cycles.
Depressurization	Endothermic heat due to recovery of *pV-work*	Endothermic heat due to recovery of *pV-work* and $Q_{loading}$

Based on the data from the Table 2 we can write the following equation for the exothermic and endothermic portions of heat generated in the material:

$$Exothermic\ Heat = Q_{loading} + (pV\ work) + Q_{excess}$$

$$Endothermic\ Heat = -Q_{loading} - (pV\ work)$$

As for excess heat produced during the fast pressurization step we can say that the power generated is proportional to the slope of pressurization times a quantity Φ (the energy content of the "fuel"), which is shown as:

$$Q_{excess} / time \propto \Phi \cdot \frac{dp}{dt}$$

The fuel in the material can be exhausted or replenished (discussed further in Chapter VI). Along with nanoparticle agglomeration, this lead to a decrease in excess heat production over an increased number of runs.

As mentioned above, the energy release, which was observed during the deuterium loading of Pd-impregnated material but not during hydrogen loading, is called an isotope effect. The isotope effect has been attributed to the nuclear nature of the excess heat generation due to deuteron-deuteron fusion inside the Pd lattice (Arata & Zhang, 2008). I ran an experiment with one of two identical samples subjected to hydrogen and the other to deuterium using the same two-step pressurization technique. The results are shown in Figure V - 2.

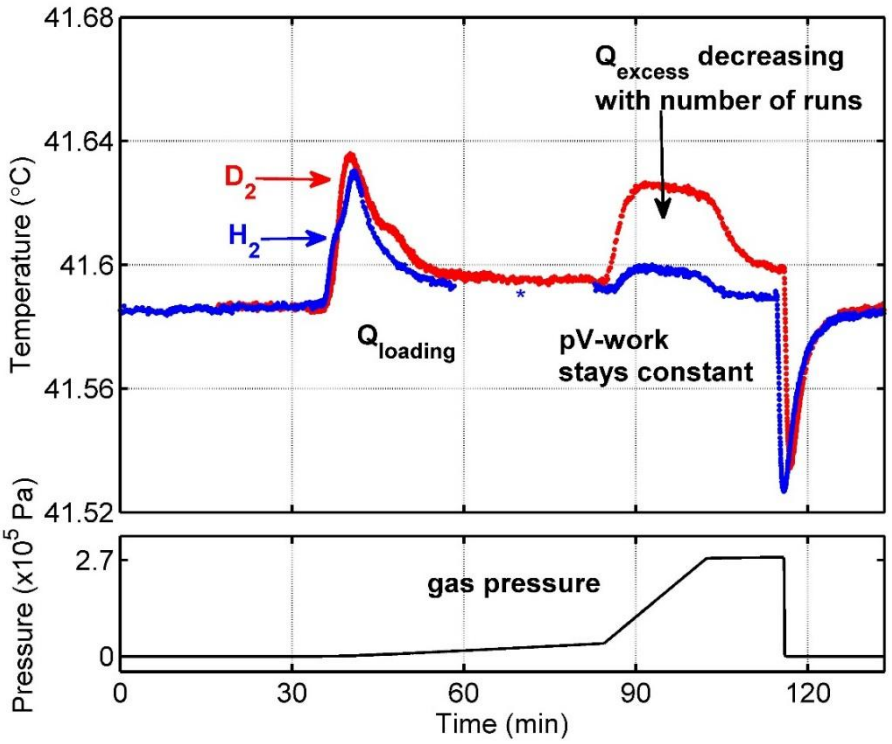

Figure V - 2 Pressure and temperature change in the system for deuterium and hydrogen pressurization. The time scale for the hydrogen run was split at the asterisk (*) in order to align the slow and fast pressurization intervals with corresponding intervals from the deuterium run.

Heat from the PdD and PdH formation ($Q_{loading}$) were similar. Endothermic heat, which consisted of $-Q_{loading} - (pV\,work)$, was the same for both materials. However, there was an isotope effect: extra heat was generated during the fast pressurization step with deuterium gas.

B. Chemical reaction hypothesis

In the absence of nuclear reaction products the question on the nature of the isotope effect and excess heat production remained unanswered. I decided to look for a conventional chemical process that could produce similar results. Because catalytic materials are known to promote chemical reactions I assumed: (1) metallic nanoparticles (Pd, Pt) dissociate hydrogen isotopes

molecules to form metal hydride and (2) initiate a spillover when deuterium and hydrogen atoms are transferred from the metal to the oxide support, and (3) the remaining water that is trapped in the material along with the OH groups on the face of the alumina act as a fuel to support a hydrogen/deuterium (H/D) exchange reaction. The H/D exchange reaction is an exothermic reaction in which deuterium substitutes for a hydrogen atom in a chemical compound. An explanation of an anomalous heating and isotope effect using the concept of H/D exchange was first proposed by D. Kidwell and colleagues (Kidwell, et al., 2009). Figure V - 3 shows the schematic representation of the H/D exchange process.

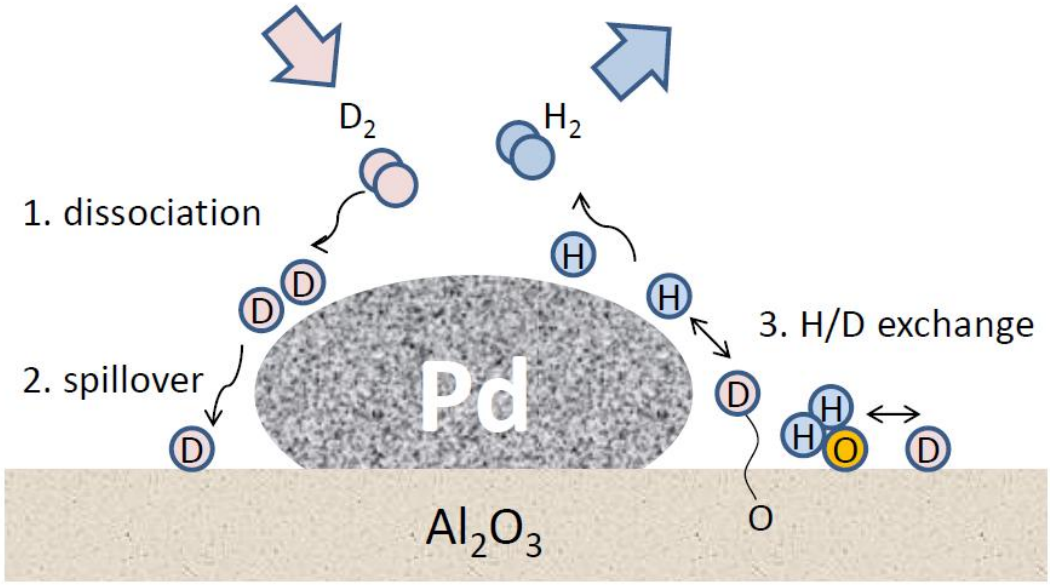

Figure V - 3 Schematic representation of the H/D exchange process: (1) deuterium is dissociated on the surface of a Pd nanoparticle forming PdD, (2) deuterium migrates to the oxide support surface where it (3) substitutes for hydrogen in water or hydroxyl group, releases hydrogen wich then recombines on the surface of palladium before leaving the system during the evacuation step.

Now let's look closer at steps (1) and (2), focusing on the dissociation, adsorption and spillover mechanisms in heterogeneous catalysts. I will focus specifically on Pd-impregnated alumina, but the same mechanisms can also be applied to a Pt-on-oxide catalyst.

1) The process of PdH (or PdD) formation is energetically preferable (the free Gibbs energy change is negative: $\Delta G < 0$), thus, the hydrogen (deuterium) molecule will dissociate on the surface of Pd nanoparticle to form a layer of PdH (or PdD), which is an exothermic reaction. I refer to this heat as $Q_{loading}$. If I assume the gas-loading ratio of Pd and D/H to be 0.86 as described in the study done by Sakamoto et al. (Sakamoto, et al., 1996), then the energy released due to the PdD formation process is -15.7 kJ/mol, and the energy released due to the PdH formation is -18.4 kJ/mol. The potential energy diagram is shown in Figure V - 4.

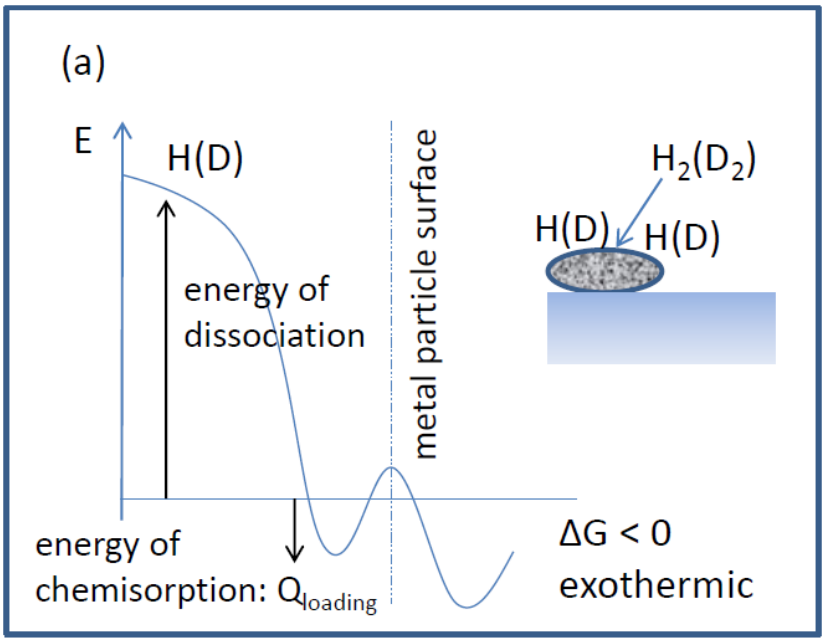

Figure V - 4 Potential energy diagram of hydrogen isotopes dissociation and PdH (or PdD) formation. H(D) in this notation means "either hydrogen or deuterium".

2) The adsorbed hydrogen (deuterium) species can then move across the surface to interface with the alumina – a process called spillover. Spillover involves active species formed in one phase (activator) migrating to the surface of another phase (acceptor) that does not absorb otherwise (Conner & Falconer, 1995). In my case the activator is a metallic (Pd, Pt) nanoparticle on the surface of the acceptor, which is the alumina support. Movement across the surfaces can take place by forming equivalent bonds between the adsorbed species and the surface, and allowing the adsorbed species to reach the interface between the activating and accepting surface. Hydrogen (deuterium) is chemisorbed on a Pd surface, and physiosorbed on alumina. Since hydrogen (deuterium) species are bonded to the metal surface more strongly than to the alumina surface, the process of breaking one bond and creating another one with the accepting surface requires energy input and may make the process slightly endothermic ($\Delta G > 0$). The potential energy diagram is shown in Figure V - 5. Diffusion across the accepting surface is expected to be a process with low-activation energy (Conner & Falconer, 1995). The potential energy diagram shown in Figure V - 6 displays hydrogen isotopes moving across the oxide support surface later engaged in a H/D exchange chemical reaction.

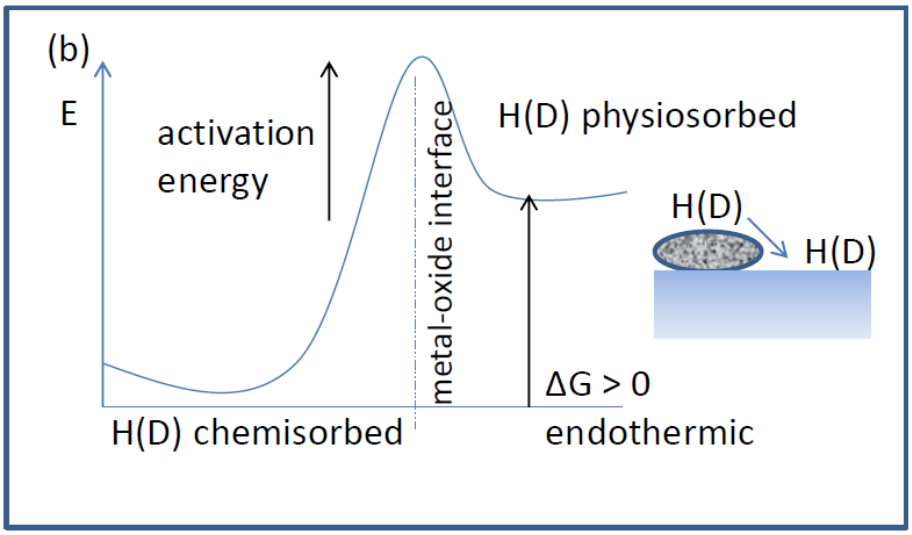

Figure V - 5 Potential energy diagram of hydrogen isotope spillover from metal to alumina.

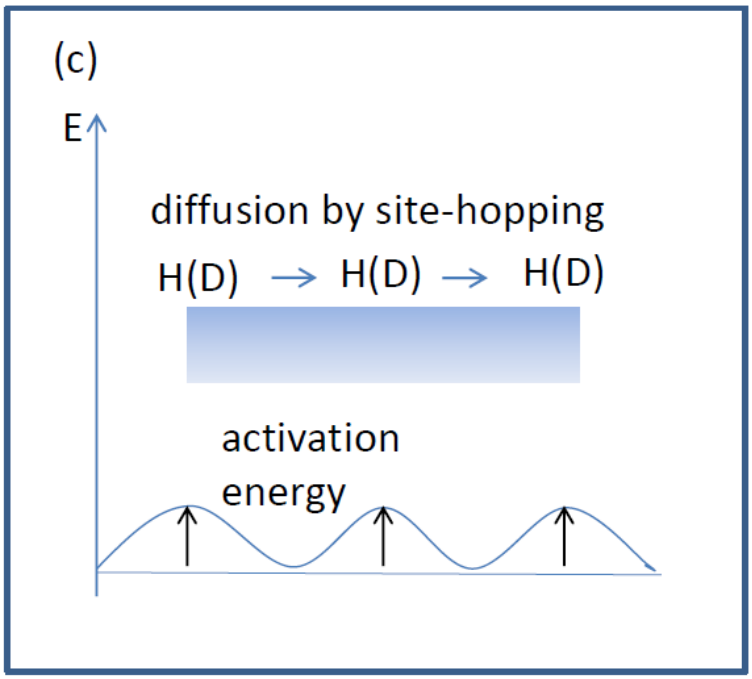

Figure V - 6 Potential energy diagram of hydrogen isotope migration on the surface of alumina.

C. Calculation of heat of reaction

The heat of reaction is the change in the enthalpy of a chemical reaction that occurs at a constant pressure. It is a thermodynamic unit of measurement used to calculate the amount of energy per mole either emitted or produced in a reaction and is typically denoted by the unit kJ/mol. When calculating the enthalpy of reaction the enthalpies of formation for reactants and products are used. The enthalpy of formation is a function of temperature (and so is the enthalpy of reaction). The temperature dependence can be calculated from the specific heat capacity of the products and reactants. The specific heat capacity of materials depends upon the temperature. For a given phase of a material the heat capacity increases with temperature. The concept comes from statistical thermodynamics: as the temperature increases, molecules can exist in a larger number of states and access various energy levels of rotation and vibration. At a finite temperature, the vibrational and rotational degrees of freedom are not fully available but when the temperature increases so does the ability of the molecules to absorb energy (thus the specific heat capacity increases with the temperature). Heat capacity data can be found using the shomate equation:

$$C_p = a + b \times T + \frac{c}{T^2}$$

where T is the temperature in Kelvin and the quantities a, b, and c are constants which depend only on the material of interest and can be found in in thermodynamic tables.

The enthalpy change of the reaction can be written as:

$$\Delta H = \Delta H_{product} - \Delta H_{reactants}$$

The derivative with respect to temperature can be written as:

$$\left[\frac{\partial H}{\partial T}\right]_p = \left[\frac{\partial(\Delta H_{product})}{\partial T}\right]_p - \left[\frac{\partial(\Delta H_{reactants})}{\partial T}\right]_p$$

Using the heat capacity terms:

$$\left[\frac{\partial H}{\partial T}\right]_p = (C_p)_{product} - (C_p)_{reactants} = \Delta C_p$$

and integrating:

$$\int \left[\frac{\partial H}{\partial T}\right]_p dT = \int \Delta C_p dT$$

and substituting $\Delta C_p = \Delta a + \Delta b \times T + \frac{\Delta c}{T^2}$, the enthalpy of the reaction as a function of temperature can be written as:

$$\Delta H_T = \Delta a \times t + {}^1/_2\, \Delta b \times t^2 - \Delta c \times \frac{1}{t} + \Delta H_0$$

where $\Delta a, \Delta b,$ and Δc are calculated from the known a, b, and c coefficients for the products and the reactants of the reaction in the same way as ΔH; t = T(K)/1000; ΔH_0 is the enthalpy change for the reaction at standard conditions in units kJ/mol.

Using the standard enthalpy of formation and shomate equation coefficients (Cox, et al., 1989) (Chase, et al., 1985) (Ruscic, et al., 2006) (Gurvich, et al., 1989) I calculated the heat associated with possible H/D and reverse H/D exchange reactions at 40˚C, which is shown in Table 3.

TABLE 3. Exothermic and endothermic heat associated with H/D exchange chemical reactions.

Chemical reaction	**Heat (kJ/mol)**
OH + D = OD + H	-5.03
$H_2O + D_2 = HDO + HD$	-4.59
$H_2O + D_2 = D_2O + H_2$	-7.91
OD + H = OH + D	5.03
$D_2O + H_2 = HDO + HD$	3.43
$D_2O + H_2 = H_2O + D_2$	7.91

As shown in the table, the reaction can be either exothermic (negative value) or endothermic (positive value). If the source of the anomalous heat in Pd nanosystems is the H/D exchange reaction, then by controlling the particular water isotope in the material and exposing it to either hydrogen or deuterium we should be able to demonstrate both exothermic and endothermic heat production in the system. Results are discussed in the following section.

Chapter V conclusions

I have confirmed the excess heat production and the isotope effect in Pd and Pt on alumina and zeolite supports. The excess heat is released during the fast pressurization step and proportional to the slope of pressurization times a quantity Φ - the energy content of the fuel. In the absence of a nuclear reaction product I looked at an H/D exchange reaction, which was a conventional chemical process that could explain the results. The heterogeneous catalyst provided a perfect environment for the H/D reaction. The oxide support is a source of the exchange sites (fuel: OH, OD, H_2O, and D_2O), while metallic nanoparticles ensure the delivery of the atomic hydrogen isotopes to the exchange sites through dissociation and spillover. Based on the enthalpy of formation I expect both, exo- and endothermic exchange reactions to happen. The concept of fuel and the way it can be controlled within the material are described in full detail in the next two chapters.

CHAPTER VI

H/D EXCHANGE AS A SOURCE OF CHEMICAL HEAT

A. Water isotope experiment

As stated in the previous chapter, the H/D exchange reaction can be either exothermic or endothermic based on which isotope is exchanged. Therefore, by controlling the particular isotope in the material and exposing it to either hydrogen or deuterium, I should be able to confirm both exothermic and endothermic heat production. The fact that material can generate or absorb heat based on a particular isotope concentration will prove that H/D exchange chemical reaction is indeed a driving mechanism for the excess heat production observed in LENR experiments.

Two different approaches were taken when loading Pd into the alumina powder (Dmitriyeva, et al., 2012, Origin of excess heat generation during loading Pd-impregnted alumina powder with deuteriu and hydrogen). My goal was to make two materials: one rich in hydrogen with very little deuterium, and the other rich in deuterium with very little hydrogen. The H-rich material was virtually free of deuterons: the material was fabricated in H_2O-based solution as described in Chapter III and any moisture absorbed from the air also came in H_2O form. I assumed that H-rich material was virtually 100% “protonated” (protium accounts for more than 99.98% of all the naturally occurring hydrogen).

The D-rich material was fabricated from D-based chemicals in argon atmosphere; however, with all the precautions used to prevent exposure to air it was only partially “deuterated”. This partial deuteration was confirmed by nuclear magnetic resonance (NMR) measurements. The NMR showed the concentration ratio of the deuterons to the protons in D-rich material to be close to 2.2. Based on this information the material was 70% deuterated.

The fabricated materials were then loaded into the experimental apparatus and exposed to deuterium and hydrogen using the scheme presented in Table 4. During the loading there was a two-minute period during which the samples were exposed to air, which resulted in some contamination of the deuterium-based material by H_2O.

TABLE 4. Four types of experiments using different combinations of materials and gases, along with the expectation of exothermic or endothermic reaction in Pd-loaded alumina powder.

Experiment number	**Material and gas**	**Expected outcome**
1	H-rich material & H_2 gas	no heat
2	H-rich material & D_2 gas	exothermic heat
3	D-rich material & D_2 gas	no heat
4	D-rich material & H_2 gas	endothermic het

At this point I hypothesized that the isotope effect demonstrated in a number of the gas-loading experiments described in the Introduction was a manifestation of the H/D exchange chemical reaction, where deuterium was introduced into material saturated with H_2O and OH-groups (experiment 2 in Table 4). As a result of the reversed H/D exchange an endothermic reaction should be observed during experiment 4 in Table 4. Little or no heat should be seen in experiments 1 and 3, where the material was prepared with the same isotope that was later introduced into the apparatus in gaseous form.

Data from experiments 1 and 2 in Table 4 along with the reference data for the empty vessel are shown in Figure VI - 1. All the curves are for the second pressurization, after the palladium precursor was reduced in the presence of hydrogen to yield metallic palladium.

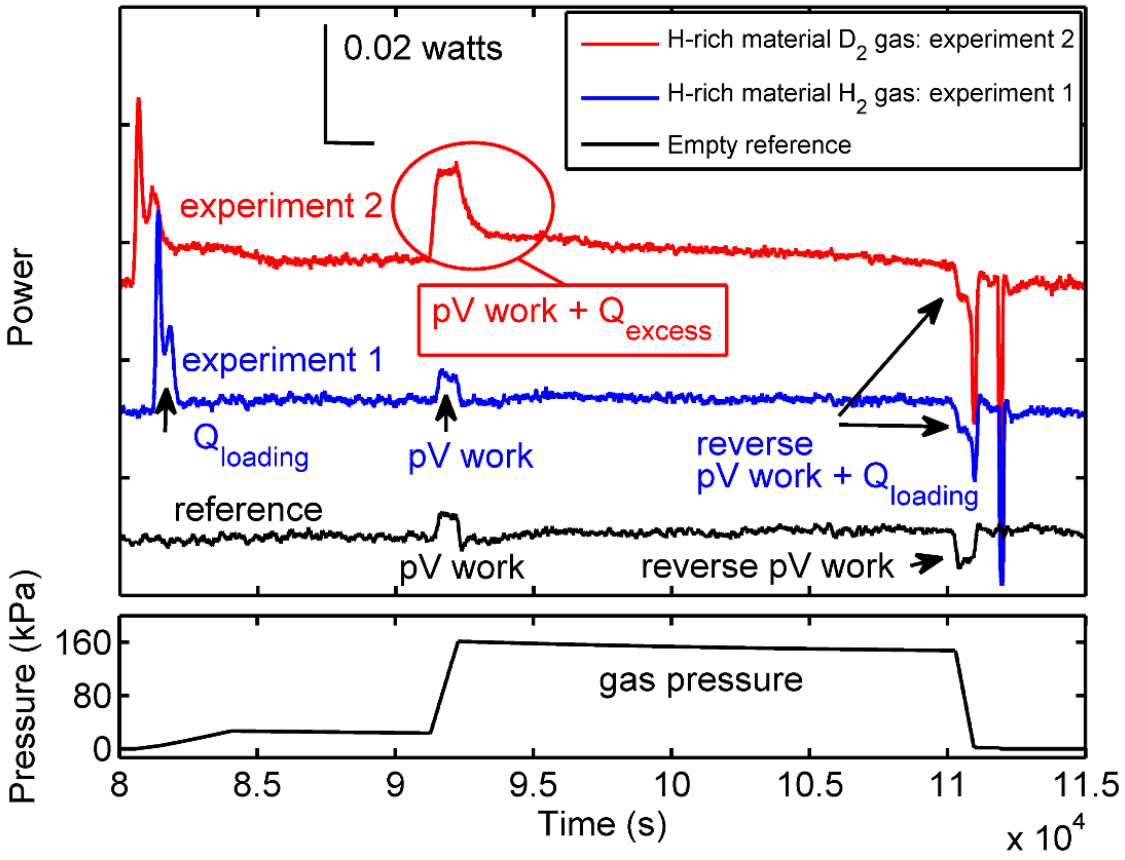

Figure VI - 1 Power in/out and pressure during hydrogen and deuterium runs on H-rich material as a function of time. The hydrogen (experiment 1) and deuterium (experiment 2) runs are both the second pressurization runs in a sequence of runs following the initial reduction runs.

There are several differences in the signals generated by the empty reference vessel, the loaded vessel exposed to hydrogen, and the loaded vessel exposed to deuterium:

1) $Q_{loading}$ for deuterium is close to $Q_{loading}$ for hydrogen when calculated as the areas underneath the curves in Figure VI - 1. For deuterium-loading this energy is (-12.9 J) and for hydrogen it is (-11.4 J). The amount of Pd by weight is 0.12 g. If we assume that the gas-loading ratio of Pd and D/H is 0.86 (Sakamoto, et al., 1996), then the maximum

possible energy released due to the PdD formation process is -16.6 J, and due to the PdH formation is -18.0 J. Exothermic heat is represented by negative values and endothermic heat by positive.

2) During the faster pressurization step:
    i) Deuterium-loading shows significant excess heat production (-23.9 J),
    ii) Hydrogen-loading shows only a *pV* work component, similar to the one generated with the reference vessel (-2.9 J).
3) The double endothermic spike during pump-out is due to a discontinuity in the evacuation process at 2.7×10^3 Pa that was introduced by collecting the RGA data (deloading of hydrogen and deuterium from Pd at 40° C occurred at approximately 4×10^3 Pa (Huang, et al., 2006). The heat associated with gas deloading from Pd is 13.4 J for the deuterium run and 12.9 J for the hydrogen run.

Now I move to a discussion of experiments 3 and 4 on D-rich material from Table 4. Data from the second pressurization are shown in Figure VI - 2.

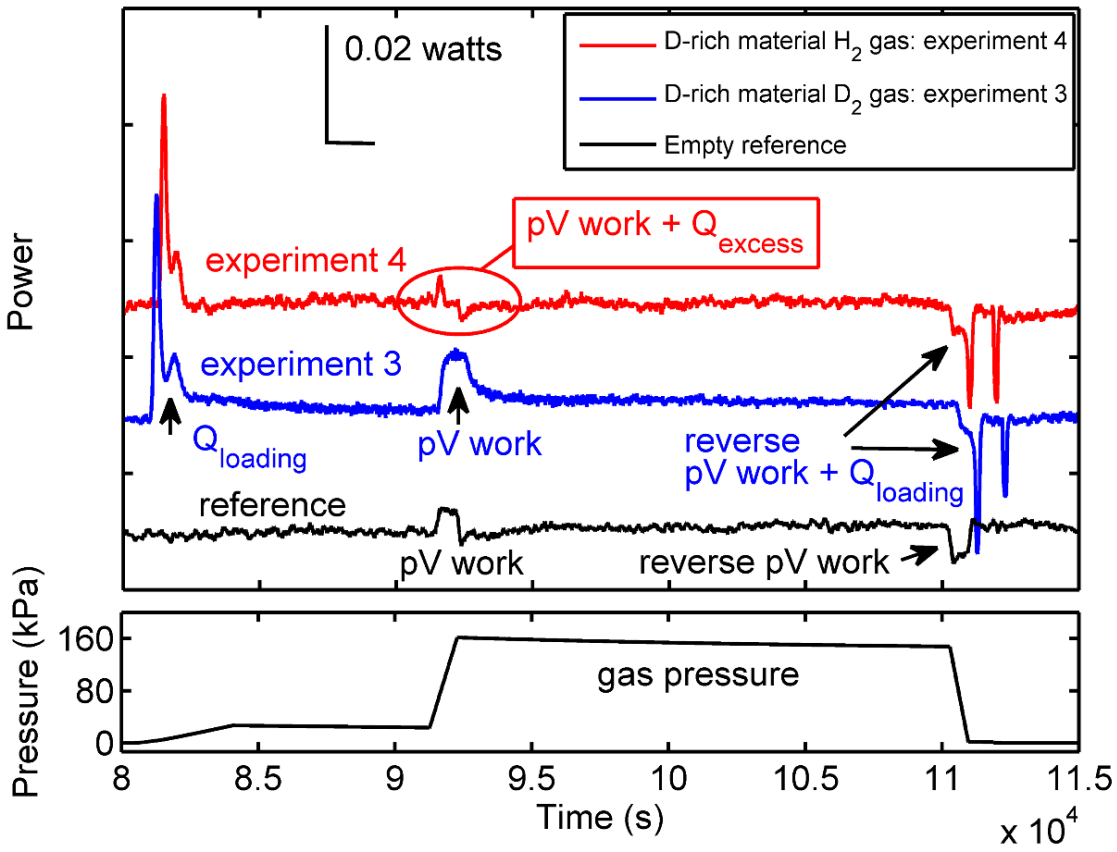

Figure VI - 2 Power in/out and pressure during deuterium and hydrogen runs on D-rich material as a function of time. Both the hydrogen (experiment 4) and deuterium (experiment 3) runs are the second pressurization runs in a sequence of runs following the initial reduction runs.

The key points are:

1) During the slower pressurization step the deuterium and hydrogen runs show $Q_{loading}$ values that are close to each other (-15.3 J and -11.2 J respectively).

2) During the faster pressurization step:

   i) The deuterium run still shows excess heat -9.7 J, but the absolute value is more than two times smaller than the value for the H-rich material (-23.9 J), as shown in Figure VI - 1.

ii) The hydrogen run shows endothermic heat during the faster pressurization step 5.4 J. The plot does not show a large endothermic dip because the heat of pressurization and the endothermic reaction heat are close in magnitude and almost compensate for each other.

3) The double endothermic spike during pump-out is the same as discussed previously (10.4 J for deuterium run and 8.2 J for hydrogen run).

Therefore, I have experimentally demonstrated a significant reduction of exothermic heat in D-rich material in the presence of deuterium (experiment 3 from Table 4) as well as endothermic heat production during the faster pressurization step (experiment 4 from Table 4).

B. Effect of depleting and replenishing of fuel

In a previous section I demonstrated that the material composition (whether fabricated with H-rich or D-rich water) affects the sign of Q_{excess}. Based on the concept of H/D exchange I suggest that the fuel is of two types: it is either H_2O and OH hydroxyl groups with its energy content, Φ_D <0, or D_2O and OD groups with its energy content, Φ_H >0 (subscript refers to the reacting gas).

By using H-rich material and switching between deuterium and hydrogen gas I found that fuels can be depleted or replenished within the material during repeated gas-loading cycles. The quantitative data are shown in Figure VI - 3 for the faster pressurization step of three sets of gas-loadings done with deuterium, hydrogen, and again with deuterium.

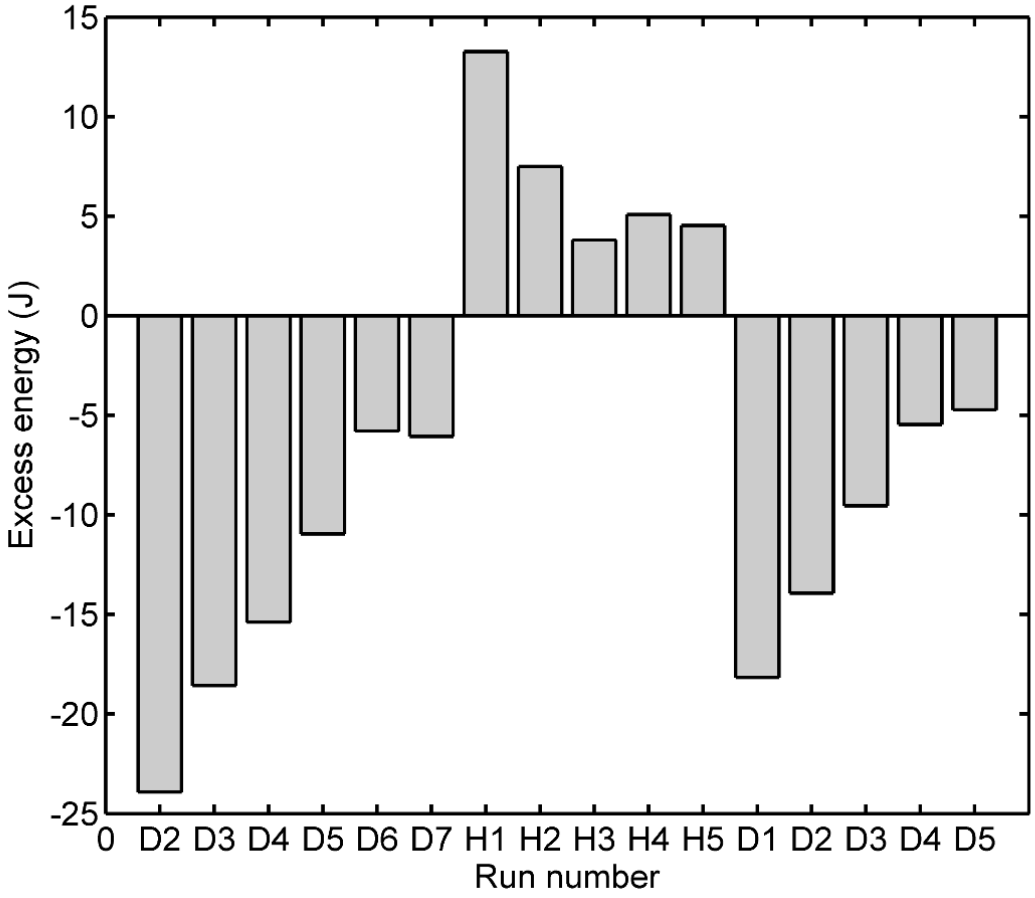

Figure VI - 3 Excess heat generated in H-rich material during deuterium and hydrogen pressurizations, as a function of run number. Data from the first run was omitted because heat generated during this run was dominated by the reduction of Pd to its metallic form.

The following processes are evident in the data of Figure VI - 3:

Depleting fuel Φ_D: During the first set of deuterium runs (D2 - D7) I see that the excess heat tapers off with repeated runs.

Generating fuel Φ_H: While Φ_D fuel was depleted, the Φ_H was generated. Switching to hydrogen in runs H1 - H5, I observe endothermic heat generation during the faster pressurization

step. As the number of hydrogen runs increases, the amount of the endothermic heat decreases in absolute value, indicating Φ_H fuel depletion.

Replenishing fuel Φ_D: After switching back to deuterium in runs D1 - D5 (second series), the system is recharged with the fuel Φ_D that supports the exothermic reaction. Notice that the excess heat levels recover only partially.

C. Process characterization

a) RGA data on H/D exchange

Residual gas analysis is an analytical technique used to identify the gaseous products present in a vacuum. A residual gas analyzer (RGA) is a mass spectrometer of small physical dimensions that can be connected directly to a vacuum system to analyze the gases inside the vacuum chamber. A small fraction of the gas molecules are ionized inside the RGA, and the resulting ions are separated, detected and measured according to their molecular masses. For each molecular mass the RGA gives partial pressure of the component.

Both of my apparatuses were equipped with SRS RGA 200 units. RGA data was collected during evacuation, first by discrete sampling every 3 min at 2.7×10^3 Pa through a capillary tube, and then every 5 min during pump-out when the pressure in the system was below 20 Pa.

The RGA data confirms the depleting and replenishing processes, as shown in Figures VI - 4 (a) and (b). These data were obtained during the evacuation step for the experimental runs of Figure VI - 3.

The processes evident in the data of Figure VI - 3 give rise to the following effects in the RGA data of Figure VI - 4:

Depleting fuel Φ_D: From the first set of deuterium runs (D1 - D7) in Figure VI - 4 (a). I see the depletion of H_2O from the material. At the same time, exchanged hydrogen is released as a result of this reaction, as shown in Figure VI - 4 (b).

Generating fuel Φ_H: The D_2O concentration increases during runs D1 - D7 as H_2O is converted to D_2O through H/D exchange. During the pump-out phase of each run only a fraction of this D_2O is removed, and so it builds up in the system.

Replenishing fuel Φ_D: The H_2O concentration increases during runs H1 - H5 as D_2O is converted to H_2O and releases exchanged deuterium, as shown in Figure VI - 4 (b). As in the previous process only a fraction of the H_2O is removed during the pump-out step, and so it builds up in the system.

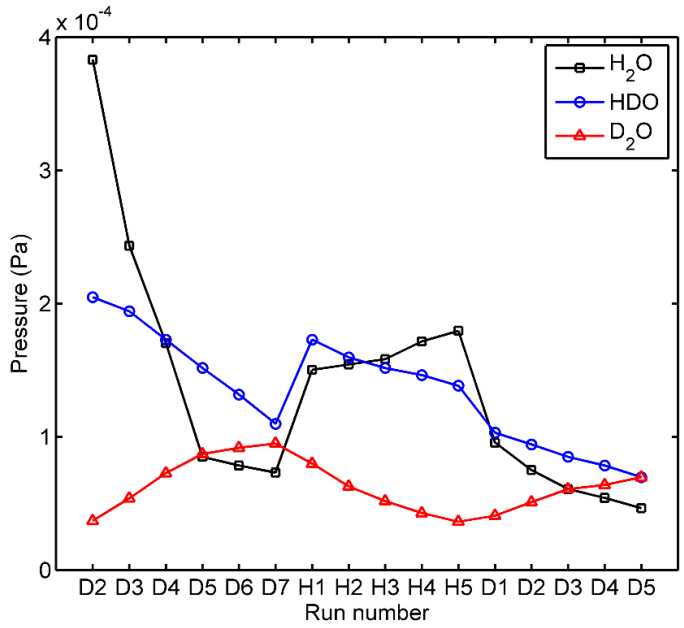

(a)

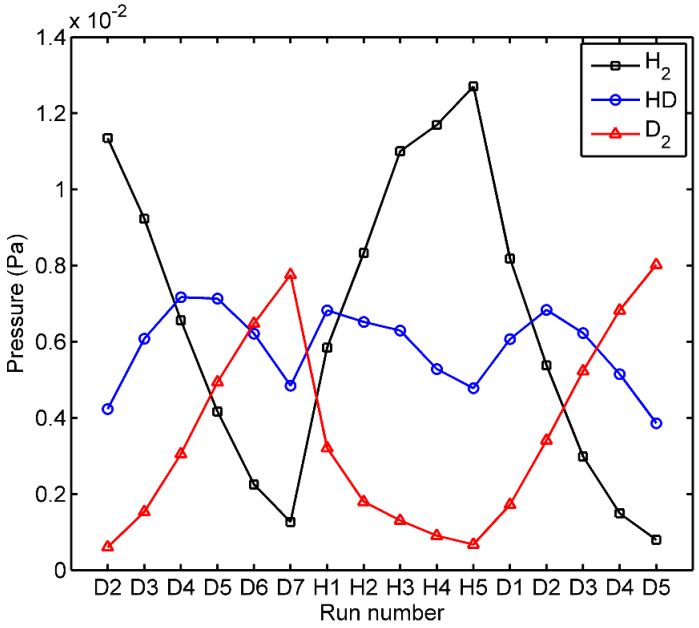

(b)

Fig. VI - 4 RGA data showing: (a) water isotopes and (b) hydrogen gas isotopes as a function of deuterium and hydrogen run sequences. Data from the first run was omitted because heat generated during this run was dominated by the reduction of Pd to its metallic form.

The ongoing chemical reaction depletes or enriches the material with either H_2O or D_2O, as shown in Figure VI - 4 (a). The change of the water isotope concentration in the three sets of runs with different gases shows this depletion or recharging process.

b) FTIR data on H/D exchange

Fourier transform infrared spectroscopy (FTIR) is an analytical technique used to identify the components of the mix (gaseous, liquid or solid). The vibrational motions of the chemically bound constituents of matter have frequencies in the infrared regime. In the infrared experiment, the intensity of an IR beam is measured before and after it interacts with the sample as a function of frequency. Absorbance of the material at a certain frequency indicates the presence of certain chemical elements/composites. Also, based on the Beer-Lambert Law, the absorbance is directly proportional to the concentration of the elements in the mixture. Thus, by analyzing the FTIR spectrum, information about the elements/composites and their concentration in the mix can be derived.

For my experiment I used a Nicolet 6700 FT-IR Spectrometer (courtesy of the Naval Research Laboratory, Washington DC). A 20 mg sample of Pd-impregnated alumina material was loaded into FTIR spectrometer using a custom-made holder, and exposed to hydrogen and deuterium at room temperature to collect the absorption spectra.

Figure VI - 5 shows the change of absorbance as a result of deuterium exposures done on H-rich material. Absorbance of the H_2O groups with O-H stretching vibrational modes around 3360 cm^{-1} decreased while absorbance of the D_2O groups with O-D stretching vibrational modes around 2400 cm^{-1} increased. Same was true for bending modes: decrease of H_2O absorbance at 1650 cm^{-1} and increase of D_2O absorbance at 1210 cm^{-1} (not shown on Figure VI-5). Thus, during deuterium runs the sample was depleted of fuel Φ_D (H_2O and OH groups) and charged

with Φ_H (D_2O and DO groups). The small changes during the first eight deuterium runs were the result of the short 30 sec gas pulses, while the large changes during the last four runs were caused by long two hour deuterium exposures.

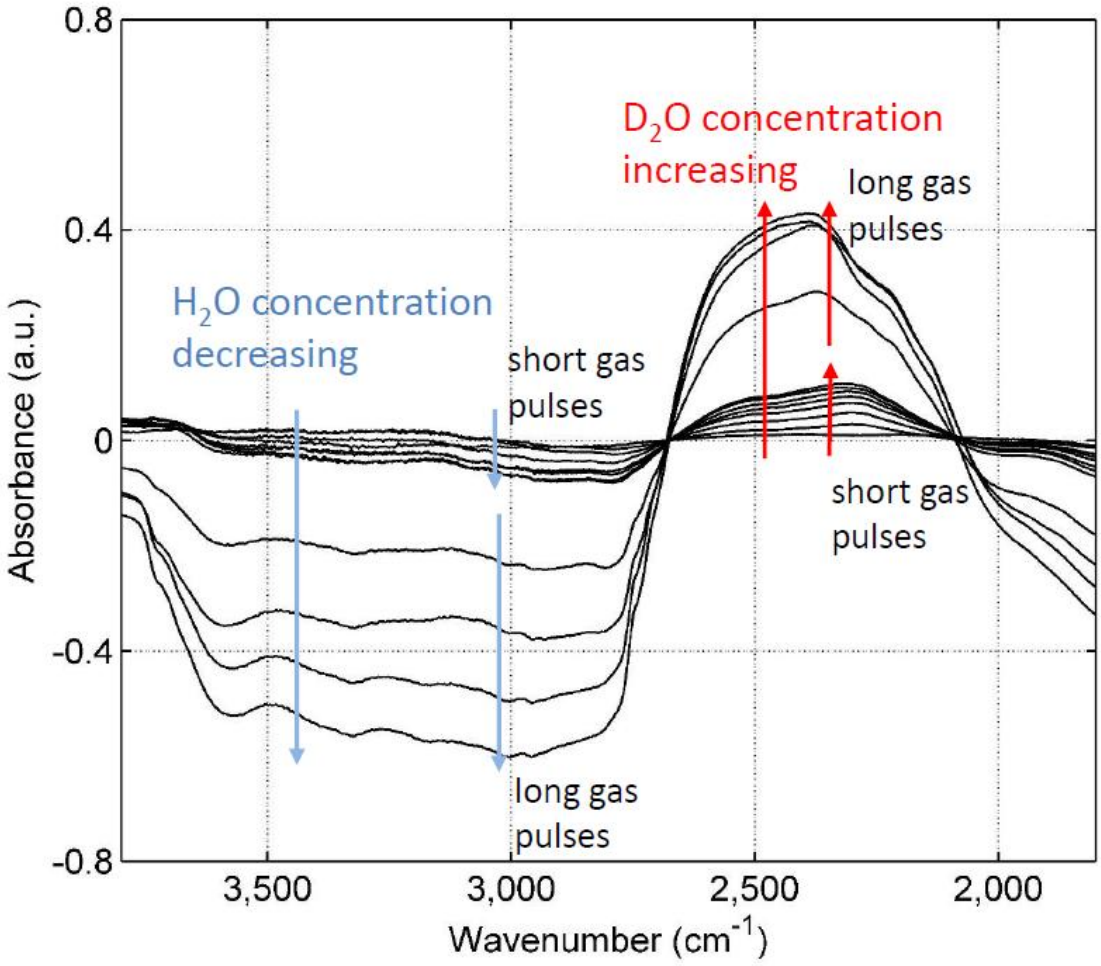

Figure VI - 5 Change of absorbance as a result of D_2 exposure to Pd-impregnated H-rich material.

Figure VI - 6 shows a 3D image of the changing intensity of the transmitted IR signal during the two hours long deuterium run as a function of wavenumber. The transmittance increases around 3300 cm^{-1} for H_2O groups and decreases around 2400 cm^{-1} for D_2O, which means the light water was converted into heavy water in the presence of deuterium. The process

saturated after $\tau_R = 120$ min. By estimating the half distance between two adjacent Pd nanoparticles, $L_D = 20$ nm from the TEM image in Figure III - 3, I calculated a mean diffusion path of the H(D) atom on the surface of the alumina using following equation:

$$D_s = \frac{L_D^2}{\tau_R}$$

The diffusion path Ds = 5.6×10^{-20} m^2/s.

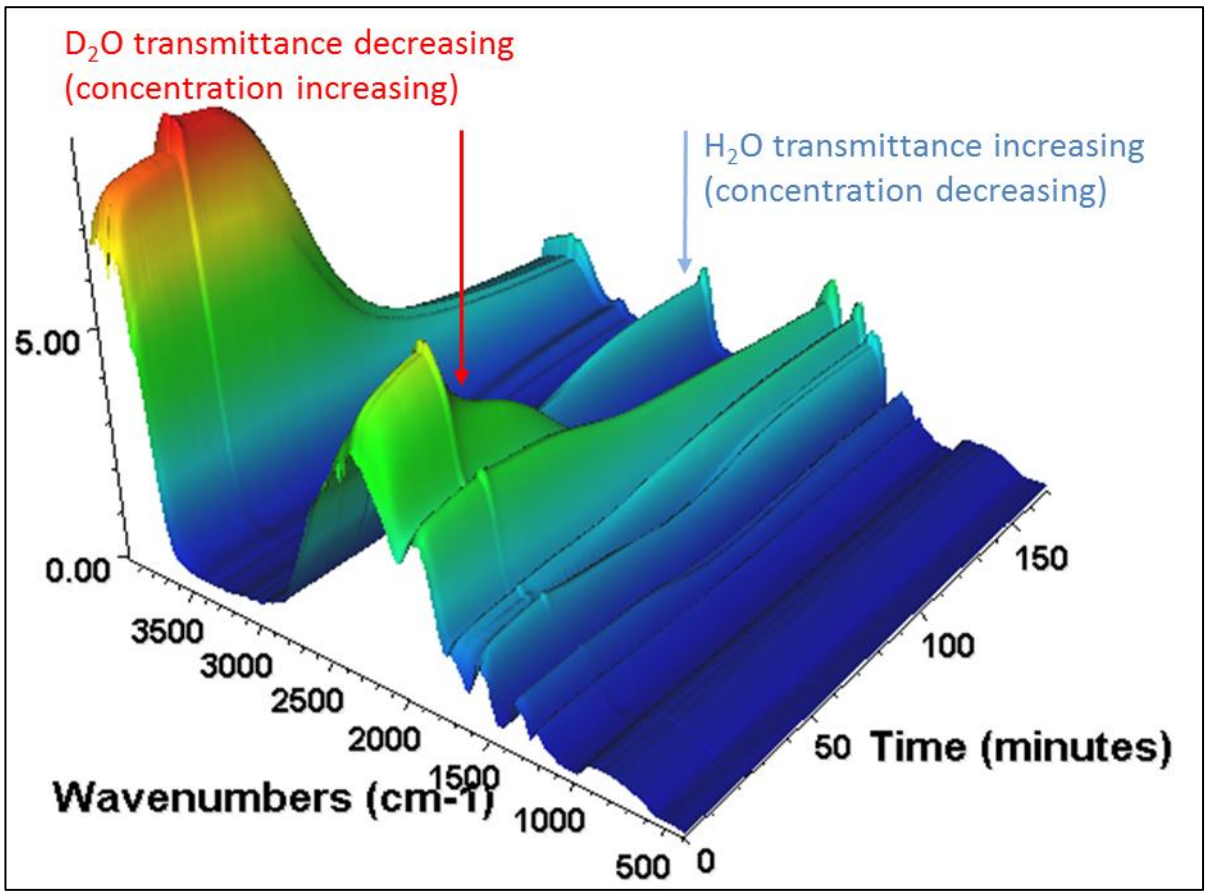

Figure VI - 6 Time-resolved FTIR transmittance spectra of Pd-impregnated H-rich material exposed to D_2 gas for two hours.

FTIR measurements were also done with D-rich material, with the number of short and long hydrogen pulses. Results are shown in Figure VI - 7. The H_2O absorbance did not change

much, possibly because the material was exposed to air and "contaminated" with protons during the loading step. However, the D_2O absorbance visibly decreased during the hydrogen exposures, which indicated a depletion of the material from D_2O - thus, the reverse H/D exchange. The last two curves shown in red are the deuterium exposures that were done after ten hydrogen runs to show that material was hydrogenated enough to start reacting with deuterium. The reverse change of absorbance can be explained by the fuel generation process in the same manner observed with RGA.

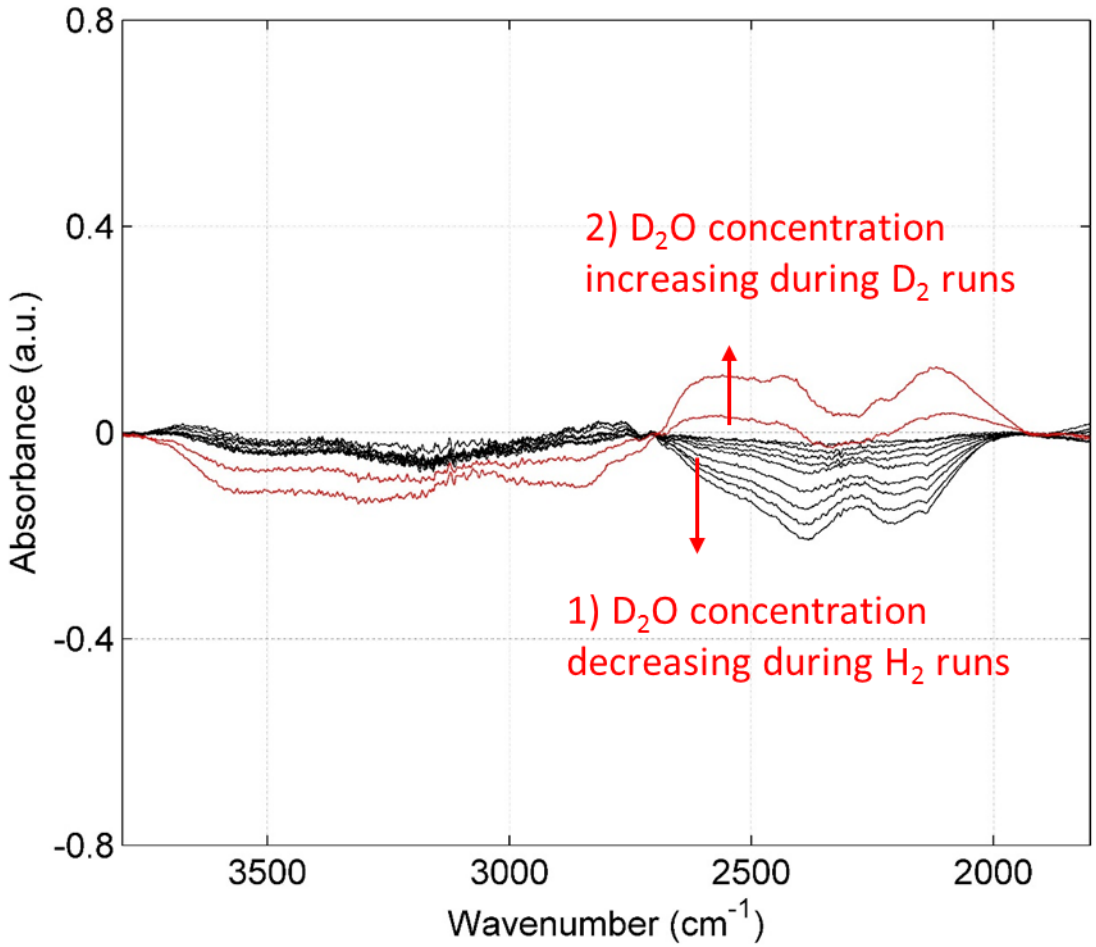

Figure VI - 7 Change of absorbance as a result of H_2 exposures done on Pd-impregnated D-rich material.

c) NMR data on H/D exchange

Nuclear magnetic resonance (NMR) spectroscopy is an analytical technique used to determine the structure of mix or compound. In the presence of an external magnetic field the nucleus can exhibit more than one spin state and can move between these states by the absorption of electromagnetic radiation of a specific frequency. Thus, the NMR can distinguish the atoms within a molecule or collection of molecules.

I used an NMR system (courtesy of the Naval Research Lab, Washington DC) to monitor the change of the number of protons and deuterons as a result of gas pressurizations. The H-rich and D-rich samples were pressurized with long (2 hours) and short (30 sec) pulses of deuterium and hydrogen inside the NMR system. Figure VI - 8 shows the results of D_2 and H_2 pressurizations on H-rich material. The measurements were done continuously in the presence of the gas and while the system was evacuated.

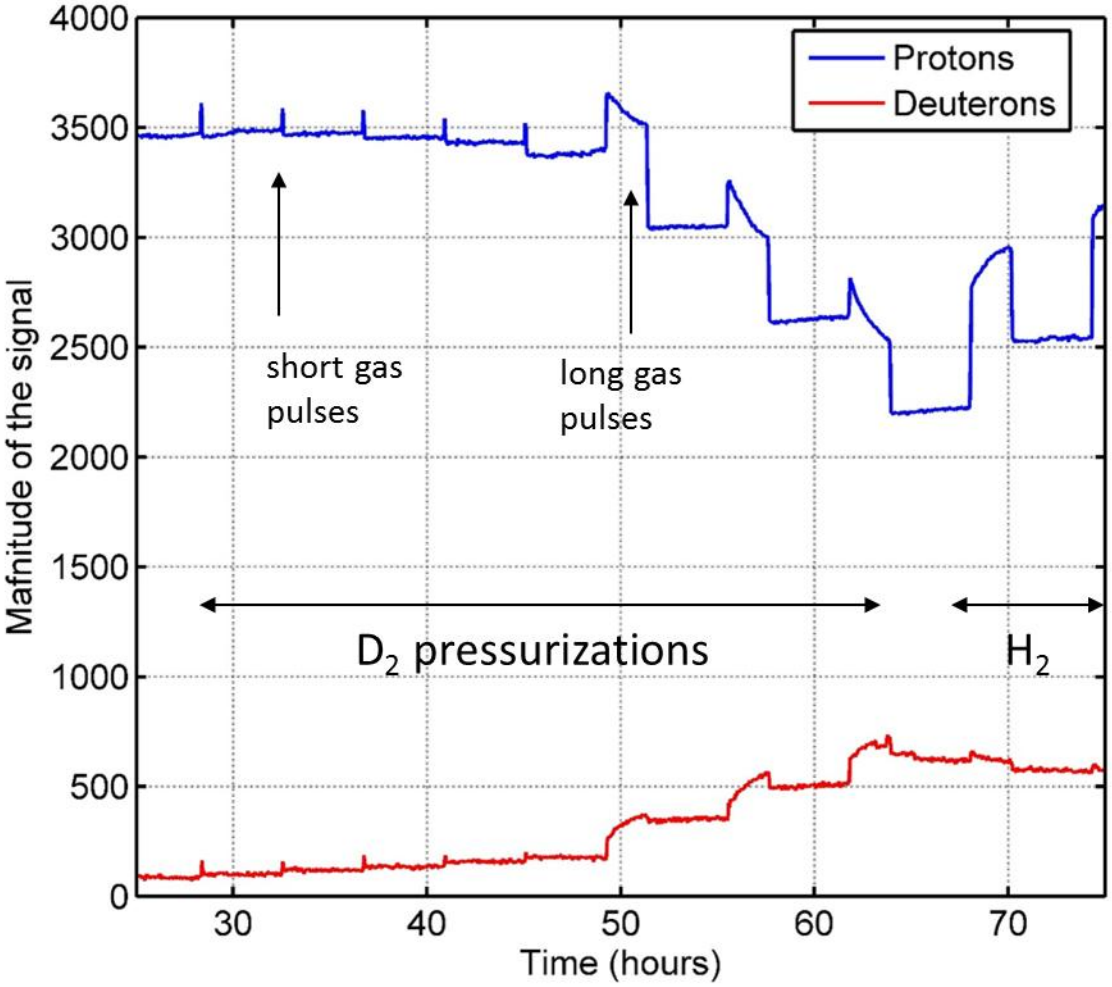

Figure VI - 8 NMR scan representing the change of protium and deuterium concentration in Pd-impregnated H-rich material as a result of deuterium and hydrogen exposures.

Five short deuterium pulses caused a slight upward shift in deuterium concentration corresponding to downward shift in hydrogen. Three long two-hour deuterium runs resulted in more pronounced shifts. During deuterium runs the sample was depleted of fuel Φ_D and charged with Φ_H. Deuterium runs were followed by two hydrogen runs, which caused a change in

hydrogen and deuterium concentration again, but in the opposite direction now, indicating a reverse H/D exchange.

Chapter VI conclusions

Several mechanisms are responsible for heat generation in Pd-loaded alumina material at different stages of the gas-loading process. While two of them (heat of loading and heat associated with the work of pressurization) are reversible, there is an additional source of excess heat that can be either exothermic or endothermic.

I fabricated different batches of material rich in protium or deuterium constituents. Using H-rich and D-rich material batches in combination with hydrogen and deuterium loading gases, I was able to demonstrate both exothermic and endothermic heat generation. I associated the particular water isotope provided to the system with a fuel, which engaged in an H/D exchange chemical reaction. RGA, FTIR and NMR time-resolved measurements independently confirmed the H/D exchange in H-rich and D-rich materials as well as the fuel depletion or generation.

CHAPTER VII

CONTROL OF HEAT GENERATION

In previous chapters I discussed the isotope dependence of heat generation in Pd-impregnated alumina and showed that Pd nanoparticles catalyze H/D exchange chemical reactions. One of the necessary reactants is a gas atom (deuterium or hydrogen), while the other reactant is a particular water isotope trapped in the material due to its hydroscopic nature. I called the water isotope fuel. This fuel can be supplied to the material in two ways: (1) the material can be enriched with a particular water isotope during the fabrication, or (2) by subsequent exposures to deuterium or hydrogen gas. The remaining question was to how to quantify the contribution of the H/D exchange in the overall heat production? One approach would be to look at the products of the reaction that occurred between the gas and the sample inside the vessel. To make a quantitative analysis using this approach I would need to know how much gas was supplied to the system, and the amount and type of gas and water isotopes that were released due to the reaction. I could calculate the energy and then compare it to the experimentally measured heat. However, there are certain obstructions associated with this approach that can seriously affect the precision of the measurements. For example, any outgasing of the stainless steel material that makes up the vessels and pipes would skew the analysis of the water content. I took a different approach to avoid these kinds of errors associated with measuring the reaction products and instead quantified the amount of fuel. In this chapter I present an approach that allowed control of the amount of water absorbed in the material, while measuring generated heat in order to quantify the contribution of the H/D exchange reaction (Dmitriyeva, et al., 2012, Using bakeout to eliminate heat from H/D exchange during hydrogen isotope loading of Pd-impregnated alumina powder).

A. Bakeout experiment

The idea for this experiment was to eliminate the fuel from the material, and therefore stop the H/D chemical reaction. Since the fuel is a particular water isotope, then baking the sample in a vacuum at elevated temperature would deplete the water from the material and stop the heat generation or absorption in the presence of gas. The experimental procedure can be described in a multistep process:

1) Heat generation/absorption

Initially, the catalyst was tested in the presence of deuterium and hydrogen to make sure the H/D exchange reaction was taking place. Figure VII - 1, Part I shows the excess heat produced in 26 runs in which the reaction gas was switched from deuterium (first 16 runs – exothermic process) to hydrogen (subsequent 10 runs – endothermic process). The amount of heat was calculated as a difference between the energy released or absorbed by the system during pressurization and evacuation.

2) Bakeout

The system bakeout was completed by ramping up the temperature in 50˚C increments to 390˚C, for a total time of about 35 hours. The bakeout was carried out in situ, so that the material was not exposed to the atmosphere between the bakeout and subsequent testing.

3) Heat depletion

Figure VII - 1, Part II shows the results of the following hydrogen and deuterium pressurizations. The first H_2 exposure resulted in an increased amount of released heat. I suggest it was due to a chemical reaction between the gas and the surface states that were activated during the bakeout. However, the temperature measurements of the subsequent 20 runs showed a

significant decrease in the amount of heat generated by the system, with no difference between deuterium and hydrogen runs. For the subsequent runs RGA testing showed no evidence of H/D exchange reactions.

4) Reabsorption of water from air

After it was unloaded from the apparatus, the material was placed on the lab scale to monitor the reabsorption of moisture from the air for the next 24 hours. On average my samples reabsorbed about 6% water by weight. Due to a delay in the transfer of the material to the scale, the percentage of absorbed water may be slightly underestimated.

5) Recovery of heat production

The material was loaded back into the apparatus and pressurized with deuterium. Figure VII - 1, Part III shows reactivation of the excess heat generation in the presence of deuterium. H/D exchange was also evident from RGA data (not shown).

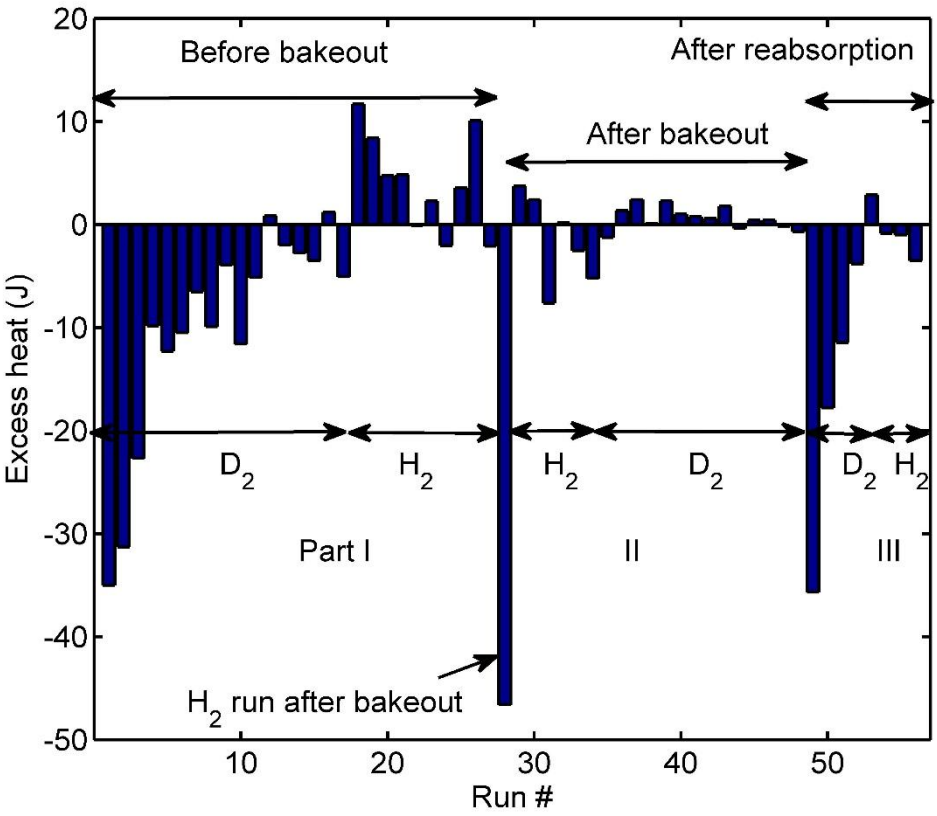

Figure VII - 1 Heat generated by the material during deuterium and hydrogen pressurizations.

B. Calculations

a) H/D exchange

Knowing how much water was available for the H/D exchange reaction I calculated the amount of energy that could be generated by the sample in the presence of D_2. 6% by weight of reabsorbed water is equal to 0.36 g. The enthalpy of the exchange reaction is 7.91 kJ/mol, which would result in 158.2 J of released heat. Based on the data presented in Figure VII - 1, Part I, I estimate that 158.7 J was generated.

b) Particle agglomeration

The agglomeration of Pd nanoparticles is a thermodynamically-driven process otherwise known as Ostwald ripening. Larger particles are more energetically stable than smaller particles due to a decrease in their overall surface area. Chemisorption analysis indicated an agglomeration of 5.7 nm particles into larger 11.5 nm particles as a result of more than 40 experimental runs (Chapter III). I used the following values to calculate the change of surface area in the nanoparticles and the energy released from agglomeration: Pd mass = 0.12 g, density ρ = 12.02 g cm^{-3}, Pd (111) surface energy $\gamma_{111} = 1.920$ J m^{-2}. I modeled nanoparticles as spheres that later agglomerated into larger spheres, therefore reducing the overall surface area. Based on my calculations, the change of surface area due to agglomeration was 2.65 m^2 (reduced from 5.26 m^2 to 2.61 m^2). As a result, the estimated energy release was 5 J.

Chapter VII conclusions

While my earlier studies showed evidence of the H/D exchange in heterogeneous catalysts, the results of this chapter confirmed that the water isotopes trapped in absorptive material are entirely responsible for the exo- and endothermic heat generation events. I described a technique that allowed me to control the heat production by depleting the fuel (residual water) through in situ bakeout at an elevated temperature. The results of my experiment showed that a 390˚C bakeout for at least 35 hours was sufficient. Allowing the material to reabsorb moisture from the air can also reactivate the reaction. Based on the material's mass loss/gain after bakeout/reabsorbtion, I calculated the energy capacity of the H/D exchange reaction and confirmed that all observed heat can be accounted for by this chemical reaction.

CHAPTER VIII

MEASUREMENT ARTIGACTS AS A SOURCE OF POSSIBLE MEASUREMENT ERROR

In Chapters VI and VII I demonstrated how the H/D exchange chemical reaction can explain the results of heat generation and absorption in heterogeneous catalysts at 40˚C. However, at temperatures above 200˚C I observed heating and cooling that could not be explained by conventional chemistry.

Figure VIII - 1 shows an example of anomalous temperature shifts at 390˚C in the presence of hydrogen and deuterium. Based on the calibration coefficients derived in Chapter IV, the estimated power production was 50 mW. The effect was observed as long as the sample was under gas pressure (the longest run was 96 hours). The effect went away when the vessel was repositioned inside the oven, which gave rise to the question as to whether measurement artifacts could account for these observations. In this chapter I describe my investigation of anomalous heating and associated measurement artifacts.

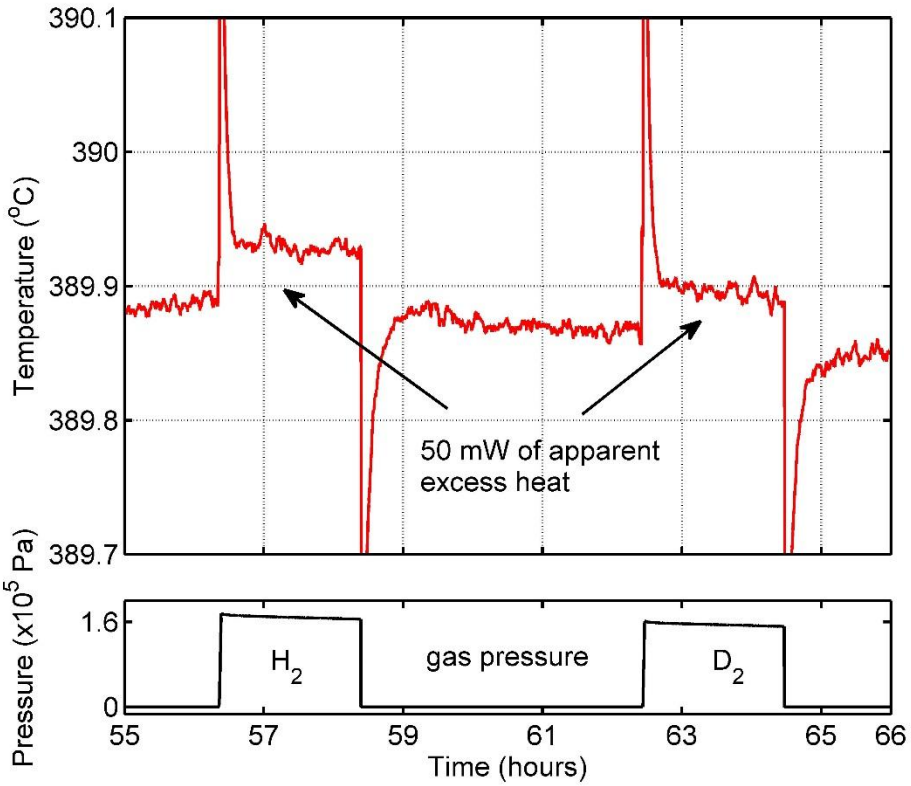

Figure VIII - 1 Temperature changes due to hydrogen and deuterium pressurizations done on material at 390˚C. There is a visible temperature baseline shift, which corresponds to 50mW of apparent excess power generated inside the vessel. The baseline shift is similar for both gases.

A. Hypothesis

The experiment was conducted in an isothermal oven. This is a high precision temperature control oven, with temperature variation kept within 10 mK. The sample vessel inside the oven went through gas pressurization/depressurization cycles to detect a temperature change due to the gas-loading process. The assumption in gas-loading experiments is that heat produced under gas pressure is an indication of a reaction inside the vessel. This is a valid assumption as long as a stable temperature baseline is established and temperature is uniform across the oven. However,

at an elevated temperature this uniformity is broken due to location-dependent variations in hot air flow from the oven heater. The effect becomes more noticeable as the temperature setting is raised. The variation can be a result of a partial blocking of hot air flow by plumbing and wiring associated with the vacuum system placed inside the oven. Local hot and cold spots are created as a result of this lack of uniformity. Because the stainless steel vessel is a poor heat conductor when it is evacuated, such hot and cold spots couple poorly to the temperature probe installed inside the vessel. However, when the vessel is pressurized, the presence of gas drastically changes the heat conduction inside it and causes the probe to couple more efficiently to the hot or cold spots in the oven than when under vacuum. This results in channeling of heat to or from the oven environment. This channeling effect can artificially shift the measurement baseline up or down, which can be mistaken for anomalous heating or anomalous cooling.

To test this hypothesis I artificially created and enhanced the hot and cold spot effect by placing a local heating or cooling element on the surface of the vessel that would later be pressurized with hydrogen, deuterium, helium, or argon. If this hypothesis is correct, the measurement baseline would shift upwards in the presence of the hot spot (dissipative resistor) when the vacuum system was pressurized, and in the presence of the cold spot (Peltier element) it would shift downwards. Moreover, the difference in the heat conduction coefficients of supplied gases would affect the magnitude of the baseline shift. While hydrogen, deuterium and helium have similar thermal conduction coefficients, argon's thermal conductivity is ten times smaller. If my assumption was correct, an argon run would show a smaller baseline shift. The presence of material inside the vessel should also affect the conduction characteristics of the vacuum system, and thus the magnitude of a baseline shift. When evacuated, a loose powdered material is a poor heat conductor due to the spacing between the particles. When under pressure,

however, the gas establishes a thermally conductive channel between particles. I expected the effect to be the result of a combination of the different factors such as the powder's packing density and the thermal conductivity of the sample.

B. Temperature gradient emulation

The hot spot was formed by placing a 150 Ω resistor on the surface of a vessel containing 6 g of Pd-impregnated alumina powder. Figure VIII - 2 (a) shows the view inside the oven, with the resistor attached on the surface of the vessel.

The oven was kept at 100˚C, and 1 W was dissipated in the resistor. In Figure VIII - 3 plot (a) shows the results of the gas pressurizations carried out in the absence of an artificially created thermal gradient. When no power was dissipated through the resistor the only temperature changes during pressurization cycles were due to absorption/desorption of the hydrogen isotopes in the Pd and the gas compression/expansion. Since neither helium nor argon is absorbed in Pd, the runs with those gases showed only temperature change associated with gas compression/expansion. However, the picture changed drastically when I powered the resistor. Figure VIII - 3 plot (b) shows a visible baseline shift whenever the vacuum system was pressurized. The baseline shift was similar for the deuterium, hydrogen and helium runs and different for argon.

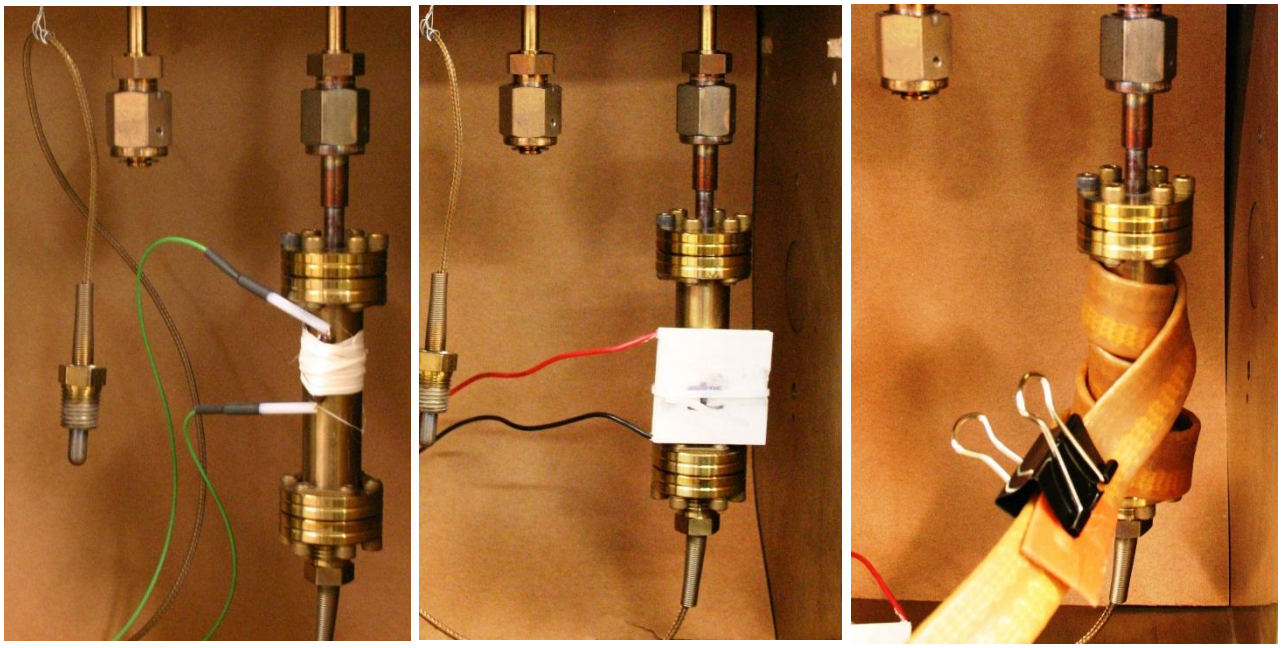

(a) (b) (c)

Figure VIII - 2 The vessel inside the oven with a (a) dissipative resistor, (b) cooling element and (c) heat sleeve attached to its surfaces.

The cold spot was formed by a Peltier element (TEC1-12706) held against the vessel surface as shown in Figure VIII - 2 (b). The oven temperature was set to 40˚C, and 0.1 W was dissipated through the Peltier element. I cycled hydrogen, deuterium, helium and argon through the vacuum system inside the oven, while having the Peltier element constantly on. The results are shown in Figure VIII - 3, plot (c). Each pressurization resulted in the downward shift of the temperature baseline. The magnitude of the shift depended on the gas used in the experiment.

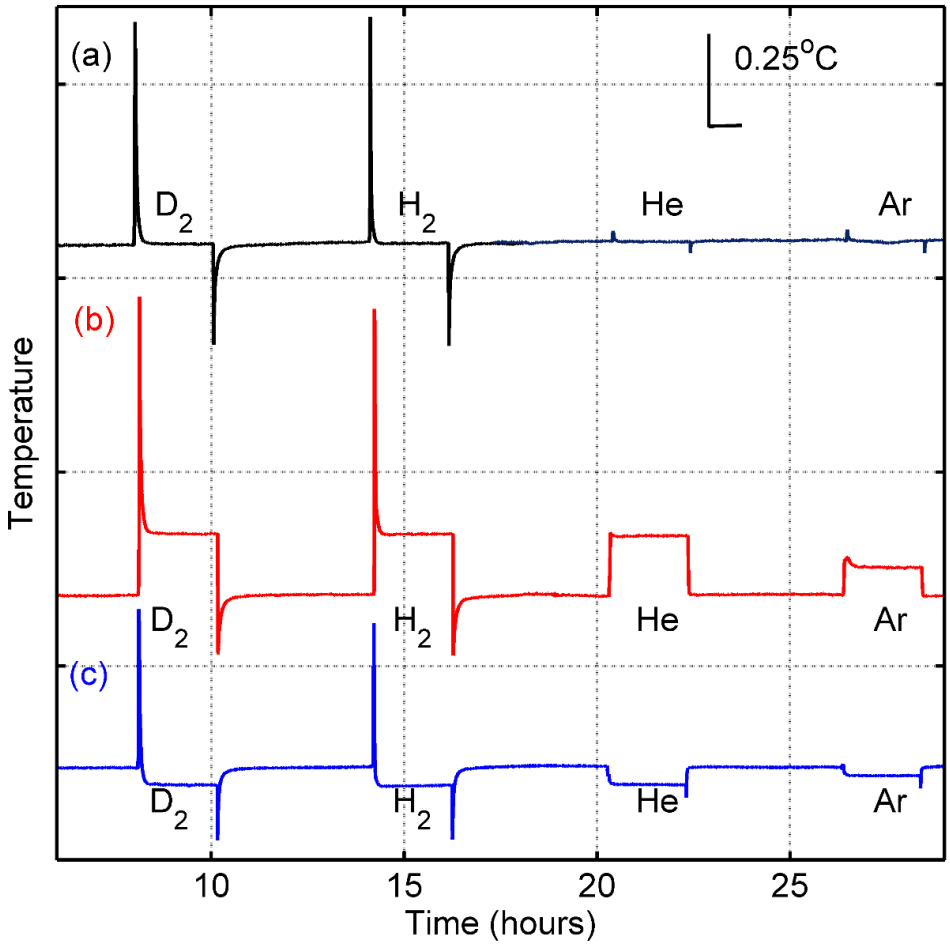

Figure VIII - 3 Temperature changes due to gas-loading of Pd-impregnated alumina (a) in the absence of an artificially produced thermal gradient; (b) in the presence of a hot spot; (c) in the presence of a cold spot. Pressurizations were carried out with deuterium, hydrogen, helium and argon.

Based on the information from the temperature measurements, I made the following conclusions: the magnitude of the shift depended on (1) the magnitude of the thermal gradient, (2) the thermal conductivity of the gas, (3) the presence of material inside the vessel.

1) Increasing the local hot spot temperature resulted in an increased amount of heat available for channeling from/to the oven's environment (and opposite for the cold spot),

affecting the magnitude of the baseline shift. I confirmed this hypothesis by dissipating different amount of power in the resistor. Doubling the power resulted in a doubling of the temperature baseline shift.

2) Gases of higher thermal conductivity (hydrogen, deuterium and helium) showed greater temperature baseline shifts, as compared to less-conductive argon. However, the trend was qualitative than quantitative. Even though argon's conduction coefficient is ten times smaller than that of helium, the baseline shift was only a factor of two smaller. I interpreted this as a mixed contribution of conductive and convective heat transfer mechanisms.

3) The presence of a sample inside the vessel resulted in 45% increase in a baseline shift as compared to the shift observed from gas-loading in an empty vessel (results not shown). Three different materials were tested: Pd-impregnated alumina, un-impregnated alumina and Ni powder. Ni is three times more thermally conductive than alumina, but a simple proportionality between the thermal conductivity of the materials and the magnitude of the baseline shift was not observed. I suggest that some other material properties (e.g., powder density) also affected the heat conduction process.

Using COMSOL commercial software for the finite element analysis I simulated heat conduction in the vessel as a result of a temperature gradient. I interpolated the hot spot experimental data to evaluate the magnitude of a temperature non-uniformity that could cause the 50 mW baseline shift shown in Figure VIII - 1. Figure VIII - 4 shows the result of the COMSOL simulation done with a stainless steel vessel of given geometry. The temperature of the surroundings was set to 390˚C. A heating stripe at 390.084˚C was simulated on the vessel's surface. Due to heat transfer and losses the probe at the bottom of the vessel would read 390.060

˚C. Based on the simulations a 0.5 K/m temperature gradient would result in 50 mW of apparent heating under the gas pressure. I did not simulate the gas flow or the change of the heat transfer inside the vessel due to the presence of the gas, but rather used the data from the hot and cold spot experiments to scale the effect. More accurate approach would be simulating pressurization of the system in the presence of the temperature gradient by linking the heat transfer to the fluid dynamics of the gas. Such direct simulations of the measurement artifacts including convection of the gas inside the vessel can be done using the CFD COMSOL Module and may be a subject of a future work.

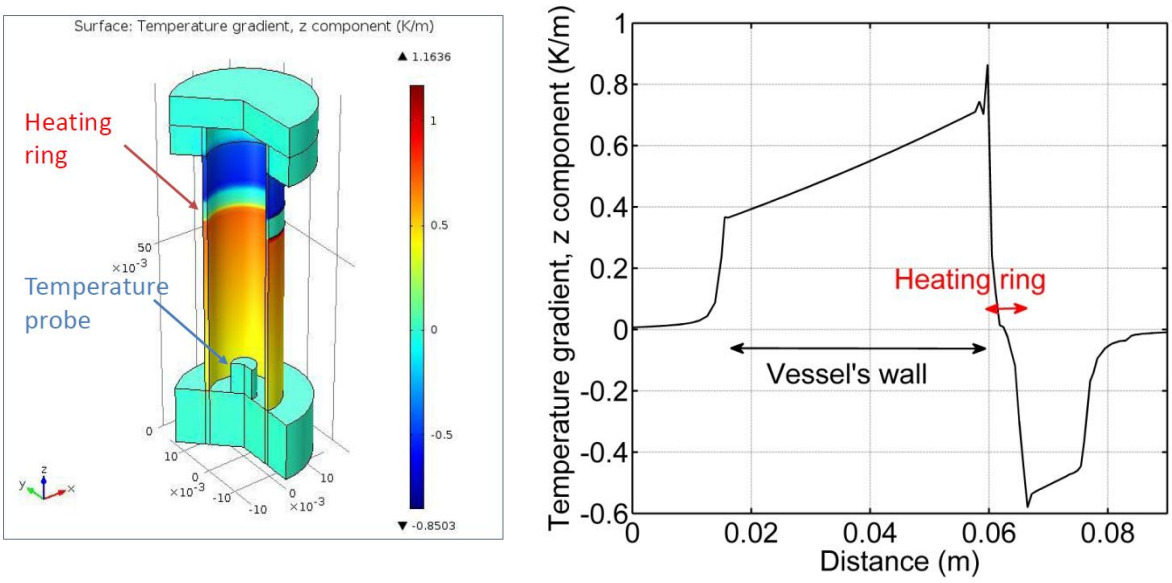

Figure VIII - 4 COMSOL simulations of the temperature gradient as a result of the local heating around the neck of the vessel. (a) 3D simulation of the temperature gradient in the stainless steel vessel; (b) the temperature gradient in the vessel along z direction.

In addition, I experimented with a heat sleeve (shown in Figure VIII - 2 [c]) that sometimes is used for LENR gas-loading experiments at elevated temperatures. I supplied 37 W of AC power to the heat sleeve. The heat sleeve created a temperature gradient across the

vacuum system and as a result, the baseline shifted during the gas pressurization step. This artificial shift is shown in Figure VIII - 5. The instability of the baseline was due to the room temperature variations, since the experiment was run with the oven shut off and opened to the ambient environment. The shifts due to the presence of the gas in the vacuum system corresponded to 1.2 W of apparent power production. The experiment with the heat sleeve provided a visual explanation of how the artificial shift of the temperature baseline could be mistaken for anomalous heating, when it is purely an artifact of temperature nonuniformities across the vacuum system.

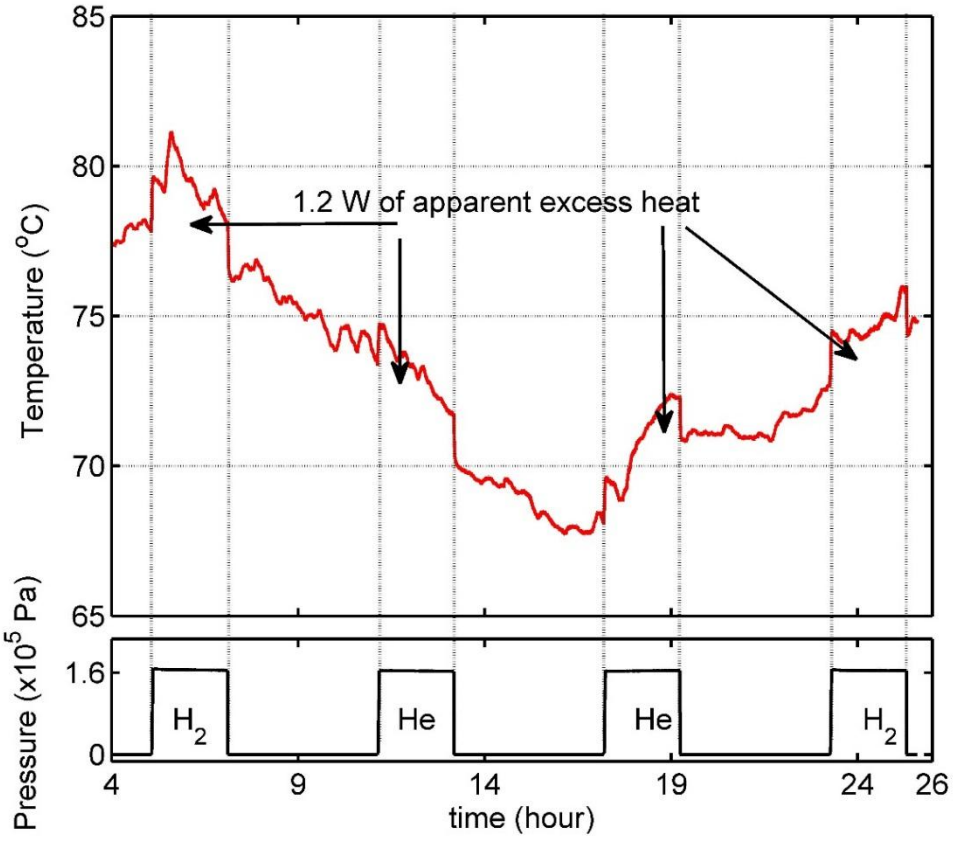

Figure VIII - 5 Temperature changes due to gas-loading of Pd-impregnated alumina in a vessel wrapped in heat sleeve. Pressurizations were done with hydrogen and helium. The experiment was carried out in an uncontrolled temperature environment, which explains why the temperature baseline is

unstable and the signal is noisy. Even with the noisy signal the temperature shifts are visible when gas is present in the system.

Chapter VIII conclusions

In this chapter I studied the influence of the temperature gradient on heat measurements during gas-loading experiments. Breaking the calorimetric requirements of the constant and uniform surrounding's temperature gives rise to the temperature gradients, and creates local hot or cold spots across the oven. These local nonuniformities would not affect the measurements if the vessel inside the oven retained the same thermal properties during the entire test, but that is not the case for the gas-loading experiments. The presence of gas inside the vacuum system drastically changes the thermal conductivity of its elements, allowing stronger coupling to the hot or cold spots, and therefore altering the temperature measurement baseline. Using COMSOL commercial software for the finite element analysis I simulated heat conduction along the stainless steel vessel. By matching the simulations to the experimental data I was able to quantify the temperature gradient. According to the simulations for my system's configuration the effect would become visible with a diminutive 0.024˚C temperature difference along the 4.5 cm long vessel wall and result in 50 mW of apparent heating. Since a number of LENR gas-loading experiments are run in elevated temperature conditions achieved by the local heating of the part of the vacuum system, this artifact can directly affect the measurements and cause the misinterpretation of the results. The way to account for this effect is to test the measurement system with the material present and an inert gas to identify potential measurement artifacts caused by temperature gradient.

CHAPTER IX

APPLYING H/D EXCHANGE THEORY TO ELECTROLYTIC EXPERIMENTS

In Chapters V-VII I discussed the mechanism of H/D exchange that involves hydrogen and water isotopes and can explain heat generation events in gas-loading experiments. The purpose of this study was to see if the same H/D exchange mechanism can explain excess heat production observed in electrochemical experiments.

I based my calculations on the data provided privately by Professor John Dash's group at Portland State University.

The "closed cell" system schematic is presented in Figure IX - 1. In this setup the cell supposed to be isolated from the environment so that no products can escape the system. For this purpose Pt/Al_2O_3 pellets were used as a catalyst to recombine H_2 (or D_2) and O_2 gases (products of the electrolysis) into water.

The cell used by the group was not a calorimetric setup. Instead, they used a two-cell system where the experimental cell contained a titanium cathode and a platinum anode, while the control cell contained a platinum cathode and a platinum anode. Each electrode was crimped to a platinum wire. Despite the presence of the recombiner both cells lost some mass. The composition of the lost mass was unknown. It could have been water vapor due to electrolyte evaporation at elevated temperatures or it could have been H_2 (or D_2) and O_2 gases escaping before they recombined. The experimental cell was calibrated using the control where both the cathode and anode were made of inert platinum and no other processes except conventional calorimetric reactions were expected. The experimental cell showed the anomalous heat generation, and the goal of the exercise was to look at the possible chemical reactions that could account for this excess heat.

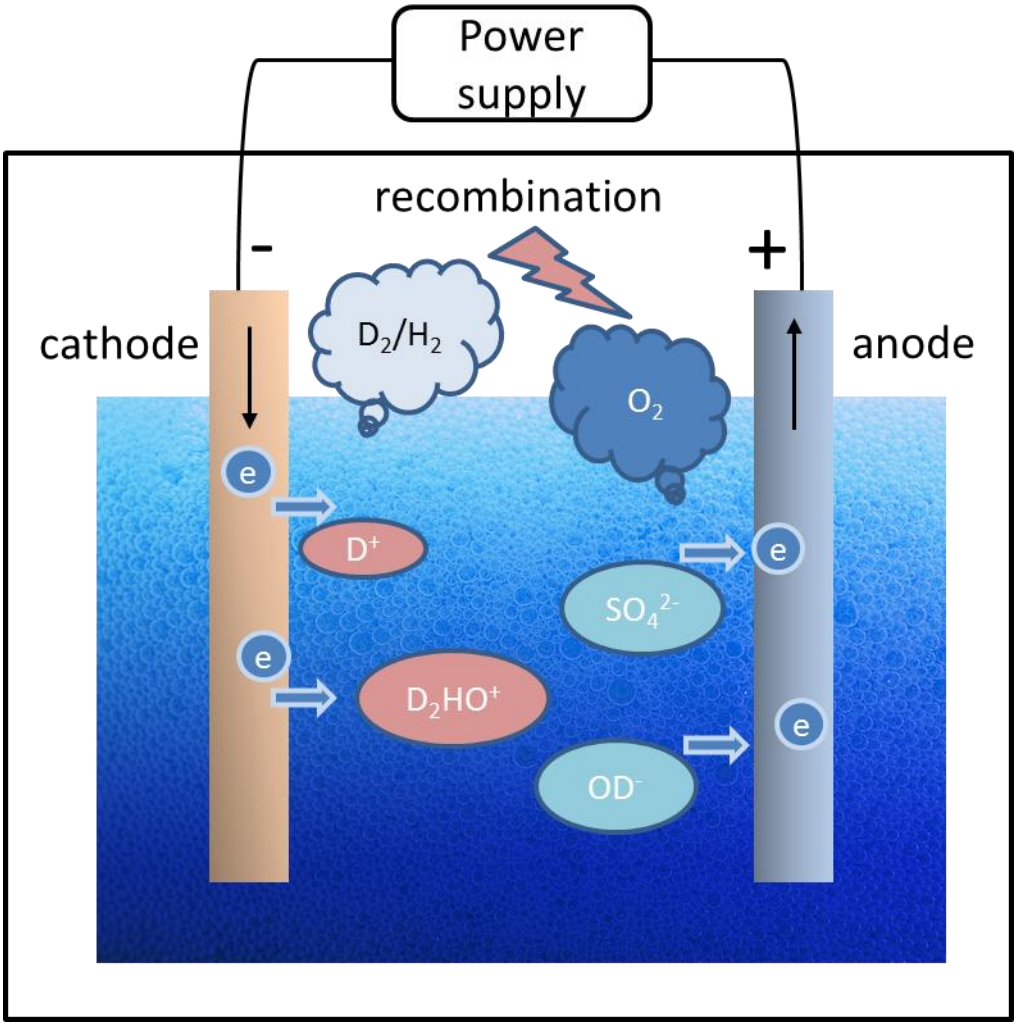

Figure IX - 1 The electrochemical cell. The electrolytic solution consists of 0.54M H_2SO_4 in D_2O. Positively charged cations travel towards the negatively charged cathode, where the reduction reaction occurs [electrons (e−), from the cathode being given to hydrogen (or deuterium) cations to form H_2 (or D_2) gas]. Negatively charged anions travel towards the positively charged anode where an oxidation reaction occurs, generating oxygen gas and giving electrons to the anode to complete the circuit. In the presence of a catalyzer (recombiner), H_2 (or D_2) reacts with O_2 to form water and returns back to the solution.

The cathode and anode in the experimental cell were submerged into a 130 ml solution of 0.54 M sulfuric acid in heavy water (0.07 mol of H_2SO_4 in 6.93 mol of D_2O). The experimental

cell was run at steady state for 25680 s and produced 0.59 W of estimated excess power, which is 110.5% of the electrical power supplied to the cell.

The hydration reaction of the sulfuric acid in heavy water and water electrolysis resulted in the creation of positive cations and negative anions that traveled to the cathode or anode where they either recombined or oxidized, providing the cell with an electrical current.

1) Knowing the hydrogen molar concentration in the electrolyte and assuming the hydrogen exists in the form of hydrones: HD_2O^+, H_2DO^+, H_3O^+, the energy of the exchange reaction is estimated as 0.07 mol x 7.91 kJ/mol = 554 J, which corresponds to 0.022 W of power. There is also a source of hydrogen in a form of water and hydroxyl groups trapped in the Pt/Al_2O_3 catalyst that is used as a recombiner. I hypothesize that 10 g of the catalyst would contain 6% water by weight based on the bakeout results from Chapter VII. Thus, the energy of the exchange reaction in the recombiner is estimated as 264 J, or 0.01 W of power. The remained question is: was this energy already accounted for as a part of a calibration routine when using a control cell? Both the experimental and control cells used the same electrolyte and the same Pt/Al_2O_3 catalyst. At this point I am going to assume that the H/D exchange in the electrolyte and the recombiner was a unique property of the experimental cell and resulted in 0.032 W of generated power.
2) Another source of exothermic heat that differed from the control cell was the hydrogenation of the titanium cathode. This reaction is reversible and the process of deloading of hydrogen from Ti after the cell was shut off should result in heat absorption. However, we assumed that the measurements were stopped when the power to the cell was shut off and no temperature measurements were taken beyond that point. Knowing

the mass of the cathode and assuming its full hydrogenation: Ti + 2H -> TiH_2 the possible generated heat is 0.0124 mol x 133.874 kJ/mol = 1.66 kJ or 0.065 W of power.

3) The mass loss was registered as a result of the electrolysis. The escaped products were unknown, however. If we assume that the electrolyte solution escaped the experimental cell in the form of water vapor after the hydrogen and oxygen recombined, then we can account for another 0.024 mol x 294.6 kJ/mol = 7.07 kJ or 0.275 W of power.

Based on these calculations the total power for which we can account by implying known chemical processes in the electrochemical cell is 0.032 W + 0.065 W + 0.275W = 0.372 W. This number represents heat that presumably was not accounted for by the control cell. However, the number 0.38 W does not fully explain 0.59 W of observed excess heat. The H/D exchange can account for only 5.4% of this excess generated power. The scale of the energy production in electrochemical cells is magnitudes higher than in gas-loading systems. Thus, the contribution of H/D exchange is insignificant, and for the particular example discussed in this chapter it cannot explain the heat production results.

Making sure the cell is closed to the environment and using calorimetric setup instead of a thermometry would improve the measurements and might result in different excess heat numbers.

CHAPTER X

CONCLUSIONS AND FUTURE WORK

A. Conclusions

The purpose of my work was to study and explain the mechanisms of heat generation in Pd-impregnated oxide materials as a result of their exposure to hydrogen isotopes. Several mechanisms are responsible for heat generation at different stages of the gas-loading process. While two of them (heat of loading and heat associated with work of pressurization) are reversible, there is an additional source of excess heat that some researchers have associated with a low energy nuclear reaction. The experiments that I carried out provided insights into this excess heat generation mechanism, and proved it to be chemical rather than nuclear.

The majority of my work was done with 2%Pd-impregnated alumina fabricated by incipient wetness impregnation. A combination of characterization methods showed that I synthesized nanoscale Pd clusters which were embedded into the alumina support. Oxide powder systems infused with Pd nanoparticles are well studied catalytic systems. I hypothesized that during deuterium and hydrogen gas-loading the catalyst promotes a chemical reaction under certain favorable conditions. If the observed reaction is indeed a manifestation of the catalytic nature of the Pd-impregnated alumina, than I should be able to demonstrate similar results using other heterogeneous catalysts. To prove my hypothesis, I fabricated samples using different supports (zeolite and silica) and different metallic inclusions (Pd and Pt). I also tested a commercially available ready-made Pd-on-alumina catalyst. The samples showed some limited variations during the gas-loading experiments. However, they all responded similarly with regards to the phenomena investigated here.

I have grouped my conclusions under the four bullet points listed below:

- No radiation above the background or alpha-particle emission was observed from the gas-loading of Pd-impregnated material, which led me to take a look at the conventional explanation of the excess heat generated by the material in the presence of deuterium. A hydrogen/deuterium (H/D) exchange chemical reaction was proposed to explain the excess heat generation phenomenon. The mechanism can be described as a multistep process: (1) deuterium gas dissociates on the surface of Pd nanoparticle, forming PdD, (2) deuterium atoms are transferred from the metal to the alumina support through a spillover process, and (3) the remaining water, which is trapped in the material along with hydroxyl groups on the surface of the alumina, engages in a H/D exothermic exchange reaction (when the hydrogen atoms are exchanged with deuterium). The H/D exchange explains the isotope effect and an observed gradual reduction of the amount of produced heat with repeated gas exposures. Based on these observations I proposed the concept of chemical fuel, which is stored in the material and supports the chemical reaction in the presence of gas.
- Chemical fuel can be of two types: H_2O and OH groups or D_2O and OD groups that are trapped in the material. My experiment with isotope materials proved that I can make a system not only generate, but also absorb heat – all based on the type of fuel provided to the sample and the hydrogen isotope used for gas-loading. Different characterization techniques confirmed the presence of the two types of fuel, and transitioning between depletion and regeneration of each type of fuel. The fact that the reactions could be both endothermic and exothermic supported the hypothesis of the chemical nature of the observed phenomenon. If a nuclear reaction initiated under these conditions had been the cause for the excess heat, it would have been exothermic only. Furthermore, the reaction

would not depend on the water isotope used during the fabrication step, as long as Pd remained in the same form and concentration and was loaded with deuterium atoms.

- A water isotope fuel can be controlled/exhausted by either continued gas cycling, which completes the H/D exchange, or by a bakeout at elevated temperature. The bakeout experiment demonstrated this elimination of the fuel, and as a result the heat generation stopped. The reaction was reactivated later through reabsorption of the water from ambient. Knowing the exact amount of the reabsorbed fuel allowed me to calculate its energy content and prove that all of the observed heat could be accounted for by the H/D exchange. I proposed the bakeout technique as a method to assess the energy released by the material due to a H/D exchange chemical reaction during the gas-loading experiments.

Besides the conventional chemistry that can explain the results of the gas-loading experiments in heterogeneous catalysts, I looked at the other processes that can be mistaken for anomalous heating in the presence of gas:

- There is a temperature measurement artifact associated with gas-loading experiments at elevated temperatures. This artifact is a result of the temperature gradients across the gas-loading system. The ruling assumption of gas-loading experiments is that heat produced under the gas pressure is an indication of the reaction. However, the presence of gas significantly changes the heat conduction inside the system. Therefore, when placed under gas pressure, the heat transfer efficiency changes. This change in heat transfer in the presence of temperature gradients artificially shifts the temperature measurement baseline, which could then be mistaken for excess heating. I have demonstrated how this

measurement artifact can alter the measurement baseline and proposed a technique that would ensure proper system calibration.

B. Future work

a) Heat transfer simulation

Coupling the experimental data to the software simulations is a powerful approach to study calorimetric systems. Commercially available finite element solvers and the simulation software package COMSOL can be used to model heat transfer inside the system via conduction, convection, and radiation. The Computational Fluid Dynamics (CFD) COMSOL multyphysics module does sophisticated fluid flow simulations, specifically: conjugate heat transfer with non-isothermal flow. The software can be used to simulate the gas flow conditions inside the oven and experimental vessel to explain and predict the rise of the measurement artifacts as described in Chapter VIII. Hydrogen, argon or helium heat conduction coefficients can be assigned when simulating flow inside the vessel. Coupling the CFD physics to the Heat Transfer in Solids physics module in the software will allow to calculate the time resolved temperature change at any point of the vacuum system.

b) Ni-H system

I looked at a gas-loading system following multiple reports of anomalous heat generated by such systems in the presence of deuterium. However, there is another large cluster of work that has been done with Ni and NiCu alloy materials and hydrogen, and for which H/D exchange reaction does not provide an explanation. Hydrogen, as a reaction gas, does not satisfy the condition for the exothermic reaction described in Table 4. Hydrogen exposure would produce either no heat if the material is saturated with H_2O, or the reaction would be endothermic if D_2O

is trapped in the sample. I do not dismiss the chemical explanation to the excess heat observed in Ni-H systems, but the details of the reaction are unknown.

Ongoing research of Ni nanopowders includes two decades of experimental work done by F. Piantelli (Piantelli, 2012), (Focardi, et al., 1999). More recent results have been reported by F. Celani, who was experimenting with NiCu Constantan wires (Celani, et al., 2012). In 2009 the Electric Power Research Institute in Palo Alto, Calif., sponsored work of B. Ahern, who repeatedly observed anomalous heating of nano-Ni composite powders under hydrogen pressure. Ahern's material was independently tested by the group of Japanese scientists from Kobe University, Osaka University, Technova Inc. and Santoku Corp., who confirmed the effect. As a result, the emphasis of their research was switched to Cu-Ni-ZrO_2 powders and hydrogen loading instead of Pd-D_2 (Sakoh, et al., 2012). Interestingly enough, the same material was tested in our laboratory using the protocol proposed by B. Ahern himself. I did not observe any anomalous heating; moreover, the results I obtained testing Ahern's material initiated the study of the measurement artifact described in Chapter VIII.

The origin of a possible heat generation mechanism in Ni-H systems is unknown and worth looking into. The effort should be applied into careful calibration of the gas-loading system to avoid measurement artifacts, since excess energy generation events from Ni-H systems were reported at the elevated temperatures. To investigate the reaction products different characterization techniques could be used in the same manner described in Chapter VI. The fact that the presence of the nano-features is essential to a successful demonstration of heat production in the material makes one expect that the catalytic properties of Ni metal play a role in initiation of a reaction.

REFERENCES

Andrews, D., 2008. A novel experiment to investigate the attenuation of alpha particles in air. *Eur. J. Phys. 29,* pp. 1077-1083.

Arata, Y. & Zhang, Y., 2008. Establishment of the "Solid Fusion" reactor. *J. High Temp Soc.,* pp. 85-39.

Biberian, J.-P., 2008. Cold fusion by gas-loading. *Proceedings of 14th International Conference on Condensed Matter Nuclear Science,* pp. 370-384.

Bloch, F., 1933. Zur bremsung rasch bewegter teilchen beim durchgang durch materie. *Ann. Phys. 16,* pp. 285-320.

Canton, P. et al., 2002. Pd/CO average chemisorption stoichiometry in highly dispersed support Pd/gamma-Al2O3 catalysts. *Lanfmuir,* pp. 6530-6535.

Celani, F. et al., 2012. Cu-Ni-Mn alloy wires, with impoved sub-micrometric surfaces, used as LENR device by new transport, dissipation-type, calorimeter. *Proceedings of 17th International Conference on Condensed Matter Nuclear Science,* in press.

Chase, M. W. et al., 1985. JANAF Thermochemical tables (third edition). *J. Phys. Chem. Ref. Data, 14.*

Chorkendoff, I. & Niemantsverdriet, L. W., 2007. *Concepts of Modern Catalysis and Kinetics.* Weinheim: WILEY-VCH Verlag GmbH & Co

Conner, W. C. & Falconer, J. L., 1995. Spillover in heterogeneous catalysis. *Chem. Rev. 95,* pp. 759-788.

Cox, J. D., Wagman, D. D. & Medvedev, V. A., 1989. *CODATA key values for thermodynamics.* New York: Hemisphere Pub. Co.

Datye, A. et al., 2000. Catalyst microstructure and methane oxidation reactivity during the Pd<-> PdO transformation on alumina supports. *Appl. Catal. A,* pp. 179-196.

Davis, E., Teofilo, V. L., Puthoff, H. E. & Nickisch, L. J., 2006. Review of experimental concepts for studying the quantum vacuum field. *Proc. of the STAIF-2006: 3rd Symposium on New Frontiers and Future Concepts, AIP Conf. Proc.,* 813, pp. 1390-1401.

Dmitriyeva, O., Cantwell, R., McConnell, M. & Moddel, G., 2012. Mechanisms for heat generation during deuterium and hydrogen loading of palladium nanostractures. *J. Condensed Matter Nucl. Sci., 8,* pp. 29-36.

Dmitriyeva, O., Cantwell, R., McConnell, M. & Moddel, G., 2012. Origin of exces heat generation during loading Pd-impregnated alumina powder with deuterium and hydrogen. *Thermochimica Acta 543,* pp. 260-266.

Dmitriyeva, O., Cantwell, R., McConnell, M. & Moddel, G., 2012. Using bakeout to eliminate heat from H/D exchange during hydrogen isotope loading of Pd-impregnated alumina powder. *Proceedings of 17th International Conference on Condensed Matter Nuclear Science,* in print.

Drits, V., Eberl, D. & Srodon, J., 1998. XRD measurement of mean thickness, thickness distribution and strain for illite and illite/smectite crystallites by the Bertaut-Warren-Averbach technique. *Clays & Clay Minerals,* pp. 38-50.

Eberl, D., Drits, V., Srodon, J. & Nuesch, R., 1996. MudMaster: a program for calculating cristallite size distributions and strain from the shapes of X-ray diffraction peaks. *USGS Open File Report,* pp. 96-171.

Fleischmann, M., Pons, S. & Hawkins, M., 1989. Electrochemically induced nuclear fusion of deuterium. *J.Electroanal.Chem.,* 261, 301 and errata in 263.

Focardi, S., Habel, R. & Piantelli, F., 1999. *Anomalous heat production in Ni-H,* Europian Patent EP0767962.

Gurvich, L. V., Veyts, I. V. & Alcock, C. B., 1989. *Thermodynamic properties of individual substances.* New York: Hemisphere Pub. Co.

Haisch, B. & Moddel, G., May 27, 2008. *Quantum vacuum energy extraction,* U.S. Patent 7,379,286.

Hansen, K. et al., 1999. Palladium Nanocrystals on Al_2O_3: structure and adhesion energy. *Phys. Rev. Lett., v.83,* pp. 4120-4123.

Hemminger, W. & Hohne, G., 1984. *Calorimetry - fundamentals and practice.* Weinheim: Verlag Chemie GmbH.

Hioki, T. et al., 2009. Hydrogen/deuterium adsorption property of Pd fine particle systems and heat evolution associated with Hydrogen/deuterium loading. *Proceedings of 15th International Conference on Condensed Matter Nuclear Science,* pp. 88-93.

Huang, S.-Y., Huang, C.-D., Chang, B.-T. & Yeh, C.-T., 2006. Chemical activity of palladium clasters: sorption of hydrogen. *J. Phys. Chem,* Volume 110, pp. 21783-21787.

Kidwell, D., Knies, D., Moser, A. & Domingues, D., 2009. Yes, Virginia there is a heat, but it is most likely of chemical origin. *Proceedings of 15th International Conference on Condensed Matter Nuclear Science,* pp. 100-109.

Kitamura, A. et al., 2008. Anomalous effacts in charging of Pd powders with high density hydrogen isotopes. *Phys. Lett. A,* pp. 3109-3112.

Langford, J. I. & Wilson, A. C., 1978. Scherrer after Sixty Years: A Survey and Some New Results in the Determination of Crystallite Size. *J. Appl. Cryst,* pp. 102-113.

Miles, M. & Fleischmann, M., 2009. New approaches to isoperibolic calorimetry. *Proceedings of 15th International Conference on Condensed Matter Nuclear Science,* pp. 22-26.

Moddel, G., 2009. Assessment of proposed electromagnetic quantum vacuum energy extraction methods. *arXiv,* 0910.5893.

Piantelli, F., 2012. *Resultes reported on Ni-H system,* Siena, Italy: 10th International Workshop on Anomalies in Hydrogen Loaded Metals.

Quantachrome Instruments, 2007. *Autosorb 1C version 1.5x operation manual.*

Ruscic, B. et al., 2006. Active thermodynamical tables: accurate enthalpy of formation of hydroxyl radical, HO_2. *J. Phys Chem. A 110,* pp. 6592-6601.

Sakamoto, Y. et al., 1996. Calorimetric enthalpies for palladium-hydrogen (deuterium) systems at H(D) contents up to about [H]([D])/[Pd]=0.86. *J.Phys.: Condens. Matter, 8,* pp. 3229-3244.

Sakoh, H. et al., 2012. Hydrogen isotope absorption and heat release chatacteristics of a Ni-based sample. *Proceedings of 17th International Conference on Condensed Matter Nuclear Science,* p. in press.

Scherrer, P., 1918. Bestimmung der Grösse und der inneren Struktur von Kolloidteilchen mittels Röntgenstrahlen. *Nachr.Ges.Wiss.Göttingen,* pp. 98-100.

Storms, E., 2007. *The science of low energy nuclear reaction.* Singapore: World Scienific Publishing Co. Pte. Ltd..

Storms, E., 2010. Status of cold fusion (2010). *Naturwissenschaften,* pp. 97:861-881.

U.S. Department of Energy, 2004. *Report of the review of low energy nuclear reactions,* Washington, DC: Department of Energy.

U.S. Department of Energy, 2011. *International Energy Outlook 2011, Report Number: DOE/EIA-0484(2011),* Washington, DC: Department of Energy.

Vitos, L., Ruban, A., Shriver, H. & Kollar, J., 1998. The surface energy of metals. *Surf. Sci 411,* pp. 186-202.

Wachs, I. E., 1992. *Characterization of catalytic materials,* Butterworth-Heinemann.

APPENDIX – A

Space, Propulsion & Energy Sciences International Forum - 2012

Test of zero-point energy emission from gases flowing through Casimir cavities

Olga Dmitriyeva[a], Garret Moddel[a,b,1]

[a]*Department of Electrical, Computer, and Energy Engineering, University of Colorado, Boulder, CO 80309-0425, USA*

[b]*Jovion Corporation, Meno Park, CA, 94025, USA*

Abstract

A recently issued patent [1] describes a method by which vacuum energy is extracted from gas flowing through a Casimir cavity. According to stochastic electrodynamics, the electronic orbitals in atoms are supported by the ambient zero-point (ZP) field. When the gas atoms are pumped into a Casimir cavity, where long-wavelength ZP field modes are excluded, the electrons spin down into lower energy orbitals and release energy in the process. This energy is collected in a local absorber. When the electrons exit the Casimir cavity they are re-energized to their original orbitals by the ambient ZP fields. The process is repeated to produce continuous power. In this way, the device functions like a heat pump for ZP energy, extracting it globally from the electromagnetic quantum vacuum and collecting it in a local absorber. This energy can be used for heating, or converted to electric power.

We carried out a series of experiments to test whether energy is, in fact, radiated from Casimir cavities when the appropriate gas flows through them. The Casimir cavity devices we tested were nanopore polycarbonate membranes with submicron pores having a density of $3x10^8$ pores/cm^2. Gas was pumped through the membranes in a stainless steel vacuum system, and emitted energy was measured using a broadband pyroelectric detector and lock-in amplifier. Emission in the infrared was clearly observed. We analyzed the emission from different gases and cavities to determine its origin. None of the conventional thermodynamic models we applied to our data fully explain it, leaving open the possibility that it is due to Casimir-cavity-induced emission from ZP fields.

PACS: 84.60._h

Keywords: Zero-point energy, quantum vacuum, vacuum energy, Casimir cavity

[1] Corresponding author. Tel.: +1-303-492-1889; fax: +1-303-492-2758
E-mail address: moddel@colorado.edu.

1. Introduction

Physical effects resulting from zero-point (ZP) energy are well established [2]. This has led to several proposals and reviews discussing the extraction of ZP energy to use as a power source [3] [4]. The extraction methods usually involve ZP energy in the form of electromagnetic ZP fields. Our approach makes use of a Casimir cavity. It consists of two closely-spaced, parallel reflecting plates. Because the tangential electric field is reduced (to zero for a perfect conductor) at the boundaries, limits are placed on the ZP field modes between the plates, and those modes having wavelengths longer than twice the gap spacing are suppressed to a degree determined by the plate reflectivity.

According to stochastic electrodynamics (SED), the energy of classical electron orbits in atoms is determined by a balance of emission and absorption of vacuum energy [5]. By this view of the atom, electrons emit a continuous stream of Larmor radiation as a result of the acceleration they experience in their orbits. As the electrons release energy their orbits would spin down were it not for absorption of vacuum energy from the ZP field. Accordingly, the orbital energies of atoms inside Casimir cavities should be shifted if the cavity spacing blocks the ZPF required to support a particular atomic orbital. An exploratory experiment to test for a shift in the molecular ground state of H_2 gas flowing through a 1 μm Casimir cavity was carried out, but without a definitive result [6].

A suitable term for this is the "Casimir-Lamb shift" [7]. The energy levels of electron orbitals in atoms are determined by sets of quantum numbers. However the electromagnetic quantum vacuum can change these energies, as exhibited in the well known Lamb shift. In the case of the Lamb shift the nucleus of the atom (a single proton for hydrogen) slightly modifies the quantum vacuum in its vicinity. The result is that the $2P_{1/2}$ and $2S_{1/2}$ orbitals, which should have the same energy, are slightly shifted since they spread over slightly different distances from the nucleus, and hence experience a slightly different electromagnetic quantum vacuum. The electromagnetic quantum vacuum can be altered in a much more significant way in a Casimir cavity. Hence the term Casimir-Lamb shift.

In a 2008 patent [1] Haisch and Moddel describe a method to extract power from vacuum fluctuations that makes use this effect of Casimir cavities on electron orbitals. The process of atoms

flowing into and out from Casimir cavities is depicted in Figure 1. In the upper part of the loop gas is pumped first through a region surrounded by a radiation absorber, and then through a Casimir cavity. As the atoms enter the Casimir cavity their orbitals spin down and release electromagnetic radiation, depicted by the outward pointing arrows, that is extracted by the absorber. On exiting the cavity at the top left, the ambient ZPF re-energizes the orbitals, depicted by the inward pointing arrows. The gas then flows through a pump and is recirculated through the system. The system functions like a heat pump, pumping energy from an external source to a local absorber.

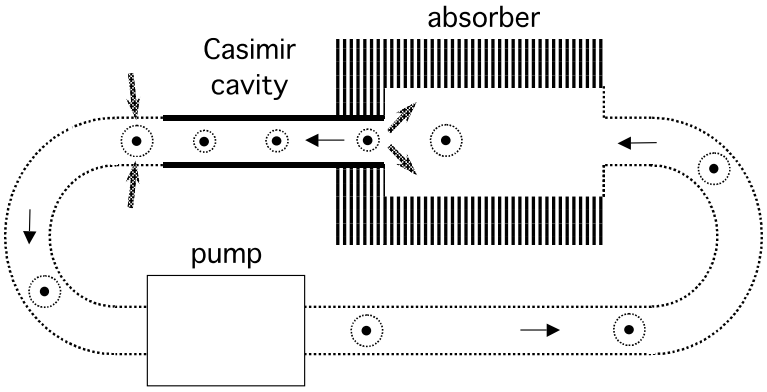

Fig. 1. Schematic representation of the vacuum-energy extraction process. Gas circulates through the system. The electronic orbitals of the gas atoms spin down to a lower level as the gas enters the Casimir cavity, radiating the excess energy to the absorber. Upon exiting the cavity the orbitals are re-energized by the ambient zero-point field. In this way, energy is collected from the ambient zero-point field and deposited on the absorber.

According to the initial analysis [1], for an electronic orbital to be suppressed inside a Casimir cavity its orbital frequency should match the frequency of a ZP field mode that is suppressed inside the cavity. For most atoms this corresponds to a Casimir-cavity gap spacing of less than 0.1 micron. So that the spacing is sufficiently large to be practically obtainable an atom with a relatively low-frequency outer orbital is required. The orbital frequency for large atoms like Xe, which has a relatively low-energy outer orbital, is lower than that for small atoms like He, where the outer orbital energy is larger. Therefore we expected that the emission would be stronger for a Casimir cavity having 0.1 μm gap and Xe gas, rather than for larger cavity spacings or smaller atoms.

In this paper we describe a test of the ZP energy harvesting concept. A series of experiments was carried out to measure radiation produced from gas flowing through Casimir cavities. The results and analysis are presented in the following sections.

2. Experimental

2.1. Choice of Casimir cavity

To form Casimir cavities we used Whatman polycarbonate Nuclepore track-etched flexible membranes with pore sizes of 0.1, 0.2, and 0.4 μm. These membranes withstand 180° C temperature stress without any visible deformation, so that they can be easily coated with metal in our thermal evaporator. The membranes are 2.54 cm in diameter, which makes them easy to handle. Gold was thermally evaporated at two angles to enhance coverage of the pore walls. The coverage was confirmed by scanning electron microscope (SEM) inspection, as shown in Figure 2. We chose gold as a coating metal since it is commonly used in the field of Casimir force measurements [8].

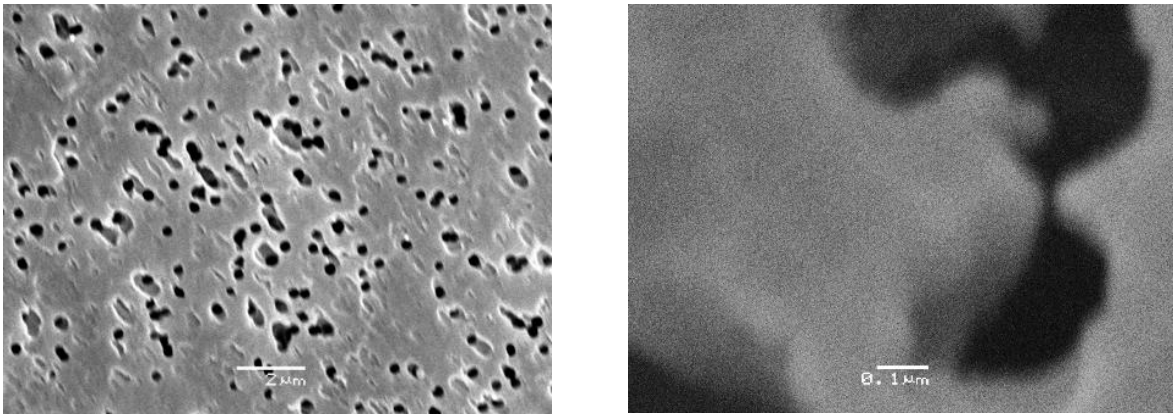

(a) (b)

Fig. 2. SEM images of the Nanopore polycarbonate membrane coated with 70 nm of palladium metal, shown at two magnifications. In (a) the white line corresponds to a length of 2 μm, and in (b) to 0.1 μm. From (b) it can be seen that top surface and the upper parts of the sidewalls are covered with metal.

Ideally, the metal coating should be highly reflective in the near-ultraviolet wavelength range to satisfy the Casimir cavity condition, since that range corresponds to twice the cavity spacing. However, modifications to the Casimir force formulation done by Lifshitz have shown that the effect occurs also for dielectric surfaces [9]. Our initial assumption was that if we were to see any quantum energy radiation

from the nanopore membrane it would be only for metal-coated filters, but we cannot exclude the possibility of observing radiation from uncoated filters, due to the Lifshitz formulation. Therefore we experimented with both, coated and uncoated membranes.

2.2. Experimental apparatus

We used a custom-machined copper holder, shown in Figure 3, to secure the filter inside the vacuum chamber.

Fig. 3. Copper holder with an uncoated nanopore polycarbonate membrane mounted in it.

The experimental set up is shown in Figure 4. Gas entered into the vacuum chamber and passed through the filter. The main chamber was made of stainless steel and used copper gaskets for sealing. It was pumped by a mechanical pump and could achieve a base pressure of 10^{-3} torr. Before each experimental run the chamber was evacuated for 20 min.

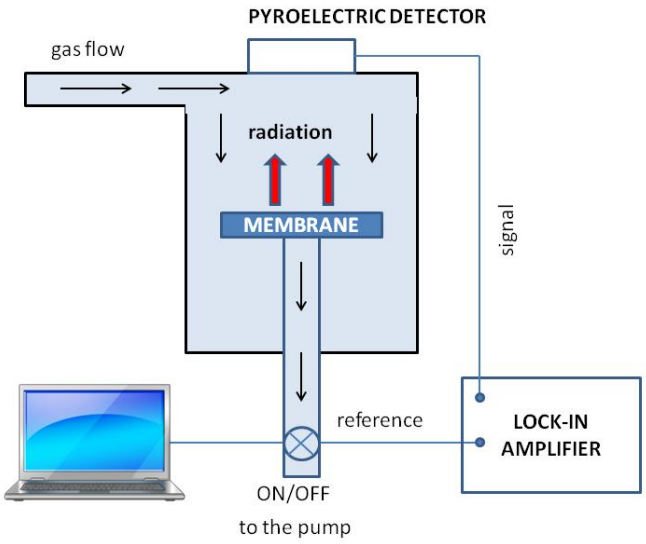

Fig. 4. Measurement setup for detection of radiation.

The flow was modulated by closing and opening the valve to the vacuum pump. We chose this approach, rather than modulating the input flow, to obtain a sufficiently small time constant, which is the inverse product of the volume and the gas flow at the given pressure. The volume of the main chamber was 320 cm^3. In contrast, the volume of the gas line to the pump was only 4.6 cm^3. Therefore, we obtained an almost 100 times faster system response by modulating the flow from the vacuum pump side than we would have by modulating the input gas flow. The main chamber pressure remained virtually unchanged while the drop of the pressure in the vacuum line modulated the flow of gas through the membrane.

A wide bandwidth SPH-49 pyroelectric detector from Spectrum Detectors Inc. was used for the radiative output measurements. The detector had a responsivity of 1.9×10^4 V/W and could detect signals at the level of nanowatts. Since the detection was based on a bolometric effect, the spectral response of the detector was flat over a wide range of wavelengths. Our device had a chromium coating, so that its response was constant from 0.6 μm to 5 μm. To reduce noise the detector was mounted inside a grounded metal box. The pyroelectric detector was placed outside the chamber facing the sample through an

infrared-transparent ZrSe window. The distance between the sample and the detector was 9 cm. We looked for a difference in the detector output, as measured using the lock-in amplifier, between the flow-on and flow-off conditions. Pressure inside the chamber was in the range of 1-10 torr. The modulation frequency for the ZPE experiment was 0.5 Hz.

At such low pressure the mean-free path length of the gas atoms was comparable to the thickness of the membrane and greatly exceeded the pore diameter. Under these conditions the flow through the filter was not laminar and can be considered to be thermal random bouncing of atoms entering and exiting the cavities with some net drift flow induced by the opening and closing the valve to the pump. If we assume that the radiation was emitted every time the atom entered the cavity, we would not be able to correlate this emission with the reference signal that modulates the flow. On the other hand, if the atom that went into the pore (or another equivalent atom) bounced back and reabsorbed the radiation it had just shed, we need to account only for the signal from the atoms that went all the way through the filter due to the net flow. In this case the emitted radiation would have the on/off frequency measured with the lock-in amplifier. We have based our experiment on this assumption.

3. Results and discussion

Both coated and uncoated membranes were tested with four different gases (He, Ar, N_2, and Xe). The measured radiation for filters with a 0.2 μm pore size is shown in Figure 5. The goal was to measure the effect of gas type on the radiation. We found clearly measureable radiation from the gases flowing into the membranes with Casimir cavities through them. However, one cannot jump to the conclusion that we found evidence for ZP energy extraction. Instead, we went to great lengths to investigate conventional mechanisms that might give rise to the observed signals.

The original expectation was that ZP radiation would be strongest and most likely to be observed when using gold-coated filters because Casimir cavities are commonly formed from metals, and Xe gas because the lower frequency atomic orbital in Xe is a closer match to the suppressed ZP energy mode in our Casimir cavities than that for the lower-mass atomic gases. Any other gas in combination with either a

coated or uncoated filter would give a smaller signal, if any at all. The results we obtained directly contradict this. The highest radiated power was observed with He gas, the smallest atomic number among four gases, and with uncoated filter. A possible explanation of the observed phenomena is presented in the following sections.

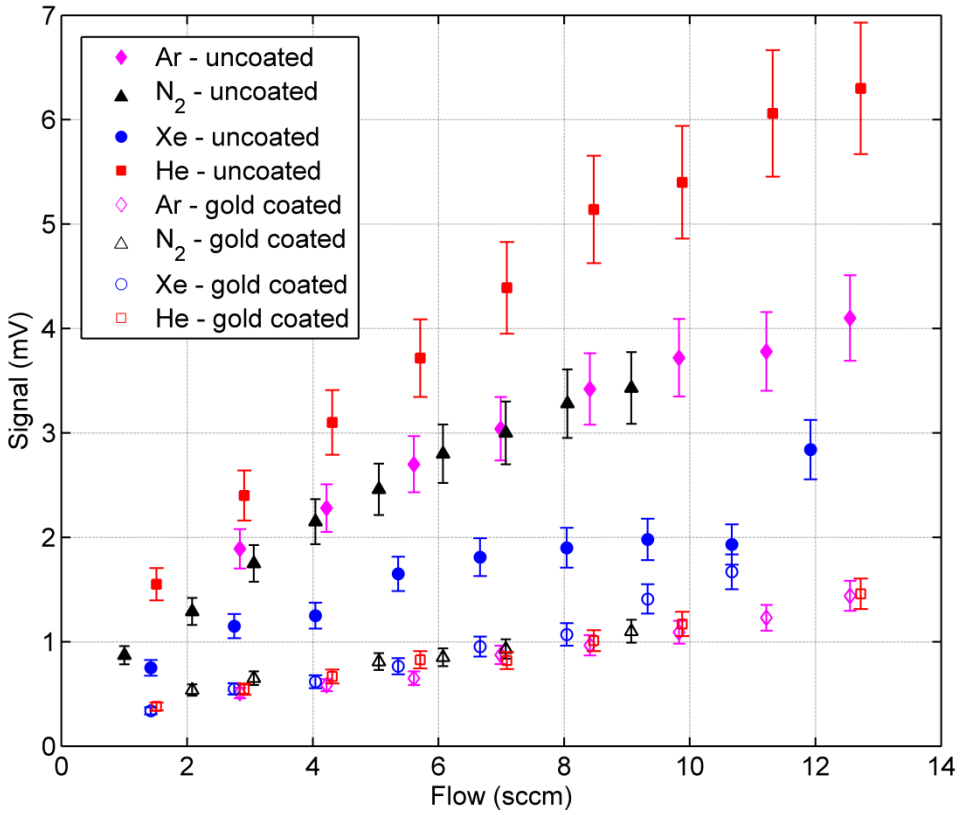

Fig. 5. Emitted radiation measured for N_2, Ar, Xe and He gasses flowing through uncoated and gold coated polycarbonate filters having 0.2 μm pore size.

3.1. Power balance and heat transfer

To analyze the power balance of the system we calculated the power provided to the system and the radiated power measured by the detector. The power in was calculated as the product of the gas flow and the pressure drop across the membrane. For a 5 sccm flow and a pressure drop of 4 torr the resulting power is ~2 x 10^{-5} W. The radiated power measured over the area of the detector at these conditions was ~10^{-7} W. If we assume that the location of the radiation source is the filter surface, then we need to account for the distance of 9 cm that separates the filter from the detector and the solid angle of 2π over

which the power is radiated. The total power output would then have been two orders of magnitude higher, bringing the number up to ~4 x 10^{-5} W and making it higher than the power in. This would mean there was source of power inside the chamber in addition to that from gas pressure. In reality, the stainless steel walls of the main chamber reflected a substantial portion of the IR radiation striking the chamber walls, making it available for detection. We analyze this quantitatively in the section on the Joule-Thomson model. At this point it appears that the power out was less than the power in and there is no need to invoke an additional power source, e.g., from ZP energy emission, inside the chamber.

Since gases were flowing inside the chamber, we must consider not only purely radiative but also conductive and convective heat transfer mechanisms. Therefore, the differences in the heat conduction coefficients of gases and their diffusivity are likely to have contributed to the measured temperature variation. It can be seen from Figure 5 that the signal levels for the different gasses flowing through the uncoated membrane followed the order of the thermal conduction coefficients and diffusivity of the gases (highest for He, lowest for Xe with N_2 and Ar in between). However, this trend is qualitative, not quantitative. The difference in the thermal conduction coefficients for He and Xe is close to 30 (He: 0.142 W/m/K, Ar: 0.018 W/m/K, N_2: 0.024 W/m/K, Xe: 0.00565 W/m/K), but the difference in the detected signal from an uncoated membrane is an order of magnitude lower, as evident from Figure 5.

For the case of metal-coated membranes, we introduce one more component into our heat transfer analysis. It is the thin gold film, which has a thermal conductivity of 30 times that of helium. An interesting observation is that with the gold-coated membrane we cannot distinguish between the signals from the different gases within measurement error, as shown in Figure 5. In this case the heat could have been conducted away through the metal film and further through the massive copper holder, and such heat transfer is no longer limited by the properties of the gases.

One factor that likely affects the magnitude of the signal is the emissivity of the material. The gases that we used in our experiment do not emit thermal radiation in the range of interest [10]. The emissivity of the gold at long wavelengths is nearly zero (0.01 to 0.1 at 1.6 μm and longer), while the emissivity for

plastic materials is approximately 0.95. This could explain why we see higher signals from the uncoated polycarbonate filter compared to the gold-coated one, as shown in Figure 5.

3.2. Heat production inside the chamber: non-Casimir-cavity-induced mechanisms

We examine several non-Casimir-cavity-induced mechanisms that might account for the observed radiation to see if there is a plausible explanation that requires only conventional thermodynamics.

3.2.1. Joule-Thomson model

To assess whether the Joule-Thomson effect [11] could be the source of the signal we first address whether we have observed it. In one of our modified experiments we were able to distinguish heating from cooling with the measurement system.

We conducted a modified experiment where the filter was replaced by a 12.5 μm thick Mylar film having a single hole 3 mm in diameter. The gas expanded through this hole into the gas line leading to the vacuum pump. The phase measured by the lock-in amplifier was positive and 180° off from the phase measured in the experiment with the nanopore filter, indicating cooling. This is how we knew the effect that we observed with gases flowing through the Casimir cavities was not due to the Joule-Thompson effect.

The signal amplitudes for the different gases followed the sequence of the gases' Joule-Thomson coefficients (highest for Xe). Based on literature values [12] Xe possesses the highest coefficient, 1.87 ºC/atm at 1 atm, while He has the smallest, –0.0625 ºC/atm at 200 atm, with Ar (0.372 ºC/atm at 1 atm) and N_2 (0.2217 ºC/atm at 1 atm) in between. These numbers, however, are for pressures higher than in our experiment. We make that assumption that for the lower pressure these coefficients follow the same trend (Xe > Ar > N_2 > He). In fact, the signal from He was so small we were not able to obtain reliable measurements from this gas.

By knowing the pressure drop at the point of gas expansion, ~2 torr, and using the above values for the Joule-Thomson coefficients we calculated the associated temperature changes. For Xe gas this temperature drop was 4.9×10^{-3} ºC. Translating the detected signal to the temperature change using black

body spectrum calculations, the number comes out to be ~0.001 K. We noted earlier that not all the radiated power reaches the detector. Our calculated value for Joule-Thomson cooling is close to the measured one for the 3 mm hole assuming that we measure 20% of total emission, rather than the reduction by two orders of magnitude calculated earlier on the assumption that there was no reflection by the inner walls of the stainless steel chamber.

3.2.2. Frictional losses model

In this model we assume that our filter works as a passive element dissipating heat in analogy with a resistor in an electrical circuit. Using this analogy the gas flow is analogous to the current and the pressure drop across the filter is similar to the voltage drop across the resistor. The pressure drop depends linearly on gas flow and the slope is different for different gases, with Xe being the most "resistive" and He being the most "conductive". These results are in agreement with the studies done by Roy and Raju on the gas flow through microchannels [13].

If these frictional losses are what produced the heating effect and gave rise to the detector signal, the power should depend quadratically on the gas flow (in the same way that electrical power depends quadratically on the electrical current passing through a passive element). In our case the power depends on the flow linearly. This does not automatically disqualify the frictional losses approach. Our system tended to stay in thermal equilibrium with the environment, with the gas in the chamber exchanging energy with the external environment through the walls and providing a channel for the heat/energy to escape. This may have affected the way power depends on the flow, causing it to show a more linear dependence.

Looking now at the variation of radiant power over different gases, the fact that the largest pressure drop at a given flow rate was associated with Xe means that this gas should have dissipated more heat than any other gas according to the frictional losses model. However, taking the heat conduction into account can dramatically change the picture. The magnitude of the signal can be affected by thermal conductivity and diffusivity of the gases, which are the highest for He and lowest for Xe. That could

explain why we observed the most radiation from He and the least from Xe, even though the frictional losses model predicts the opposite outcome.

Based on the lack of a quadratic power dependence on flow and the opposite gas order for frictional losses and measured power, it appears that the frictional losses model does not explain the observed behaviour. However, as noted above, it may be possible to explain the result if the heat conduction and diffusivity of the gases are included. To better assess whether these factors can account for the observed behaviour will take additional experimental and analytical investigation.

3.2.3. Absorption/adsorption and release model

When a gas is brought into contact with a solid, molecules are pulled from the gas and are either absorbed inside of the solid, or adsorbed on the outside, attached to the surface. The absorption/ adsorption process is exothermic. It may be possible that the heating we see is due to adsorption on the membrane when the gas pressure rises. In the absence of gas flow we would then observe desorption, which is an endothermic process. Adsorption is proportional to the pressure of the gas and the number of vacant sites for adsorption. The number of such sites depends on the surface area. We used three different pore size filters, 0.1 μm, 0.2 μm and 0.4 μm, which have surface area of 9.42 cm^2, 18 cm^2 and 12.56 cm^2, respectively. Signal from these different filters measured at pressure of ~5 torr did not follow the expected trend of surface areas. Based on this result we have rejected the absorption/adsorption model as a possible explanation for the radiation we observed.

3.2.4. Turbulence model

Turbulence is another possible heat source. The theory of energy dissipation in locally isotropic turbulence was developed in the early 1940s by Kolmogorov [14]. In our experiment the rate at which the gas flowed through the nanopore cavities was below 2 cm/s. The resulting Reynolds number is far below what would be required to cause turbulence at the exit. Also, the viscosities of the gases used in the experiment have values that are very close to each other (Ar: 2.1×10^{-4} poise, N_2: 1.66×10^{-4} poise, Xe:

$2.1x10^{-4}$ poise, He: $1.86x10^{-4}$ poise). This means that even if turbulence did cause the radiation from the filter it alone could not explain the differences in signal levels for the different gases.

3.3. Heat production inside the chamber: Casimir cavity-induced model

After failing to explain the observed radiation using conventional thermodynamics, we analyze the data as if the signal were the result of ZP energy emission. If we assume that each atom releases on the order of 10% of its energy, approximately 1eV per transaction upon entering the cavity, it is straightforward to calculate how much output power we should see from the gas flowing through a given nanopore filter. It is on the order of milliwatts, which is thousands times larger than the measured power, assuming that we detect at least 20% of emitted radiation.

If the radiation is due to Casimir cavity effects there are several factors that are likely to have reduced the radiated power and would account for its being lower than expected:

- The filters contain a range of nanopore sizes and shapes, as shown in Figure 2. Given that only a small fraction of the nanopores within the filter satisfy the Casimir cavity conditions, the number of atoms experiencing a large change in ZP field density was reduced substantially. Thus, the amount of power radiated by the atoms passing through the membrane was reduced.
- Atoms may need to undergo a collision in order to radiate power. Since we were running our experiments at low pressure (several torr), the mean-free path length of the gas atoms inside the cavity is on the order of 10 μm, which exceeds the dimension of the cavity itself. This means a fraction of the atoms could have passed through the cavity undisturbed, retaining their electrons in their initial unperturbed states without radiating any power.

Because the underlying SED theory is still under development, we cannot predict precisely what wavelengths of the ZPE field support the atomic orbitals, and hence what the optimum Casimir cavity dimensions are for shifting the orbitals. We cannot predict the emission wavelengths, and so the majority of the emission may lie outside the range of our detector. There may be other factors that can influence the change in the orbital size inside the Casimir cavity. Therefore the fact that the measured power was far

below that expected from ZP energy-induced radiation does not disqualify that as a possible source for the observed radiation.

4. Conclusions

A clear infrared signal has been measured for gases flowing through polycarbonate Casimir cavity nanotubes, both when uncoated and when coated with gold. The signal was obtained for all gases tested, N_2, Ar, Xe and He. In an attempt to explain the results in terms of conventional thermodynamics, we analyzed them to see if Joule-Thomson cooling, frictional heating, adsorption/absorption heating, or turbulence could account for the results. None of these clearly fit the data, but it is possible that a combination of effects could. At this point it appears that ZP energy extraction from the quantum vacuum remains a possible explanation for the observed radiation. More experimental work will be required to determine if this is the correct explanation.

Acknowledgements

Many thanks to B. Haisch for illuminating discussions about vacuum energy, to R. Cantwell and M. McConnell for help with the experiments, and to B. L. Katzman for comments on the manuscript. This work was supported by HUB Lab, and based on prior work supported by DARPA under SPAWAR Grant No. N66001-06-1-2026.

References

[1] B. Haisch and G. Moddel, "Quantum vacuum energy extraction," U.S. Patent 7,379,286, May 27, 2008.

[2] P. W. Milonni, *The Quantum Vacuum*. Boston: Academic Press, 1994.

[3] E. Davis, V. L. Teofilo, H. E. Puthoff, and L. J. Nickisch, "Review of experimental concepts for studying the quantum vacuum field," in *Proc. of the STAIF-2006: 3rd Symposium on New Frontiers and Future Concepts, AIP Conf. Proc.*, vol. 813, 2006, pp. 1390-1401.

[4] G. Moddel, "Assessment of proposed electromagnetic quantum vacuum energy extraction methods," *arXiv:0910.5893v1*, 2009.

[5] T. H. Boyer, "Random electrodynamics: the theory of classical electrodynamics with classical electromagnetic zero-point radiation," *Phys. Rev. D*, vol. 11, pp. 790-808, 1975.

[6] H. E. Puthoff, S. R. Little, and M. Ibison, "Engineering the zero-point field and polarizable vacuum for interstellar flight," *J. Brit. Interplanetary Soc.*, vol. 55, pp. 137-44, 2002.

[7] B. Haisch, private communication.

[8] M. Bordaga, U. Mohideen, and V. M. Mostepanenko, "New developments in the Casimir effect," *Phys. Reports*, vol. 353, pp. 1-205, 2001.

[9] V. Mostepanenko, N. N. Trunov, and R. L. Znajek, *The Casimir Effect and its Application*. Oxford: Clarendon, 1997.

[10] G. L. Stephens, *Remote Sensing of the Lower Atmosphere: an Introduction*. New York: Oxford University Press, 1994.

[11] D. V. Schroeder, *An Introduction to Thermal Physics*. San Francisco: Addison Wesley, 2000.

[12] D. Green and R. Perry, *Perry's Chemical Engineers' Handbook, Eighth Edition*. New York: McGraw-Hill, 2007.

[13] S. Roy and R. Raju, "Modeling gas flow through microchannels and nanopores," *J. Appl. Phys.*, vol. 93, no. 8, pp. 4870-4879, 2003.

[14] A. Kolmogorov, "The local structure of turbulence in incompressible viscous fluid for very large Reynolds numbers," *Proc. R. Soc. London A*, vol. 434, pp. 9-13, 1991, first published in Russian in Docl.Akad. Nauk SSSR, 1941, translated by V. Levin.